

Review

Polymers and Polymer-Based Materials for the Detection of (Nitro-)explosives

Olga S. Taniya ¹, Albert F. Khasanov ¹, Leila K. Sadieva ¹, Sougata Santra ¹, Igor L. Nikonov ^{1,2}, Wahab K. A. Al-Ithawi ^{1,3}, Igor S. Kovalev ¹, Dmitry S. Kopchuk ^{1,2}, Grigory V. Zyryanov ^{1,2,*} and Brindaban C. Ranu ^{1,4}

¹ Chemical Engineering Institute, Ural Federal University, 19 Mira Str., 620002 Yekaterinburg, Russia; olga.tania@urfu.ru (O.S.T.); a.f.khasanov@ya.ru (A.F.K.); l.k.sadieva@urfu.ru (L.K.S.); sougatasantra85@gmail.com (S.S.); rodonid93@mail.ru (I.L.N.); valitkhavi@urfu.ru (W.K.A.A.-I.); ekls85@yandex.ru (I.S.K.); dkopchuk@mail.ru (D.S.K.); bcranu@gmail.com (B.C.R.)

² I. Ya. Postovsky Institute of Organic Synthesis of RAS (Ural Division), 22/20 S. Kovalevskoy/Akademicheskaya Str., 620219 Yekaterinburg, Russia

³ Energy and Renewable Energies Technology Center, University of Technology-Iraq, Baghdad 10066, Iraq

⁴ School of Chemical Sciences, Indian Association for the Cultivation of Science, Jadavpur, Kolkata 700032, India

* Correspondence: gvzyryanov@gmail.com; Tel.: +7-3433754501

Abstract: Methods for the remote detection of warfare agents and explosives have been in high demand in recent times. Among the several detection methods, fluorescence methods appear to be more convenient due to their low cost, simple operation, fast response time, and naked-eye-visible sensory response. For fluorescence methods, a large variety of fluorescent materials, such as small-molecule-based fluorophores, aggregation-induced emission fluorophores/materials, and supramolecular systems, have been reported in the literature. Among them, fluorescent (bio)polymers/(bio)polymer-based materials have gained wide attention due to their excellent mechanical properties and sensory performance, their ability to recognize explosives via different sensing mechanisms and their combinations, and, finally, the so-called amplification of the sensory response. This review provides the most up-to-date data on the utilization of polymers and polymer-based materials for the detection of nitroaromatic compounds (NACs)/nitro-explosives (NEs) in the last decade. The literature data have been arranged depending on the polymer type and/or sensory mechanism.

Keywords: polymers; nitro-explosives; materials; detection methods; fluorescent materials



Citation: Taniya, O.S.; Khasanov, A.F.; Sadieva, L.K.; Santra, S.; Nikonov, I.L.; Al-Ithawi, W.K.A.; Kovalev, I.S.; Kopchuk, D.S.; Zyryanov, G.V.; Ranu, B.C. Polymers and Polymer-Based Materials for the Detection of (Nitro-)explosives. *Materials* **2023**, *16*, 6333. <https://doi.org/10.3390/ma16186333>

Academic Editor: Ana Arenillas

Received: 15 August 2023

Revised: 17 September 2023

Accepted: 18 September 2023

Published: 21 September 2023



Copyright: © 2023 by the authors. Licensee MDPI, Basel, Switzerland. This article is an open access article distributed under the terms and conditions of the Creative Commons Attribution (CC BY) license (<https://creativecommons.org/licenses/by/4.0/>).

1. Introduction

In the last several decades, terroristic threats have become an actual problem worldwide, and these threats are mainly associated with the use of warfare agents or explosive devices against civilian transport and/or objects of civilian infrastructure. Therefore, approaches to the remote detection of warfare agents and explosives are in high demand. Concerning the latter, the use of detection dogs is widely considered the most effective and adaptive tool for explosive detection [1]. However, there are several disadvantages to using dogs for that purpose. First of all, dogs are unable to work by themselves, only functioning in tandem with a handler, who is fully responsible for correctly judging the dog's behavior during the explosives search. Second, dogs cannot be worked as intensely as a piece of machinery (not more than half an hour). Third, dogs are also vulnerable to distraction by external factors, such as new surroundings, bright lights and loud noises, fatigue, and even alluring scents left behind by canine members of the opposite sex. Therefore, studies on using other mammals/rodents, such as pigs [2] or rats [3], are in progress. And thus, the olfactory systems of rats and pigs are considered promising objects for studies on explosive detection [4]. Some other studies are associated with investigating insects/insect-based biodevices for explosive detection [5–9].

Other approaches to explosive detection include using physical methods, such as mass spectrometry [10], differential mobility spectrometry [11], electrochemical methods [12], microcantilever devices [13], neutron techniques [14], nuclear quadrupole resonance methods [15], X-ray diffraction methods [16], millimeter-wave [17] or terahertz imaging [18], and, finally, laser-based detection methods [19]. The main disadvantages of these methods are the lack of portability, a need for special algorithms for transferring the sensory event to a readable signal, a noticeable time delay from the sensing event to the physical signal, the high cost of equipment, and, in most cases, the requirement for operation by highly trained personnel. In this regard, the use of colorimetric [20,21] or fluorescence methods [22] seems to be more convenient due to their low cost, simpler operation, fast response time, and naked-eye-visible sensory response. For fluorescence methods, a large variety of fluorescent materials, such as small-molecule-based fluorophores, aggregation-induced emission fluorophores/materials, and supramolecular systems, have already been reported in the literature [22]. Among them, fluorescent (bio)polymers/(bio)polymer-based materials [23–25] have gained wide attention due to their excellent mechanical properties and sensory performance, their ability to recognize explosives via different sensing mechanisms and their combinations, and, finally, the so-called amplification of the sensory response.

For the evaluation and comparison of the quenching efficiency of sensors and probes, the Stern–Volmer mathematical model is usually used. If the static quenching mechanism takes place, the quenching constant (Stern–Volmer constant), K_{SV} , should increase linearly with the quencher concentration, as described by the Stern–Volmer equation (Equation (1)):

$$\frac{I_0}{I} = 1 + K_{SV} \cdot [Q] \quad (1)$$

where I_0 and I are the fluorescence intensity before and after the addition of a nitroaromatic compound (quencher); $[Q]$ is the concentration of the quencher, mol/L; and K_{SV} is the value of the quenching constant, M^{-1} .

According to Equation (1), the plot of I_0/I vs. $[Q]$, or the so-called Stern–Volmer plot, should give a straight line with a slope equal to K_{SV} .

During the static quenching mechanism, the lifetime of the luminescence does not depend on the concentration of the quencher and remains unchanged as the quencher concentration increases.

Dynamic quenching is usually associated with collisions between molecules of a sensor and an analyte, and the Stern–Volmer equation is represented as Equation (2):

$$\frac{I_0}{I} = 1 + k_q \tau_0 \times [Q] \quad (2)$$

where k_q and τ_0 are the bimolecular quenching constant and the lifetime of the fluorophore in the absence of a quencher, respectively.

This review provides the most up-to-date data on the utilization of polymers and polymer-based materials for the detection of nitroaromatic compounds (NACs)/nitro-explosives (NEs) in the last decade. The literature data are arranged depending on the polymer type and/or sensory mechanism.

2. Common Approaches to the Detection of NACs by Using Polymer-Based Materials

Conjugated polymers (CPs) are considered attractive materials for the fluorescence detection of various (bio)analytes since, in most cases, CPs have high fluorescence quantum yields, large extinction coefficients, and efficient optical signal transduction, and the synthetic versatility of CPs allows the incorporation of a wide selection of functional groups into the polymer backbone or into the side arms for better performance. Below, several common approaches to using polymers for explosive detection are highlighted.

2.1. Linear Conjugated Polymers

Batool and coworkers designed fluorene-based fluorometric and colorimetric conjugated polymers (CPs) (Figure 1) for the sensitive detection of PA in an aqueous medium at the picomolar (pM) level [26]. These polymers possess a high conjugation degree and electron-donating ability due to the presence of fluorene units. Therefore, these CPs demonstrated great sensitivity and selectivity toward picric acid (PA) over other NACs, with Stern–Volmer quenching constant, K_{SV} , values of $4.27 \times 10^6 \text{ M}^{-1}$, $3.71 \times 10^6 \text{ M}^{-1}$, and $2.13 \times 10^6 \text{ M}^{-1}$ in an aqueous solution ($\text{H}_2\text{O}/\text{THF}$ (3:2, v/v)) for CP1, CP2, and CP3, respectively (Figures 2 and 3). The limits of detection (LODs) for PA were calculated to be 3.2, 5.7, and 6.1 pM, respectively. For all of the CPs, the static quenching mechanism could be inferred from the high linearity of the Stern–Volmer plots (Figure 2d), bathochromic shifts in UV/Vis absorption spectra upon the addition of PA, and the insignificant overlap between the absorption of PA and the fluorescence emission of the CPs. The authors confirmed the PET mechanism by analyzing the HOMO–LUMO energy levels of CPs and PA. In this case, CP1, CP2, and CP3 were characterized by higher-lying LUMO levels (−1.63, 1.73, and −1.84 eV, respectively) compared to PA (−4.56 eV), with the smallest ΔE_{LUMO} calculated for CP1, which agrees with the experimental data. In addition, CPs exhibited a naked-eye-visible response after the addition of 500 nM PA to $\text{H}_2\text{O}/\text{THF}$ (3:2, v/v) solutions (Figure 4).

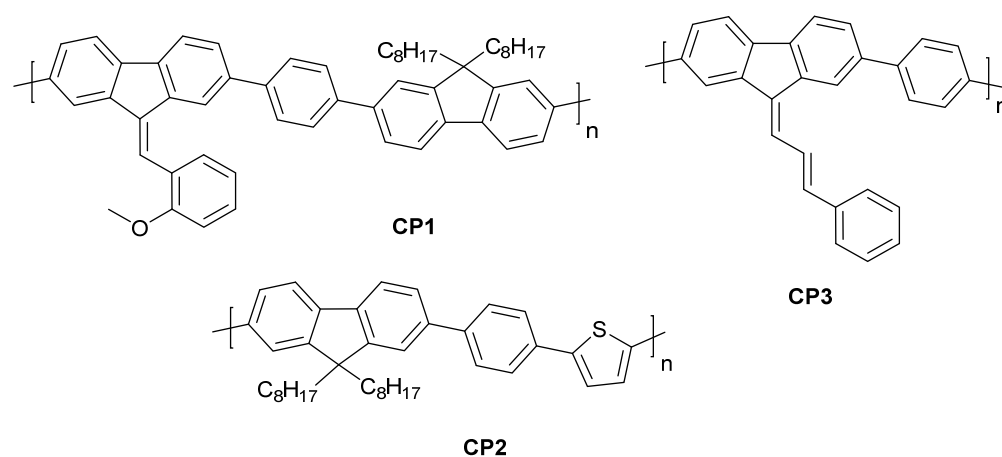


Figure 1. Structures of CP1, CP2, and CP3.

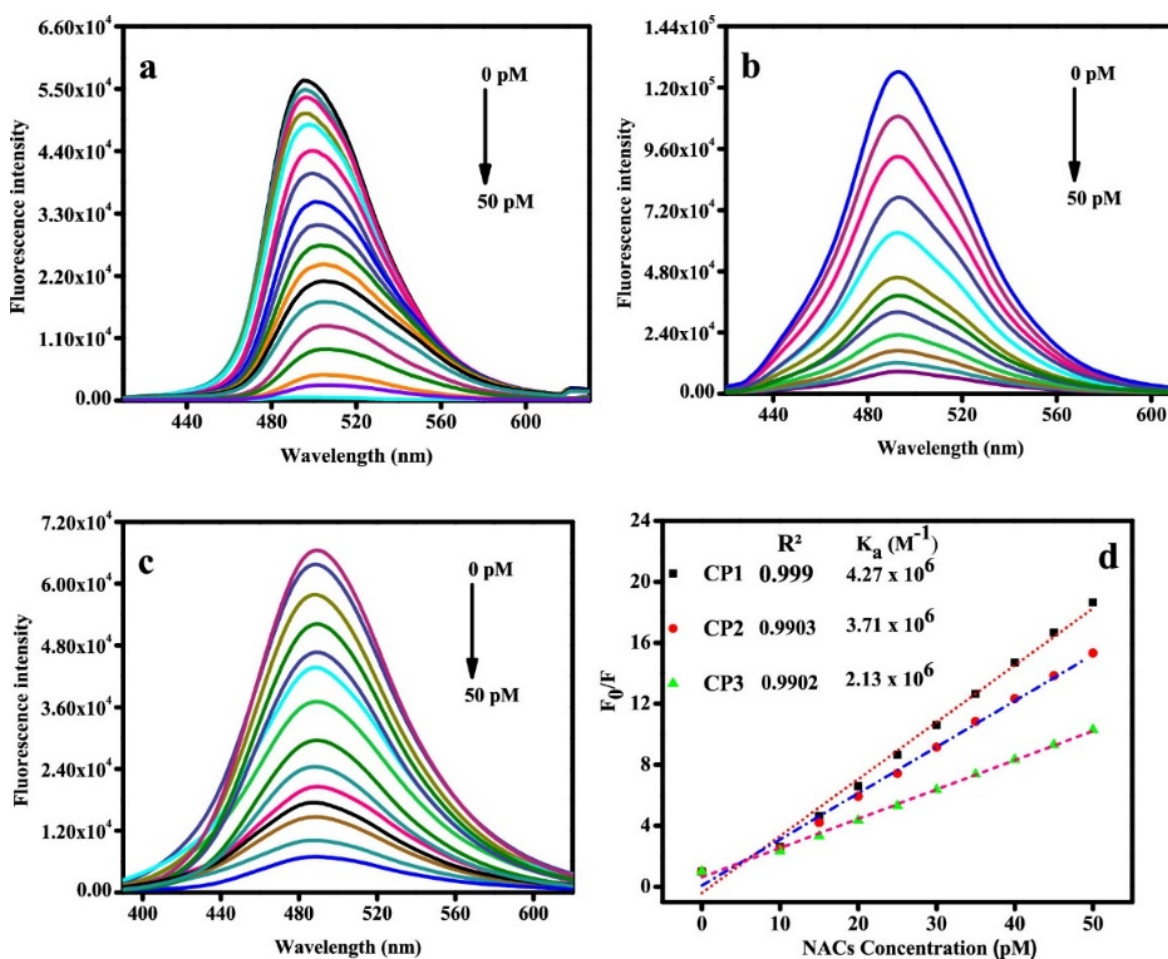


Figure 2. Spectral change in fluorescence emission behavior of the polymers (a) CP1, (b) CP2, and (c) CP3 (10 μ M) in aqueous solution (H_2O/THF (3:2, v/v)) and (d) changes in the SV plot of polymers CP1, CP2, and CP3 treated with different concentrations of TNP explosive (0–50 pM). Reproduced with permission from reference [26]. Copyright © ACS Publications 2022.

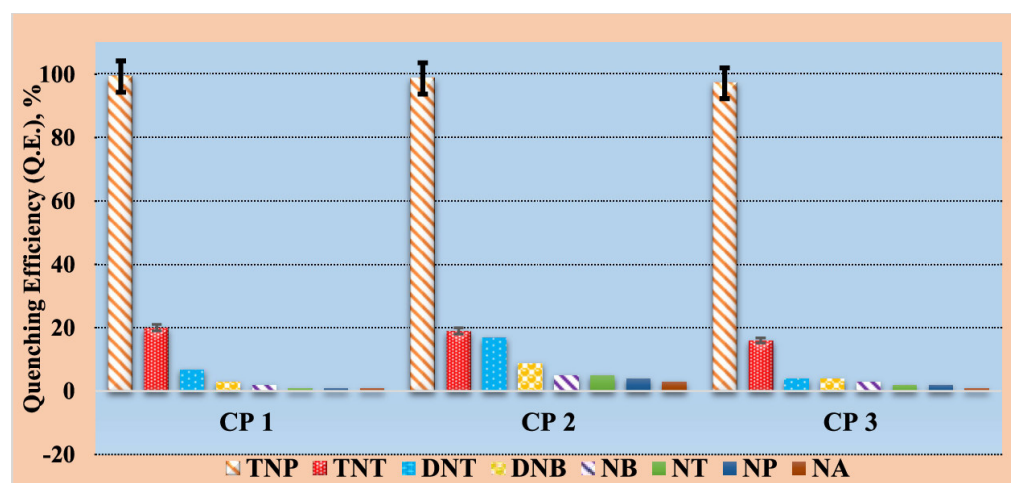


Figure 3. Graphical representation of quenching efficiency of polymers CP1, CP2, and CP3 (10 μ M) treated with different NACs, including TNP, TNT, DNT, DNB, NB, NT, NP, and NA. Reproduced with permission from reference [26]. Copyright © ACS Publications 2022.

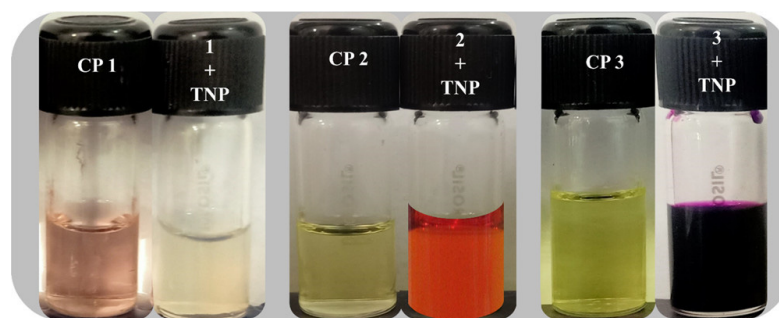


Figure 4. Polymers **CP1**, **CP2**, and **CP3** (10 μM) changing to different colors with the addition of 500 nM PA in daylight. Reproduced with permission from reference [26]. Copyright © ACS Publications 2022.

Giri and Patra reported 1,2,3-triazolyl-functionalized carbazole- (**P1**), fluorene- (**P2**), and thiophene-based (**P3**) A-alt-B-type π -conjugated copolymers for the selective and sensitive detection of NACs in aqueous media and the vapor phase [27]. Due to the high conjugation degree based on typical donating units, these **P1–P3** copolymers demonstrated highly intense fluorescence with quantum yields in the range of 18–20%. The **P1–P3** polymers exhibited a fluorescence-quenching response to NACs with high quenching efficiency (Figure 5). PA was found to be the most efficient quencher for all of the polymers, with the highest $K_{\text{SV}} = 6.4 \times 10^4 \text{ M}^{-1}$ for **P2** (Figure 6b). Based on the high linearity of the Stern–Volmer plot (Figure 6a) and the higher-lying LUMO levels of **P1–P3** compared to those of the NACs, the authors declared that static quenching occurred by the PET mechanism. **P1–P3**-based thin films demonstrated luminescence quenching of 91%, 53%, and 48%, respectively, after exposure for 200 s (Figure 7a). In addition, the authors demonstrated the reusability of the films based on the number of cycles of exposure and washing with water (Figure 7b), showing the applicability of the prepared probes.

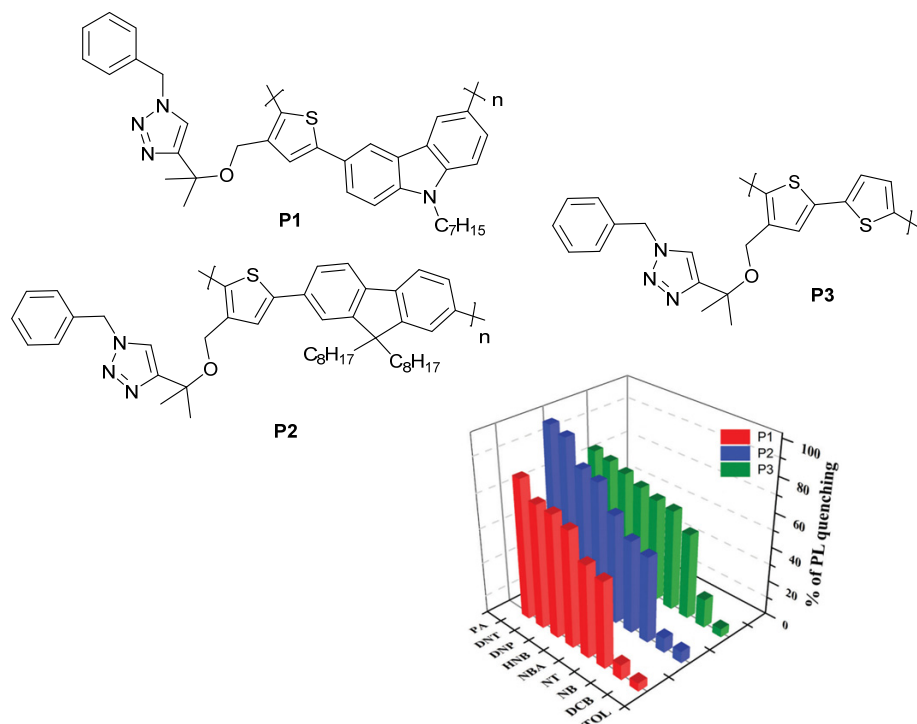


Figure 5. Emission-quenching percentage for polymers **P1–P3** toward different NACs and non-nitroaromatic compounds in chloroform. Reproduced with permission from reference [27]. Copyright © Royal Society of Chemistry 2020.

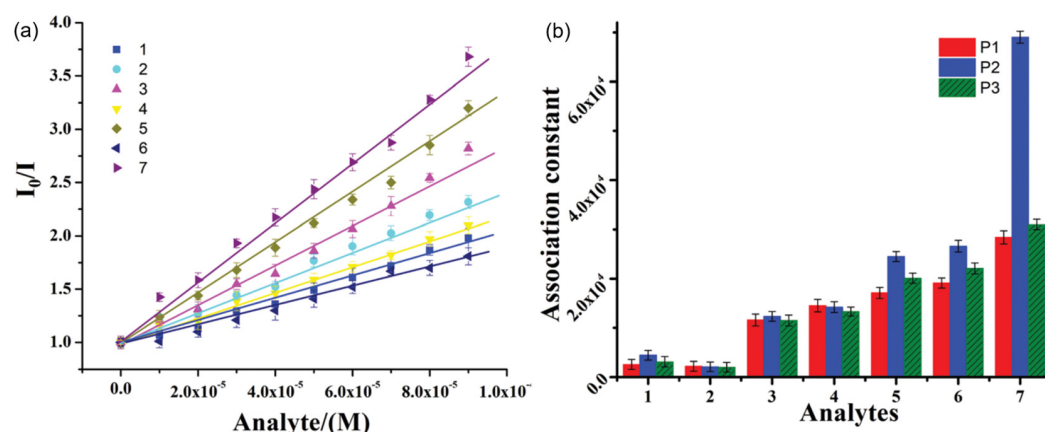


Figure 6. (a) Results in Stern–Volmer plot for polymer **P2**. (b) Graphical representation of the association constant comparison of polymers **P1–P3** for different nitroaromatics (1: NB; 2: NT; 3: NBA; 4: HNB; 5: DNP; 6: DNT; 7: PA). Reproduced with permission from reference [27]. Copyright © Royal Society of Chemistry 2020.

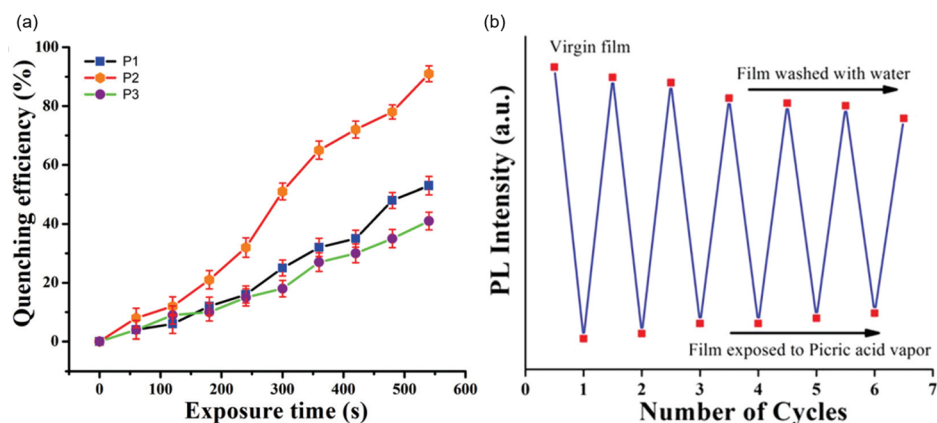


Figure 7. (a) Graphical representation of the superiority of polymer **P2** over polymers **P1** and **P3**, as indicated by the relative quenching efficiency. (b) Emission-quenching cycles and demonstration of reusability through recovery after exposing the probe film to PA vapor for 200 s. Reproduced with permission from reference [27]. Copyright © Royal Society of Chemistry 2020.

Liu and coworkers reported the three-component conjugated polymers **P4** and **P5** (Figure 8) and their application as super-rapid-response fluorescent probes to DNT vapor [28]. **P4** and **P5** thin films demonstrated selectivity toward DNT vapor over other common explosives (Figure 9). The authors performed fluorescence-quenching experiments in the vapor phase only. The fluorescence-quenching ratios of **P4** and **P5** to DNT reached 93% and 96% in 5 s, respectively. In addition, **P4** and **P5** thin films have comparable quenching efficiency toward DNT and TNT, while **P4** shows remarkably higher quenching efficiency toward other analytes compared to **P5**. The authors attributed such behavior to the possible stacking of pyrene units, which is easier to achieve compared to anthracene ones. Therefore, **P4** can form looser films to increase the diffusion of analyte molecules, thus enhancing the sensing performance. The higher selectivity toward DNT and TNT could be explained by the higher vapor pressure of these analytes in comparison with other less volatile explosives. **P4** and **P5** demonstrated a fast response time: that is, after 5 s of exposure to DNT vapor, 93% and 96% of the fluorescence was quenched, respectively (Figure 10a,b). The fluorescence-quenching ratios of **P4** and **P5** films to TNT were found to be only 46% and 43% in 5 s, respectively. The reusability of **P4** and **P5** films was also investigated. They demonstrated almost the same level of fluorescence-quenching performance (93% and 94% after exposure to DNT vapor for 5 s) after three cycles of quenching/recovery.

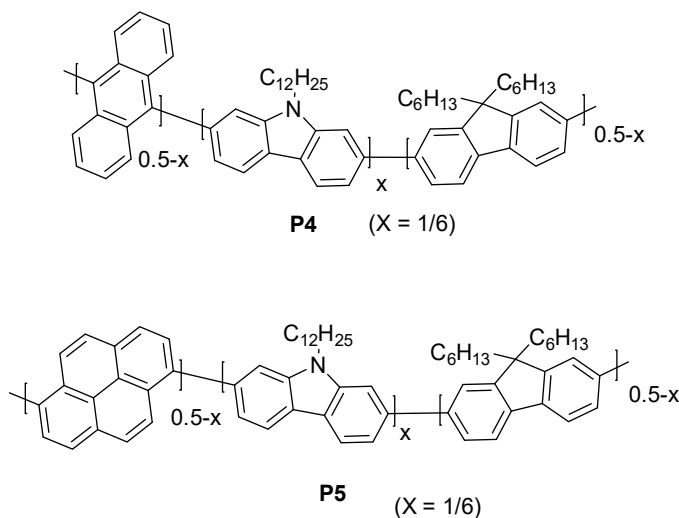


Figure 8. Structures of polymers P4 and P5.

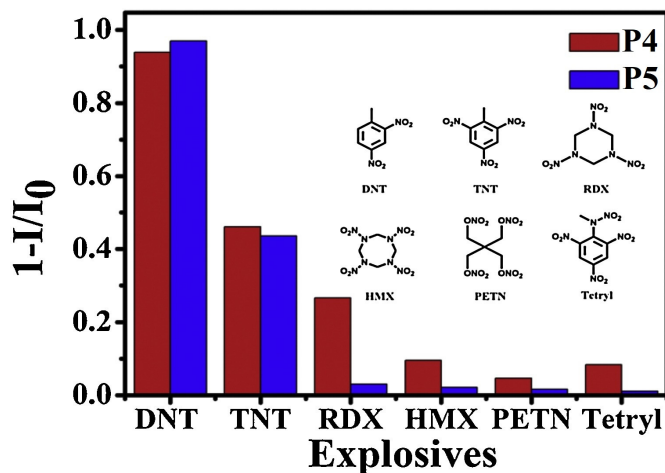


Figure 9. Graphical representation of different fluorescence-quenching ratios of polymers P4 and P5 exposed to nitro-explosives DNT, TNT, RDX, HMX, PETN, and Tetryl vapor for 5 s. Reproduced with permission from reference [28]. Copyright © Elsevier 2019.

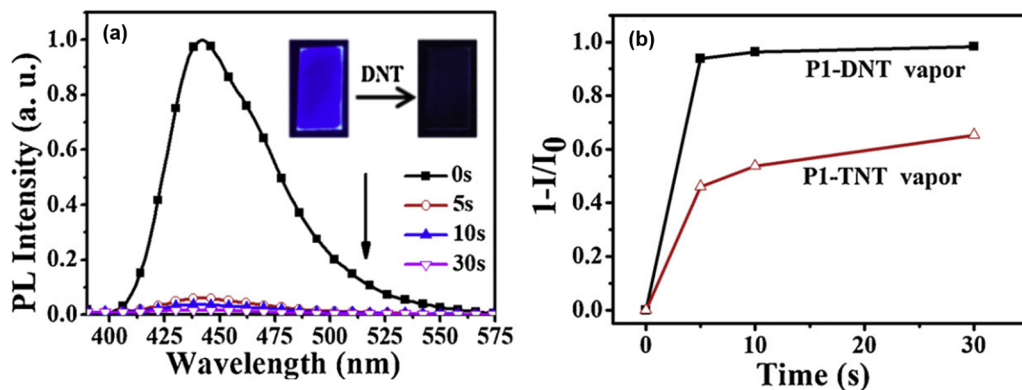


Figure 10. (a) Graphical representation of fluorescence intensity of P1 films exposed to DNT vapor. Inset: Depiction of P1 and P2 films exposed to DNT vapor for 0 s and 5 s. (b) Graphical representation of fluorescence-quenching ratios of P1 films to TNT and DNT. Reproduced with permission from reference [28]. Copyright © Elsevier 2019.

2.2. Conjugated Microporous Polymers

Porous polymers have a large specific surface area, which has unique advantages in the fluorescence detection of explosives. This allows for an improved mass-transfer capability so that explosives in solution or in the gaseous state can be pre-concentrated within the polymer, increasing the concentration of nearby fluorophores. On the other hand, it can promote the diffusion of explosive molecules into the pores of the polymer and provide a full-contact interface for the interaction of explosive molecules with fluorophores, thereby improving the detection sensitivity. In this case, the determination of porosity properties, such as the Brunauer, Emmett, and Teller surface area (S_{BET}), pore volume and size, micropore volume ratio ($V_{\text{micro}}/V_{\text{total}}$), etc., plays an important role in the estimation of a polymer as a sensor for any analyte, including NACs. Therefore, the control and tuning of porosity and surface parameters are of great importance and can be achieved by choosing certain building blocks and types of implemented organic reactions. In addition, porous polymers can be applied in a field of molecular separation for the selective extraction of an analyte from a mixture, followed by recyclization by washing, centrifuging, etc., with subsequent reuse, which is very practical.

Nailwal et al. designed [29] and developed three luminescent truxene-based CMPs (**Tx-CMPs**) via the Suzuki–Miyaura cross-coupling reaction (Figure 11). All **Tx-CMPs** exhibited a high BET surface area, $S_{\text{BET}} = 788\text{--}915 \text{ m}^2 \text{ g}^{-1}$ (based on nitrogen gas uptake isotherms, Figure 12a), and good thermal stability. Based on nonlocal density functional theory (NLDFT), **Tx-CMPs** mainly possess a pore size of 1.38–1.41 nm (Figure 12b) with a pore volume of 0.57–0.90 $\text{cm}^3 \text{ g}^{-1}$, accompanied by the formation of aggregates of small globular particles with an amorphous character (Figure 12c–e). It should be noted that a negligible presence of the palladium metal residue was detected by SEM–EDS. Due to the extended aromatic conjugation system based on fluorene units and flexible aromatic linkers, **Tx-CMPs** avoid the ACQ effect and demonstrate intense luminescence. All **Tx-CMPs** were insoluble in all tested organic solvents, with the most well-dispersed suspensions of **Tx-CMPs** obtained in THF, which was chosen as the solvent for further fluorescence experiments.

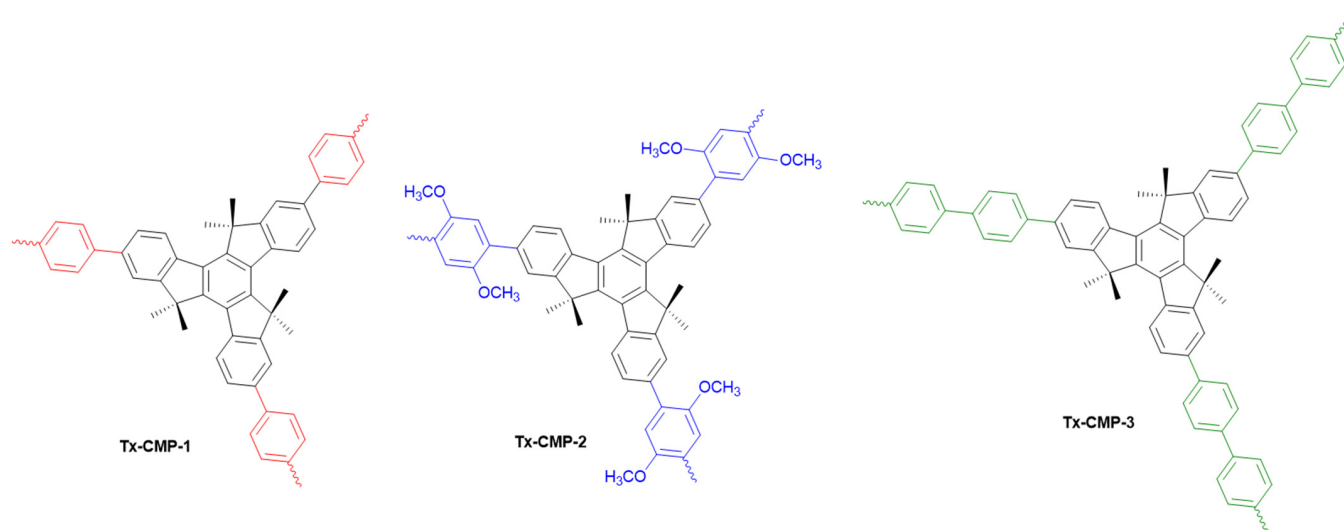


Figure 11. Structures of **Tx-CMPs**.

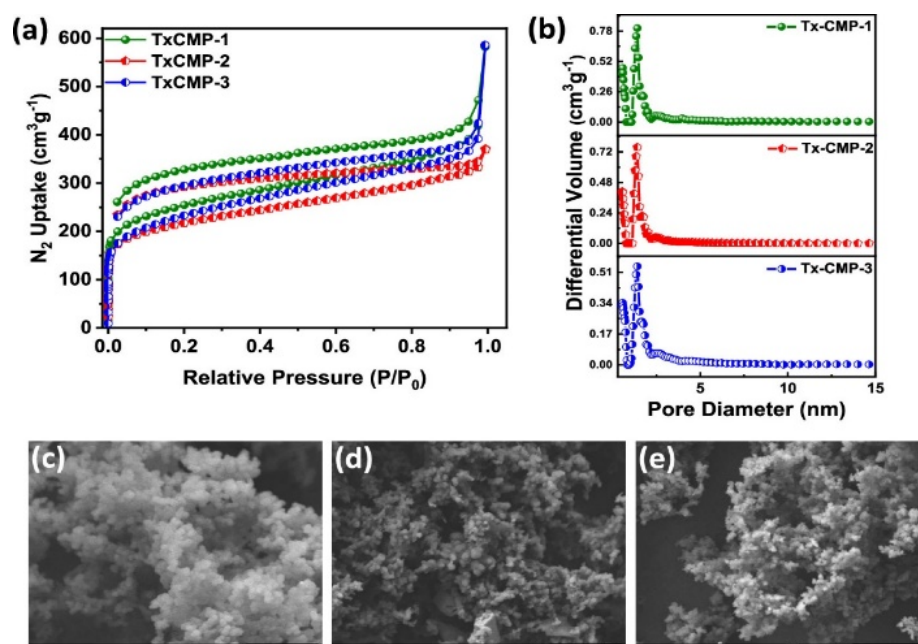


Figure 12. (a) Nitrogen adsorption and desorption isotherms of Tx-CMPs. (b) Pore-size distribution curves of Tx-CMPs. (c–e) FE-SEM images of Tx-CMP-1, Tx-CMP-2, and Tx-CMP-3, respectively. Reproduced with permission from reference [29]. Copyright © ACS Publications 2022.

Among various nitroaromatic explosives, Tx-CMPs demonstrated a selective luminescence turn-off sensing response to PA with K_{SV} values in the range of $2.39\text{--}7.35 \times 10^4 M^{-1}$. For comparison, K_{SV} values for other nitroaromatics (2,4-DNP, 4-NP, 3-NP, 1,3-DNB, and 2,4-DNT) were in the range of $0.48\text{--}4.15 \times 10^3 M^{-1}$, which is more than 10 times less, accompanied by a significantly lower quenching efficiency (Figure 13). The LODs for Tx-CMP-1, Tx-CMP-2, and Tx-CMP-3 were calculated at 1.86, 4.05, and 2.11 nM, respectively. According to time-resolved fluorescence quenching experiments, negligible changes in the average lifetime values were observed ($\tau_{av} = 0.39$ ns for Tx-CMP-1), suggesting a static quenching process in this case. Based on the HOMO–LUMO distribution for Tx-CMPs and PA, the authors declared that the quenching process occurred by the PET mechanism, with the largest difference between the LUMO of the sensor and the LUMO of the analyte calculated for Tx-CMP-2, exhibiting the most efficient quenching of luminescence.

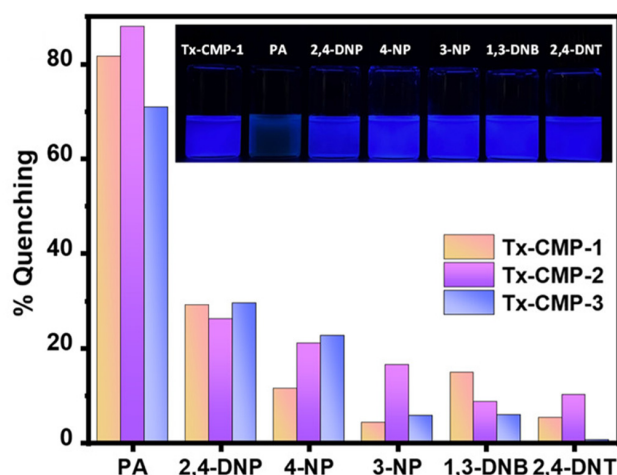


Figure 13. Graphical representation of fluorescence-quenching efficiency of different nitroaromatic compounds ($100 \mu M$) toward Tx-CMP-1, Tx-CMP-2, and Tx-CMP-3 in THF. Reproduced with permission from reference [29]. Copyright © ACS Publications 2022.

Mothika et al. reported the electrochemical generation of three **CMP** thin films (**PTPETCz**, **PFLCz**, and **PTPEFLCz**) with high porosity and their fluorescence response to TNT vapor [30]. These three polymers exhibited different luminescence behaviors arising from the structures of the original monomers. Only the **PTPETCz** and **PTPEFLCz** polymers, which include an aggregation-induced emissive TPE core, demonstrated a sensing response to TNT vapor, with LODs of 10 ppb (Figure 14a) and 0.2 ppm (Figure 14d), respectively. **PFLCz** turned out to be irresponsive even under a higher TNT vapor pressure (0.2 ppm). The authors ascribed this contrasting behavior to the increased electron-accepting character of **PFLCz** due to its fluorenone units. In addition, **PTPETCz** appeared to be remarkably selective toward TNT compared to other analytes because of either a lower LUMO to initiate the PET process or the insufficient volatility of the nitroaromatic molecules (Figure 14b). Meanwhile, such low LOD values for TNT originated from the high microporosity of **CMP** films. S_{BET} values were calculated at 930 and 509 m^2/g , with average pore diameters of 1.71 and 1.72 nm and total pore volumes of 0.40 and 0.22 $\text{cm}^3 \text{g}^{-1}$ for **PTPETCz** and **PTPEFLCz**, respectively, resulting in the better diffusion of TNT into the **CMP** matrix. The S_{BET} values of the thin films were lower than those of the corresponding bulk **CMP** powders synthesized via FeCl_3 -assisted chemical oxidation from the corresponding monomers due to the impact of the selected preparation method. However, thin films are more applicable to device and chip fabrication and demonstrate higher sensitivity to TNT vapor (Figure 15b). In this case, the authors estimated the role of film thickness and reported more efficient quenching at a lower thickness (15 nm over 61 nm).

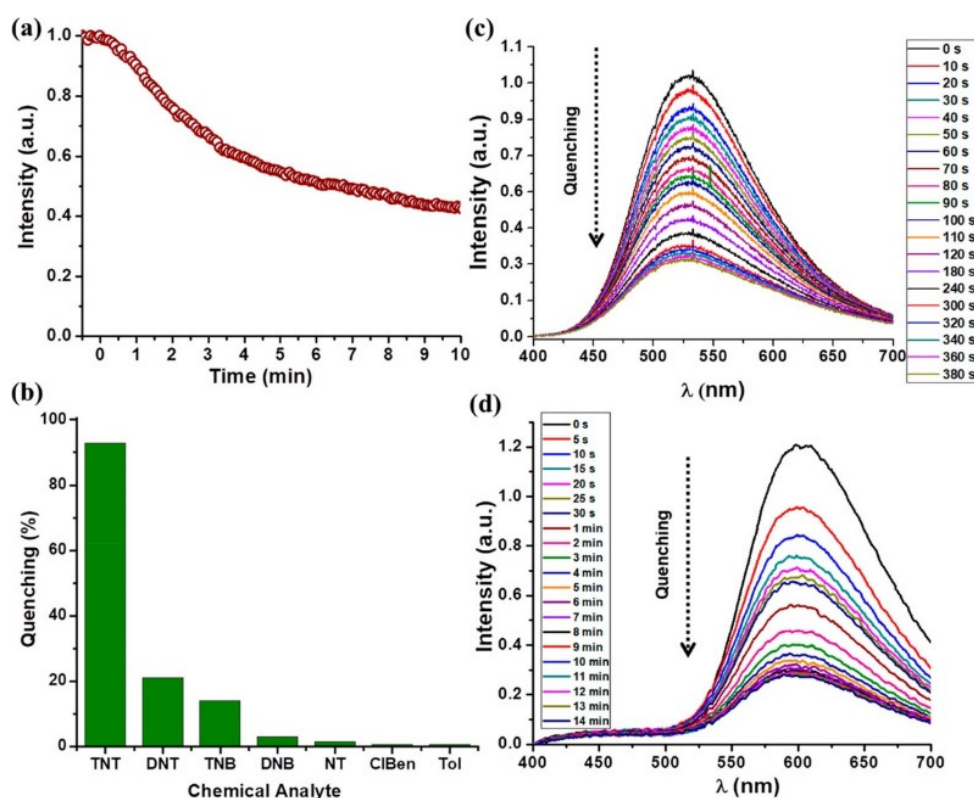


Figure 14. (a) Graphical representation of fluorescence quenching of **PTPETCz** film in presence of TNT vapor (10 ppb); (b) emission quenching of **PTPETCz** films after exposure to various analyte vapors: TNT (33 ppb, 3 min), TNB (10 ppb), 1,3-DNB (47 ppb), 2,4-DNT (saturated vapor), NT, chlorobenzene (ClBen), and toluene, exposure time 5 min. (c) Fluorescence intensity change with time in presence of TNT vapor (33 ppb) for **PTPETCz** films of ca. 61 nm thickness and (d) fluorescence intensity change with time in presence of TNT vapor (0.2 ppm) for **PTPEFLCz** films. Reproduced with permission from reference [30]. Copyright © ACS Publications 2018.

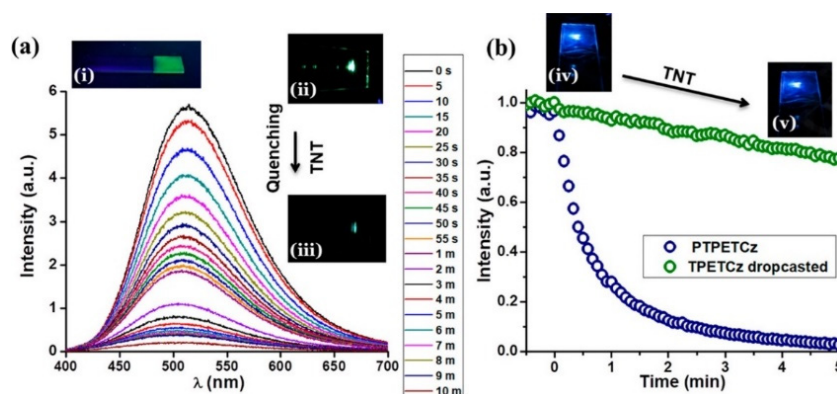
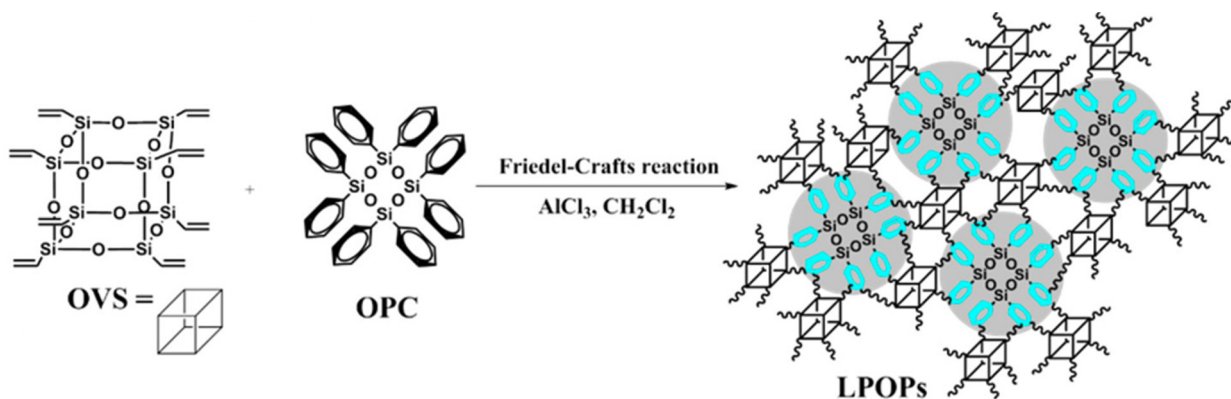


Figure 15. (a) PTPETCz emission decreasing during exposure to TNT vapor (33 ppb) over time. Inset: Illuminated PTPETCz thin films on ITO (i) under UV lamp and (ii), (iii) before and after exposure to TNT under a laser source, respectively. (b) Fluorescence quenching of PTPETCz films (blue) with time in presence of TNT vapor (33 ppb) compared to the fluorescence quenching of a drop-casted monomer film (TPETCz) when exposed to TNT vapor (0.2 ppm). (Inset) Illuminated TPETCz film (iv) before and (v) after TNT exposure. Reproduced with permission from reference [30]. Copyright © ACS Publications 2018.

Gou and colleagues presented siloxane-based nanoporous polymers, **LPOPs**, with a narrow pore-size distribution prepared by the Friedel–Crafts reaction of octaphenylcyclotetrasiloxane with octavinylsilsesquioxanes with different ratios (Scheme 1) [31]. **LPOPs** exhibited a narrow pore-size distribution, a monomodal micropore structure, excellent fluorescence properties, a high surface area, high thermodynamic stability, and sensing properties. According to the nitrogen adsorption–desorption isotherm and pore-size distribution (Figure 16), **LPOP-2** (the ratio of the starting reactants is 1:0.2) demonstrated a higher porosity degree with an S_{BET} of $967 \text{ m}^2\text{g}^{-1}$ and a corresponding micropore volume ratio ($V_{\text{micro}}/V_{\text{total}}$) of 0.94, with the monomodal nanopores centered at approximately 0.59 nm, as well as the most intense luminescence both in the solid state and in suspension at approximately 450 nm. Moreover, this intense luminescence of **LPOP-2** could be efficiently quenched by NACs, with K_{SV} constants of 2.32×10^4 , 1.63×10^4 , and $2.42 \times 10^4 \text{ M}^{-1}$ for NT, DNT, and TNT, respectively. The authors revealed the synergetic effect of dynamic adsorption, electron transfer, and electrostatic interaction between the nanoporous materials and analytes. In addition, Gou and colleagues demonstrated the quenching of the luminescence of **LPOPs** by using paper strips.



Scheme 1. Schematic representation of the synthesis of polymers (**LPOPs**). Reproduced with permission from reference [31]. Copyright © ACS Publications 2018.

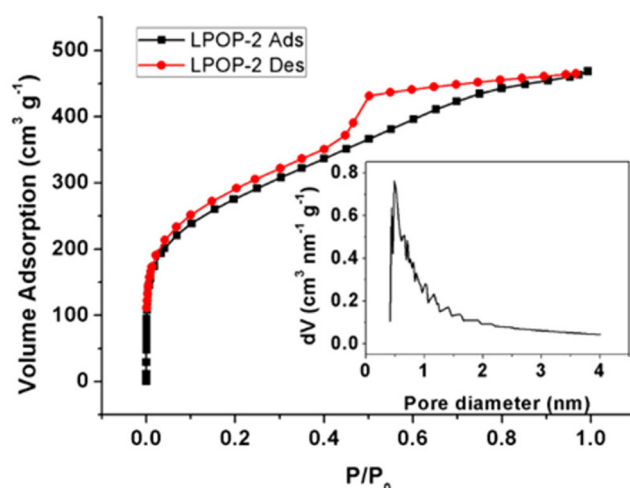
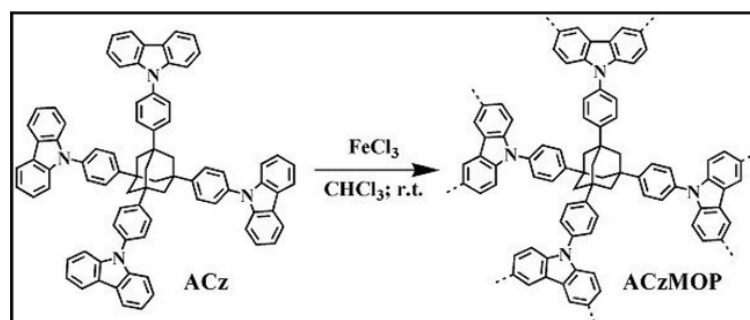


Figure 16. Nitrogen adsorption–desorption isotherm and pore-size distribution curve (inset) of LPOP-2. Reproduced with permission from reference [31]. Copyright © ACS Publications 2018.

Manna and co-authors developed the adamantane- and polycarbazole-based CMP **ACzMOP** for the detection of NACs in aqueous and gaseous phases (Scheme 2) [32]. **ACzMOP** demonstrated fluorescence sensitivity to NT, NB, TNP, DNP, NP, and NA analytes with high K_{SV} values, especially toward DNT, with a K_{SV} of approximately $1.6 \times 10^6 \text{ M}^{-1}$ and a quenching efficiency of 70% (Figure 17). Moreover, these K_{SV} constants were obtained in aqueous media; K_{SV} for DNT was calculated in both normal and seawater media and indicated no influence of the type of aqueous medium (Figure 17b). The LOD was found to be 0.32 ppb for DNT, which is well below the maximum permissible limit of 2 ppb in drinking water. In addition, the authors characterized the quenching mechanism as highly dynamic in nature because of the reduction in the fluorescence lifetime upon the addition of different concentrations of DNT. With high values of S_{BET} of $1568 \text{ m}^2 \text{ g}^{-1}$, total pore volume of $1.58 \text{ cm}^3 \text{ g}^{-1}$, and pore diameter around 1.17 nm (for the major fraction), **ACzMOP** exhibited high sensitivity to vapors of NACs such as DNT, NT, and NB, with quenching efficiencies of 95%, 99%, and 99%, respectively, after a 20 s exposure time (Figure 18). As can be seen, despite differences in vapor pressure, DNT, NT, and NB demonstrated comparable quenching efficiencies for **ACzMOP**, which led the authors to speculate about the negligible role of vapor pressure, making it possible to detect TNT vapor. The structural similarity between DNT and TNT should facilitate this as well. In addition, the process of reversible “ON-OFF” switching was also demonstrated for an **ACzMOP** thin film. After 30 min in a laboratory vacuum oven at $50 \text{ }^\circ\text{C}$, the same fluorescence intensity was restored, allowing this process to repeat for many cycles. Moreover, the possibility of detecting NACs by using paper strips with **ACzMOP** was shown. In addition, the authors successfully applied **ACzMOP** for the aqueous phase separation of nitroaromatics with high efficiency due to its very high porosity.



Scheme 2. Synthetic approach for **ACzMOP**.

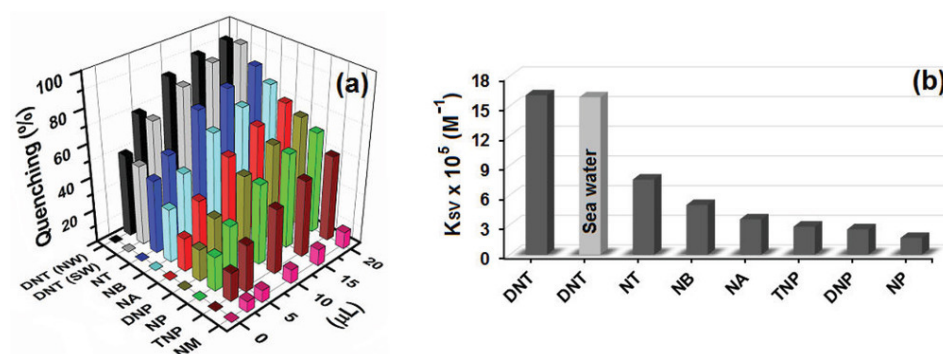


Figure 17. (a) Fluorescence quenching (%) results for different analytes. (b) Nitroaromatics' Stern–Volmer quenching constant (NW = normal water; SW = sea water). Reproduced with permission from reference [32]. Copyright © Wiley 2021.

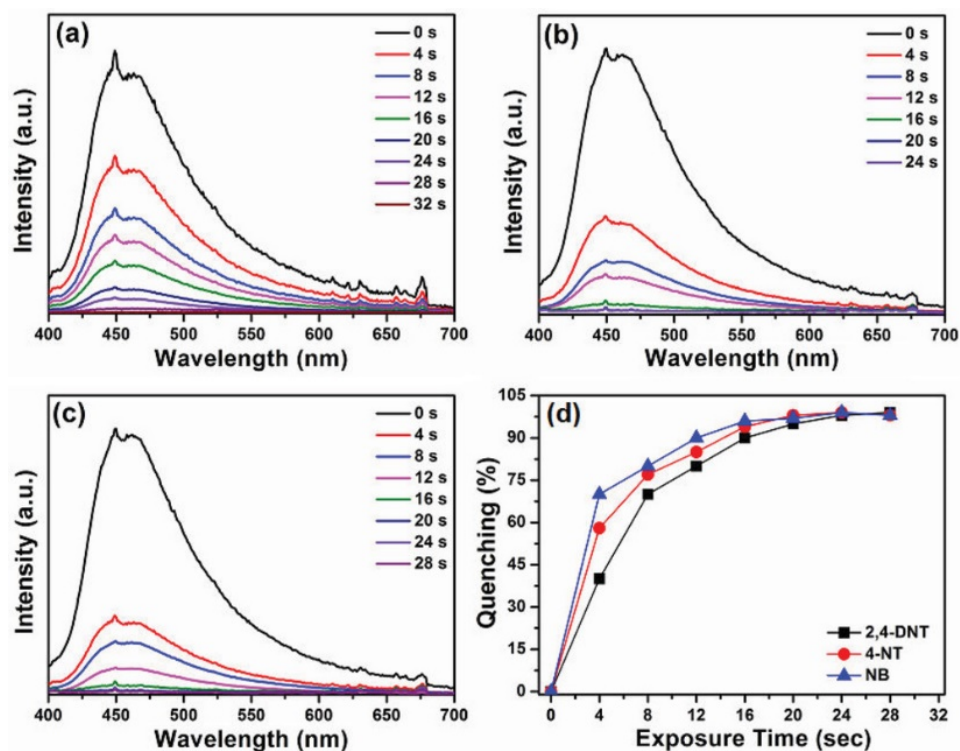


Figure 18. Studies of fluorescence quenching of ACzMOP thin layer (time-dependent) when exposed to saturated vapor of (a) DNT, (b) NT, and (c) NB and (d) fluorescence quenching (%) comparison by corresponding analytes. Reproduced with permission from reference [32]. Copyright © Wiley 2021.

2.3. Branched Polymers

Hyperbranched polymers are composed of three parts: dendritic links, linear links, and end links. Dendritic units and linear units are randomly distributed over the macromolecular backbone, which leads to randomly branched structures and the polydispersity of the molecular weight. At the same time, hyperbranched polymers have a large number of modifiable end groups, which can conveniently be further adjusted for the fluorescent and sensory properties of the polymers through the functionalization of the end groups. However, in this case, the polymer performance depends strongly on the nature and number of end groups, as they are not part of the polymer system.

Gupta and Lee [33] reported recyclable polymeric thin films based on a pyrene-derived polymeric probe, P6 (Figure 19a), for the selective detection and separation of PA with $K_{SV} = 7.75 \times 10^4 \text{ M}^{-1}$ in aqueous media (Figure 19b,c). At lower pH, trialkylamine groups

could be protonated, turning off the PET process and amplifying the luminescence intensity (Figure 20). This provides a favorable way to sense PA via quenching of this amplified luminescence. Because of the nonlinear nature of the K_{SV} plot, the lower-lying LUMO energy level of PA compared to **P6**, and the overlap between the fluorescence spectra of **P6** and the absorption spectra of PA, the authors declared a combination of PET and FRET mechanisms. The LOD for PA was determined to be 56 μM . Based on the **P6** polymer, the corresponding **P2** film was fabricated with higher sensitivity to PA. The authors reported that only 11.4 attograms (10^{-14} M) was required to initiate fluorescence quenching by PA. They also attributed this amplified fluorescence quenching of the **P6** film to the π - π stacking of the pyrene units, which enabled an exciton-hopping process via intermolecular electronic coupling, facilitating long-range exciton diffusion in the well-assembled solid state. The authors demonstrated the possibility of applying the **P6** film to separate PA from a mixture of different nitroaromatics in a MeCN solution.

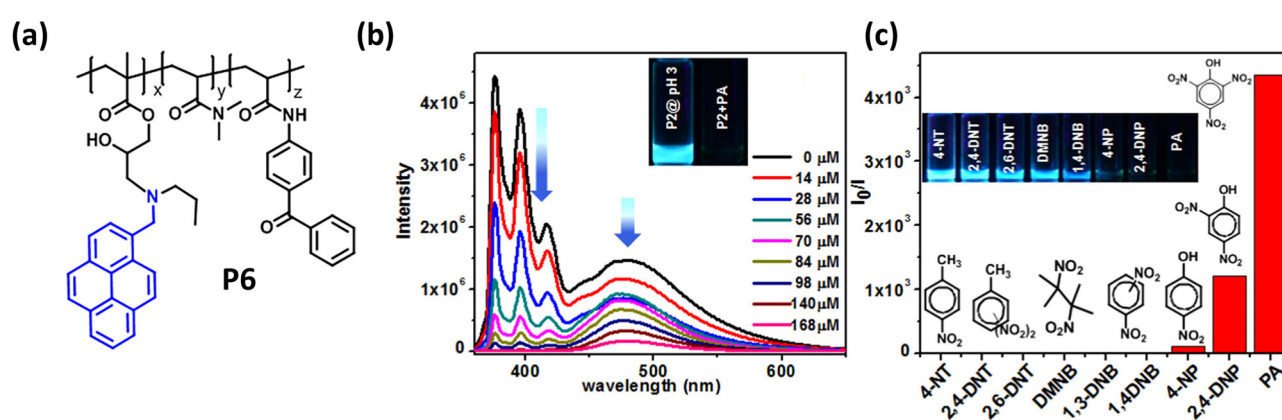


Figure 19. (a) Structure of **P6**. (b) Changes in emission spectra of **P6** (2.1×10^{-7} M pyrene units) on addition of PA (0–0.168 mM) at pH 3 in aqueous media and (c) **P6** selectivity in water with other structurally similar analytes. Reproduced with permission from reference [33]. Copyright © ACS Publications 2018.

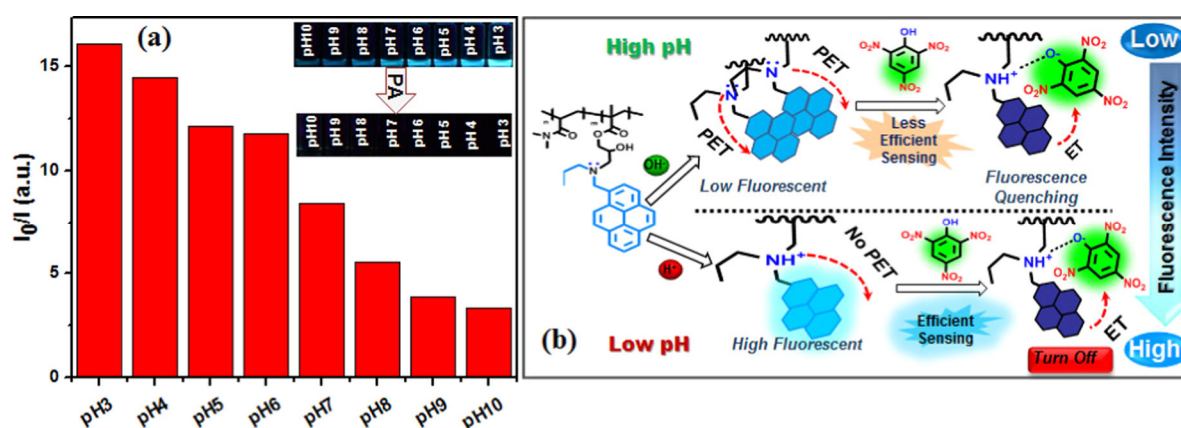


Figure 20. (a) Emission quenching extent upon PA (0.168 mM) addition at various pH; inset: **P6** (2.1×10^{-7} M pyrene units) before and after the addition of PA. (b) Mechanistic pathway of pH-tunable detection sensitivity of **P6** upon PA addition in H_2O . Reproduced with permission from reference [33]. Copyright © ACS Publications 2018.

Kumar et al. reported the synthesis and multimodal sensing applications of an emissive alanine-based dansyl-tagged copolymer P(MMA-*co*-Dansyl-Ala-HEMA) (**DCP**) (Figure 21) synthesized by RAFT copolymerization [34]. This polymer demonstrated high sensitivity and selectivity toward PA, as well as toward other NAC explosives, such as

DNT and TNT, with lower quenching efficiency in THF solutions (Figure 22a,b). The DCP polymer demonstrated K_{SV} values of $1.1 \times 10^3 \text{ M}^{-1}$ and $1.3 \times 10^3 \text{ M}^{-1}$ for DNT and TNT and a large value of $1.6 \times 10^4 \text{ M}^{-1}$ for PA. The authors characterized the mechanism of quenching as a combination of static and dynamic processes based on fluorescence up-conversion and time-resolved fluorescence data. In addition, the vapor sensing of NACs by a 20 nm thin film of DCP was demonstrated, with quenching efficiencies in the order $\text{DNT} > \text{TNT} > \text{PA}$ associated with the higher vapor pressure of DNT over TNT and PA.

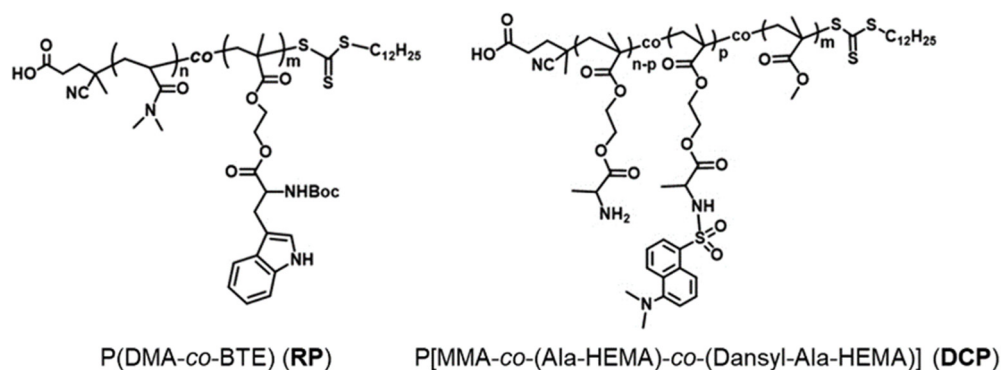


Figure 21. Chemical structures of copolymers RP and DCP.

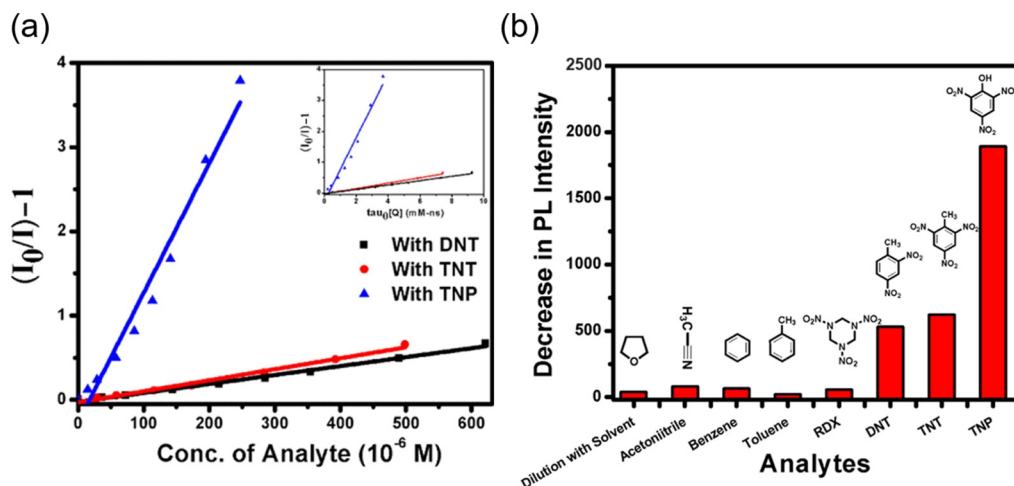


Figure 22. (a) Stern–Volmer plots for PA, DNT, and TNT. (b) Histogram for DCP selectivity test. Reproduced with permission from reference [34]. Copyright © Springer Nature 2019.

In addition, they demonstrated the possibility of detecting NACs with a polymer–small-molecule donor–acceptor FRET pair, using the tryptophan copolymer poly[(*N,N*-dimethylacrylamide)-co-(Boc-tryptophan methacryloyloxyethyl ester)] (also known as (P-[DMA-co-(Boc-Trp-EMA)])) (RP) (Figure 21) as the donor and carbazole (CZ) as the acceptor. This RP:CZ system demonstrated high sensitivity to NACs, with $K_{SV} = 2.9 \times 10^4 \text{ M}^{-1}$, $5.3 \times 10^3 \text{ M}^{-1}$, and $5.7 \times 10^3 \text{ M}^{-1}$, as well as LOD values of 1.4 μM , 6.4 μM , and 5.9 μM for PA, DNT, and TNT, respectively. This unique and high-sensitive detection works based on the FRET process, where the FRET mixture is excited at the donor's (RP) characteristic wavelength (291 nm). This excitation energy of the donor is resonantly transferred to the acceptor because of the great overlap between the fluorescence of RP and the excitation of CZ (Figure 23a), followed by a dramatic increase in the PL emission of CZ at 325–425 nm (Figure 23b). This emission is further weakened with the increase in the DNT, TNT, and TNP concentrations (Figure 23c for PA). A time-resolved spectroscopic study confirmed the occurrence of the FRET process with a considerably good energy transfer efficiency $\phi_E = 35\%$ and a decrease in the average lifetime of PA from 1.6 to 1.0 ns. The authors also

calculated the Förster critical distance R_0 and the distance between donor and acceptor molecules r at 25.51 Å and 28.28 Å, respectively, which are in the range of 10–100 Å and applicable to the FRET process.

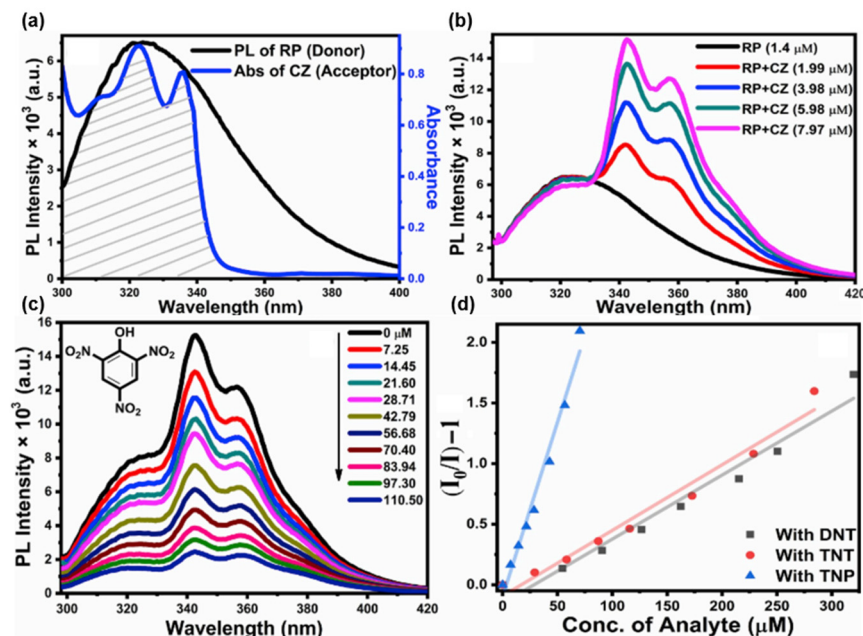


Figure 23. (a) Fluorescence of RP and absorption of CZ (spectral overlap); (b) FRET signal for donor–acceptor pair at the excitation wavelength of donor (291 nm); (b,c) fluorescence quenching of FRET pair with addition of PA. (d) Stern–Volmer plots for PA, DNT, and TNT. Reproduced with permission from reference [34]. Copyright © Springer Nature 2019.

Moreover, in their subsequent research [35], the authors reported the polymer–polymer donor–acceptor FRET pair RP:DCP, with the copolymer RP as the donor and the copolymer DCP as the acceptor (Figure 21). The sensitivity of this copolymer toward NACs is based on the same FRET pair principle as RP:CZ, with the dominance of the PET quenching mechanism (Figure 24a). Kumar and colleagues demonstrated that changing the excitation source for DCP from an outer source to the FRET approach is favorable for NAC detection. The K_{SV} values appeared to be comparable to those of the RP:CZ FRET pair and were $2.2 \times 10^4 \text{ M}^{-1}$, $6.3 \times 10^3 \text{ M}^{-1}$, and $7.6 \times 10^3 \text{ M}^{-1}$ with LODs of 0.4 μM (0.1 ppm), 5.4 μM (0.98 ppm), and 2.3 μM (0.53 ppm) for PA, DNT, and TNT, respectively. However, this system demonstrated values approximately 6 orders of magnitude higher than the reported K_{SV} values for the DCP polymer, indicating the key role of the FRET pair in the quenching of NACs. In addition, the authors provide deep insight from optical, time-resolved spectroscopic, and ultrafast transient absorption studies to establish the mechanistic aspects of the interactions between RP:DCP and NACs. They demonstrated the selectivity of the RP:DCP pair toward PA, DNT, and TNT over other analytes (Figure 24b).

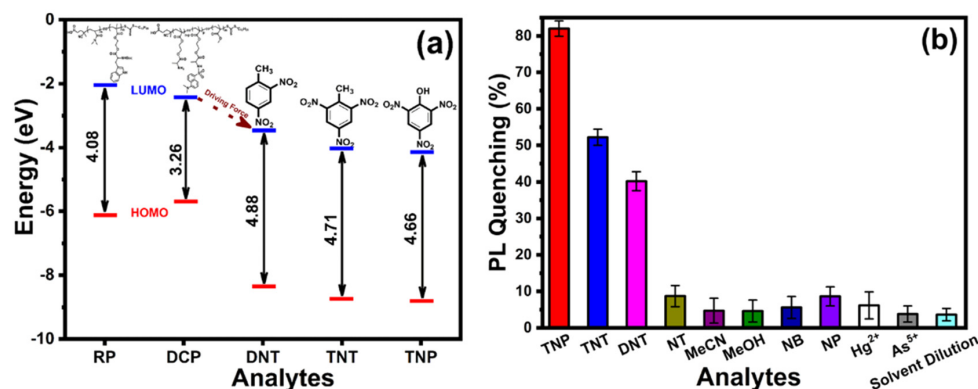


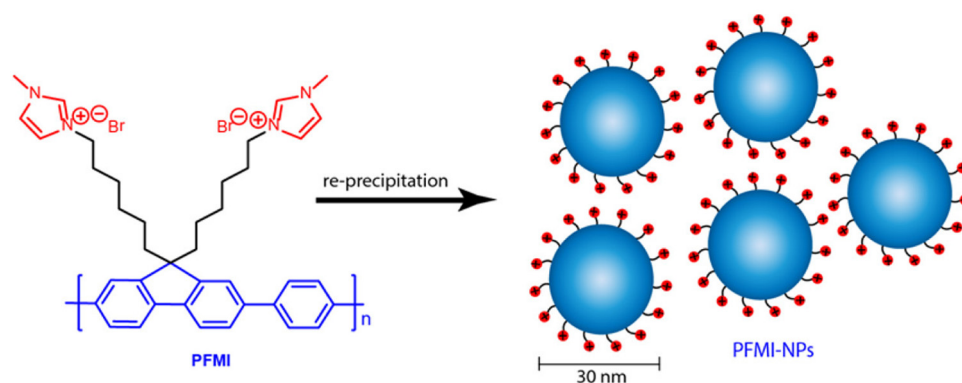
Figure 24. (a) Energy levels for RP, DCP, and the analytes and (b) quenching efficiency by different NACs and other analytes. Reproduced with permission from reference [35]. Copyright © ACS Publications 2021.

3. Modern Accents/Trends in the Development/Research of Polymers/Polymer-Based Materials for the Detection of NACs

3.1. Polymer Nanoparticles for Detection in Aqueous Media

One of the main disadvantages of polymer-based materials is their flat surface, which prevents the deep penetration of NACs into the polymer body, especially on hard surfaces. When π -conjugated polymers are converted into nanostructures, the properties of the polymer are enhanced by additional nanoscale characteristics, including the ability to functionalize the inside or outside of nanostructures and increase solubility in various solvents, including water [36]. Conjugated nanostructured polymers have high quantum yields, molar extinction coefficients, brightness, and photostability. Due to these properties, polymer-based nanoparticles (PNs) have found wide applications in optoelectronics and biomedicine [37]. Small PNs with high specific surface areas for maximum sensitivity are considered promising probes for detecting nitro-containing analytes.

Malik et al. fabricated a fast and sensitive platform based on conjugated polymer nanoparticles (PFMI-NPs) with an average particle size of 30 nm for the selective detection of PA (Scheme 3) [38]. With the pendant cationic imidazolium groups attached to the side chains of the PFMI polymer, it became water-soluble and obtained a specific recognition site for PA in polar solvents. This led PFMI-NPs to demonstrate higher sensitivity for PA over other NACs, with $K_{SV} = 1.12 \times 10^8 \text{ M}^{-1}$ (Figure 25a,b) and a LOD of 30.99 pM/7.07 ppt in water. The exceptional selectivity and sensitivity toward PA remained unchanged in the presence of a variety of cations and anions yet were reduced by 50% in a 1 M NaCl aqueous solution, demonstrating sensitivity to PA at relatively high electrolyte concentrations in aqueous media. Because of the nonlinear Stern–Volmer plot at higher concentrations of PA (Figure 25c), the authors described the quenching mechanism as a combination of the “molecular-wire effect”, electrostatic interactions, and PET and possibly RET mechanisms. Moreover, the authors fabricated a two-terminal sensor device for PA vapor detection (Figure 25d) with high sensitivity and selectivity, a high signal response (6 s), and fast recovery.



Scheme 3. Preparation of PFMI-NPs.

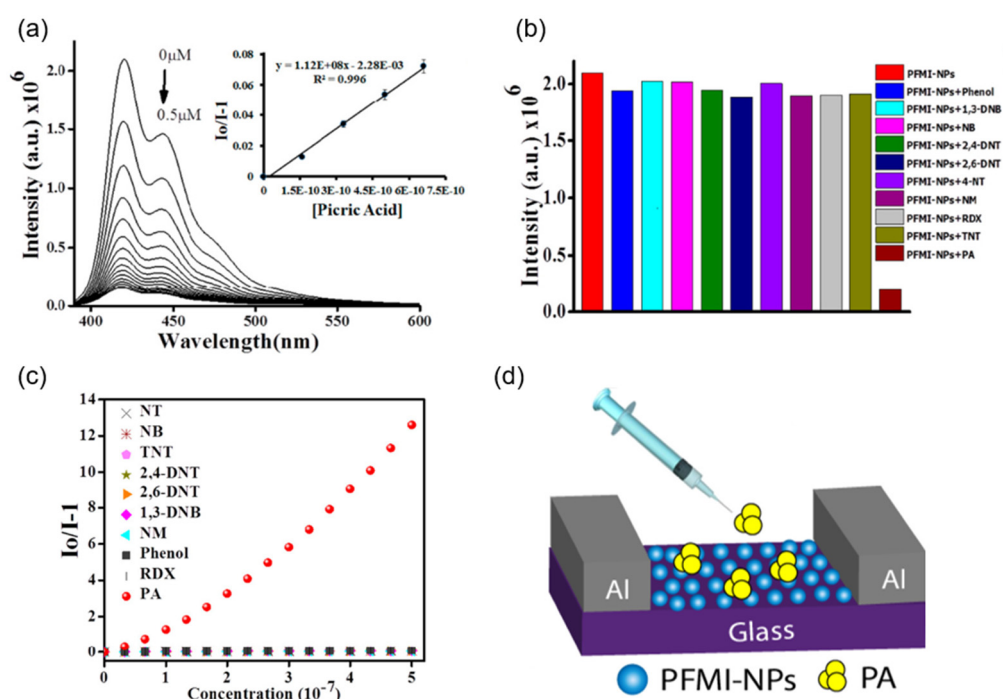


Figure 25. (a) Emission spectra of PFMI-NPs with variable concentrations of PA in aqueous media. Inset: Stern–Volmer plot at lower PA concentrations. (b) Effect of different nitro-explosives (5×10^{-7} M) on the emission of PFMI-NPs. (c) Stern–Volmer plots for various nitro-explosives. (d) Two-terminal sensor device (schematic representation). Reproduced with permission from reference [38]. Copyright © ACS Publications 2015.

Ouyang and co-authors reported *l*-PANtPE and PANtPE polymer nanoparticles based on anthracene and tetraphenylethene units (Figure 26) for the detection of nitroaromatics in aqueous media [39]. Despite the difference in molecular structure, both *l*-PANtPE and PANtPE polymers demonstrated similar fluorescence emission with maxima at 455 and 448 nm, respectively. However, PANtPE exhibited higher efficacy for the quenching of PA in water, with a K_{SV} of 4.0×10^4 M $^{-1}$, compared to *l*-PANtPE, with a K_{SV} of 1.4×10^4 M $^{-1}$ (Figure 27), as well as higher sensitivity, with a LOD of 439 nM compared to 663 nM. The better sensing activity of PANtPE is due to its surface parameters. Both particles possessed an average size of 73 nm and spherical morphology. However, porosity with a pore size centered at ca. 3.5 nm and an S_{BET} of 49 m 2 /g for PANtPE was observed, thus facilitating contact and the adsorption/diffusion of the analyte in the polymer. *l*-PANtPE possessed no porosity due to its linear molecular structure. K_{SV} values for other NACs were much lower, while the presence of different cations and anions had an insignificant

effect, indicating high selectivity toward PA (Figure 28). The authors revealed a static mechanism of quenching based on time-resolved fluorescence decay data, a prerequisite for the PET mechanism due to higher LUMO values of *l*-PAnTPE and PAnTPE (−2.68 and −2.53 eV, respectively, vs. −3.90 eV for PA), as well as for the FRET mechanism due to the overlaps between the absorption spectra of PA and the fluorescence spectra of *l*-PAnTPE and PAnTPE. The authors also note the possibility of the appearance of an inner-filter effect because of overlaps between the excitation spectra of PA and the fluorescence spectra of *l*-PAnTPE and PAnTPE.

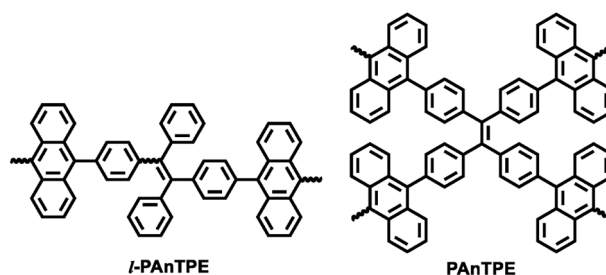


Figure 26. Structures of *l*-PAnTPE and PAnTPE nanoparticles.

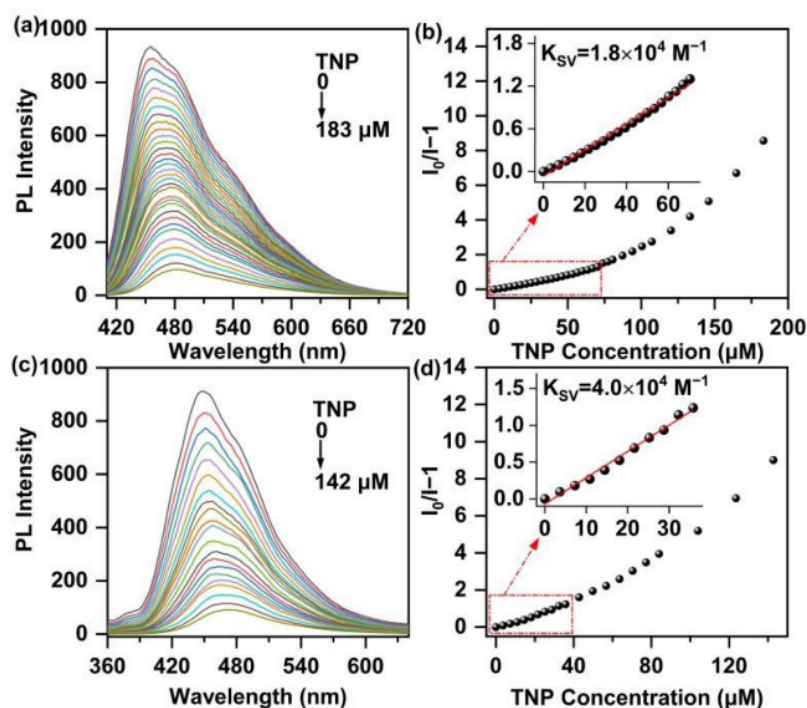


Figure 27. (a) Emission spectra of *l*-PAnTPE; (b) S–V plots of PL intensity ($I_0/I - 1$) vs. TNP concentration of *l*-PAnTPE; (c) emission spectra of PAnTPE; (d) S–V plots of PL intensity ($I_0/I - 1$) vs. TNP concentration of PAnTPE. Reproduced with permission from reference [39]. Copyright © MDPI 2022.

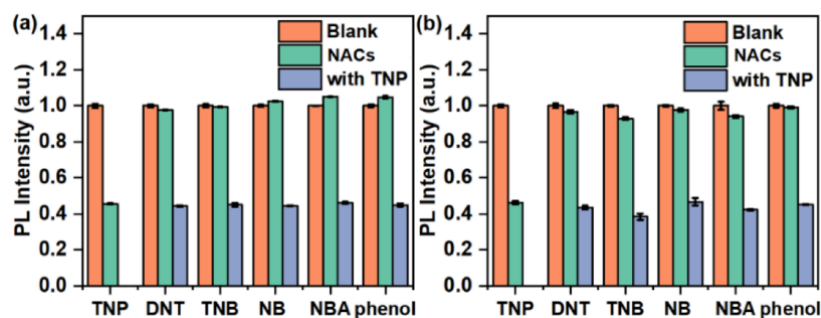


Figure 28. The quenching degree of *I*-PAnTPE (a) and PAnTPE (b). Reproduced with permission from reference [39]. Copyright © MDPI 2022.

Wang and colleagues reported aggregation-enhanced FRET-active conjugated polymer nanoparticles, **P7** (Figure 29a), with an average diameter of 117 nm (Figure 29b) and orangish-red fluorescence emission with a maximum at 572 nm in 1,4-dioxane-water media ($f_w = 92\%$) and applied them for PA sensing in an aqueous solution [40]. **P7** exhibited high sensitivity and selectivity toward PA (Figure 29c), with $K_{SV} = 3.4 \times 10^4 \text{ M}^{-1}$, a LOD of $0.51 \mu\text{M}$, and, according to the authors, a conjectural PET mechanism of quenching. Other NACs demonstrated much lower efficiency (Figure 29d). The presence of different cations and anions did not influence the quenching performance of **P7**.

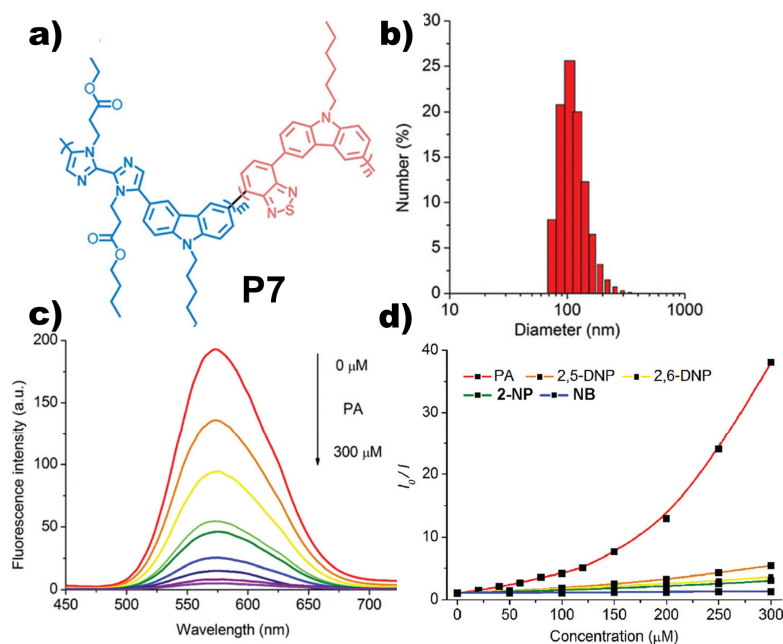
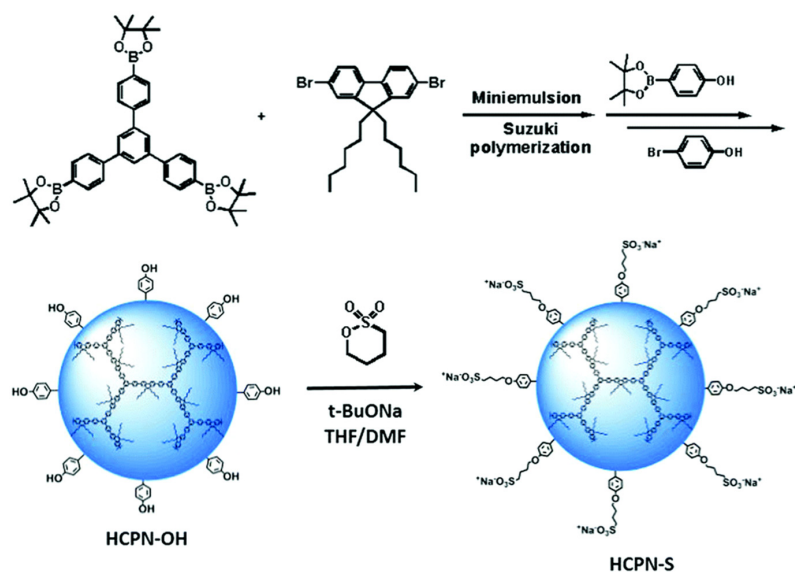


Figure 29. (a) 2,2'-Biimidazole-containing polymer **P7** ($m/n = 9/1$) (chemical structure); (b) data of dynamic light scattering (DLS) of the nanoparticles from **P7** in aqueous solution; (c) fluorescence spectra in presence of increasing concentrations of PA; (d) Stern–Volmer plots of **P1** for various nitroaromatics. Reproduced with permission from reference [40]. Copyright © Royal Society of Chemistry 2018.

Wu and co-authors presented water-dispersible hyperbranched conjugated polymer nanoparticles with sulfonate terminal groups (**HCPN-S**) for the amplified fluorescence sensing of TNT traces in an aqueous solution (Scheme 4) [41]. This polymer was prepared by Suzuki coupling polymerization in an oil-in-water miniemulsion followed by post-functionalization with the attachment of hydrophilic sulfonate terminal groups to the hydrophobic hyperbranched conjugated polymer core. The resulting NPs had an average diameter of around 25 nm and demonstrated a high fluorescent response to TNT in

aqueous media, with $K_{SV} = 1.21 \times 10^6 \text{ M}^{-1}$ and a LOD of 3.7 nM (0.8 ppb) (Figure 30a,b). **HCPN-OH**, which is the corresponding precursor of **HCPN-S** with OH groups, exhibited a significantly lower $K_{SV} = 2.21 \times 10^3 \text{ M}^{-1}$, determining the key role of sulfonated groups in the detection of TNT. In addition, the authors prepared linear conjugated polymer nanoparticles (**LCPNs**)—the linear analog of **HCPN-S**. These **LCPNs** demonstrated a much lower $K_{SV} = 2.12 \times 10^4 \text{ M}^{-1}$ and a LOD of 3.0 μM (Figure 30b), indicating the pivotal contribution of the nature of the hyperbranched core. The inner cavities of the core of **HCPN-S** resulted in an enhanced encapsulation ability, providing a large PET interface and a more efficient quenching performance (Figure 30c). The authors investigated the quenching performance of other NACs in water as well and observed high selectivity toward TNT (Figure 31a). Even PA, which is the most common NAC, exhibited a high K_{SV} value ($8.39 \times 10^4 \text{ M}^{-1}$), but it was more than 14-fold lower than that of TNT (Figure 31b).



Scheme 4. Synthetic approach for **HCPN-S**. Reproduced with permission from reference [41]. Copyright © Royal Society of Chemistry 2017.

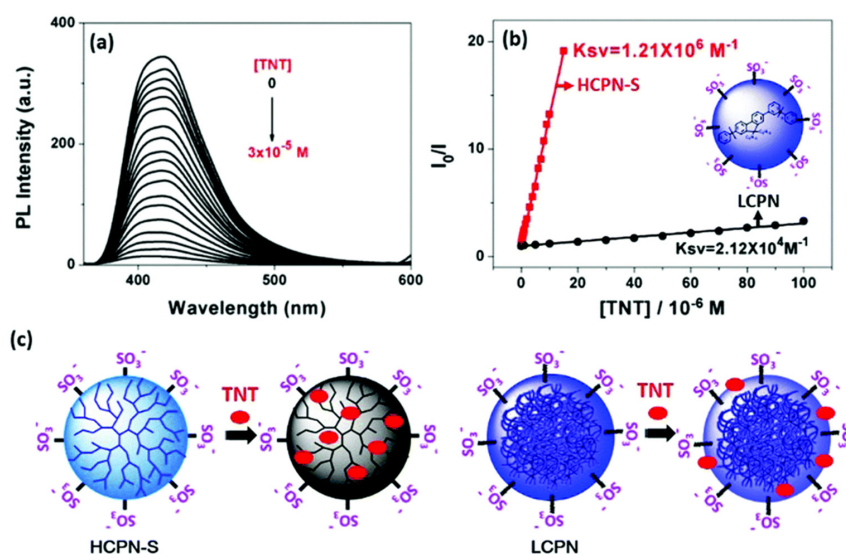


Figure 30. (a) Fluorescence response of **HCPN-S** dispersion during addition of TNT. (b) Stern–Volmer plots of **HCPN-S** at 419 nm and **LCPN** at 394 nm. (c) Proposed mechanistic pathway for different sensitivities between **HCPN-S** and **LCPN**. Reproduced with permission from reference [41]. Copyright © Royal Society of Chemistry 2017.

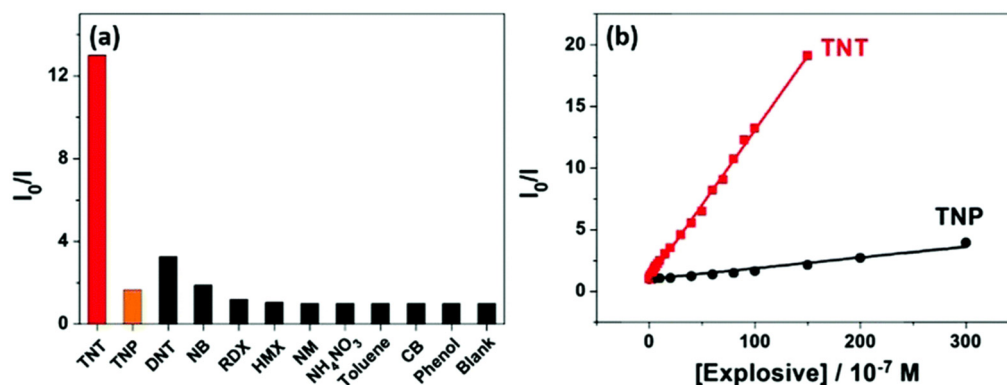


Figure 31. (a) Fluorescence response of HCPN-S upon addition of different analytes (concentrations: 10 μ M for TNT, TNP, DNT, and NB; 100 μ M for other analytes). (b) Stern–Volmer plots of HCPN-S at 419 nm. Reproduced with permission from reference [41]. Copyright © Royal Society of Chemistry 2017.

3.2. Aggregates of Polymeric Probes

At high concentrations of both small-molecule-based and polymeric fluorophores, in most cases, the fluorescence decreases dramatically due to such common phenomena as aggregation-induced quenching or aggregation quenching (AQ), which significantly hampers the application of most fluorescent materials for the fluorescence detection of NACs. In 2001, Tang et al. reported, for the first time, the emission of fluorophores, which did not appear in solution but appeared during aggregation, and this phenomenon was named “aggregation-induced emission” (AIE) (opposite of AQ) [42]. AIE-active polymer probes and materials have been successfully applied to detect explosives, and the number of published papers in this area has rapidly increased over the last 10 years [24,43]. The high fluorescence efficiency, synergistic effect, and large contact area in the aggregated state endow AIE polymers with a “super-amplification effect” and make them ideal candidates for constructing sensors with high sensitivity [44]. AIE sensors have been developed for ions, explosives, and biomolecules [45]. In the solid state, non-AIE-based sensors suffer from partial or complete emission quenching, which makes their practical application difficult [24,43]. The opposite of ACQ, the aggregation-induced emission (AIE) phenomenon, has arisen in the molecular engineering of luminescent materials and has generated curiosity among various scientific fields [46]. Luminogens with AIE characteristics (AIEgens) are used as an approach to overcome the problem connected with ACQ, the most popular of which is the tetraphenylethene (TPE) functional group.

This section provides a wide range of readers with updated information on current trends in the development and research of optical sensors based on polymer aggregates with a linear, branched, or porous structure for the detection of nitro-containing pollutants. This includes several reports comparing the sensitivity of ACQ, AIE, and AEE polymers as probes for detecting explosives under the same conditions, as well as sensors based on through-space conjugated polymers.

3.2.1. Linear Conjugated Polymers

To study the relationship between the quenching mechanism of polymer sensors and the sensitivity/selectivity of the detection of nitro-containing analytes, three linear polymers were synthesized with tetraphenylethane (TPE), fluorene, and thiophene moieties, namely, an aggregation-caused quenching (ACQ)-active polymer (PF), an aggregation-induced emission (AIE)-active polymer (PFTPE), and an aggregation-enhanced emission (AEE)-active polymer (PTTPE) (Figure 32) [47]. Then, polyurethane foams modified with three polymers, PU-PF, PU-PFTPE, and PU-PTTPE, were prepared as carriers using the ultrasonic processing method.

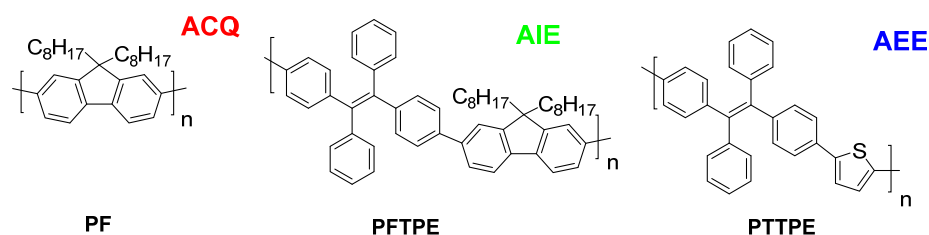


Figure 32. Structures of linear conjugated polymers **PF**, **PFTPE**, and **PTTPE**.

A comparative study of polymer sensors on polyurethane foam with a three-dimensional mesh structure for the detection of explosives was carried out. It was shown that significant quenching of fluorescence was observed with the introduction of TNP solutions. All **PU-PF**, **PU-PFTPE**, and **PU-PTTPE** sensors showed excellent sensitivity to TNP solutions at various concentrations. Typically, the ACQ phenomenon results in reduced emission in the aggregate or solid form of fluorescent samples, which reduces their potential for practical applications [48]. However, the ACQ **PU-PF** polymer was shown to provide better sensory performance than polymers with AIE or AEE characteristics. Thus, the highest TNP extinguishing efficiency for **PU-PF** was 96.2%, while it was 93.5% for **PU-PFTPE** and 86.7% for **PU-PTTPE**. The probable explanation for the efficiency lies in the modification of the fluorene domain and the choice of a suitable carrier.

Although fluorene-containing chemosensors have ACQ properties due to their planarity, the active methylene (C-9) position of the fluorene core results in easy functional modification, making it suitable for use in fluorescent materials and sensors for detecting analytes [49]. For example, three conjugated polymers based on C9-functionalized fluorene domains (**CP1**, **CP2**, and **CP3**) were found to be highly sensitive for the fluorescence detection and colorimetric detection of PA in an aquatic environment [26] (Figures 2–4).

A number of articles present typical linear AIE polymer sensors based on **TPE** luminogens for the selective detection of 2,4,6-trinitrotoluene in solution and the gas phase. For example, Xu et al. obtained and studied four linear polyacrylate polymers, **PAP1a–b** and **PAP2a–b**, containing two AIE luminogens as side units, namely, 3,6-bis(1,2,2-triphenylvinyl)carbazole (**BTPC**) and bis(4-(1,2,2-triphenylvinyl)phenyl)-amine (**BTPPA**), in high yields via a free radical polymerization reaction in the presence of an azobisisobutyronitrile catalyst. The polymer structures are shown in Figure 33 [50]. The spectrofluorometric analysis of polymer nanoaggregates in THF/water showed that **BTPPA**-based polymers gave a more sensitive fluorescent response to nitroaromatic compounds, including 2,4,6-trinitrotoluene, with a maximum K_{SV} value of 12870 M^{-1} for **PAP2b**, than **BTPC**-based polymers.

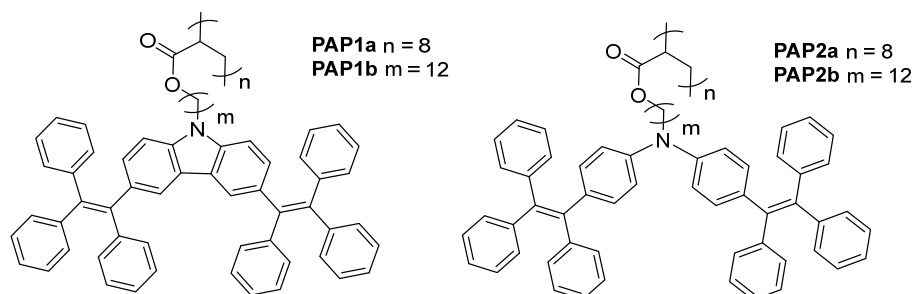


Figure 33. Structures of linear polymers **PAP1a–b** and **PAP2a–b**.

Tetraphenylethene-based arylenethynylene-type polymers (**TPEPs**) were synthesized through the Sonogashira coupling of diethynyl-**TPE** and three diiodobenzene struts carrying branched oligoethylene glycol, hexyl, or hexyloxy side chains (Figure 34). The presence of aggregates in a mixture of THF/water (5:95) was proved using a scanning electron micro-

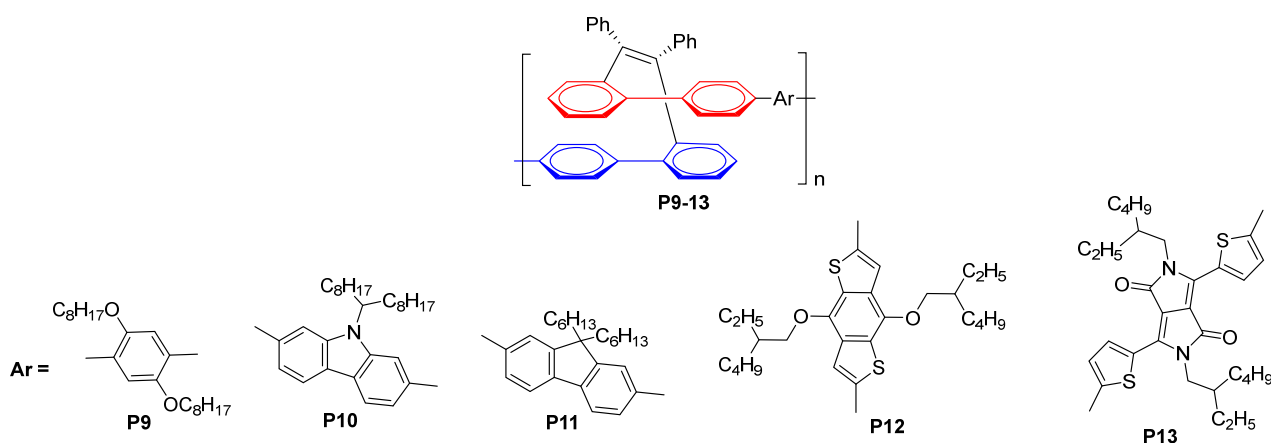


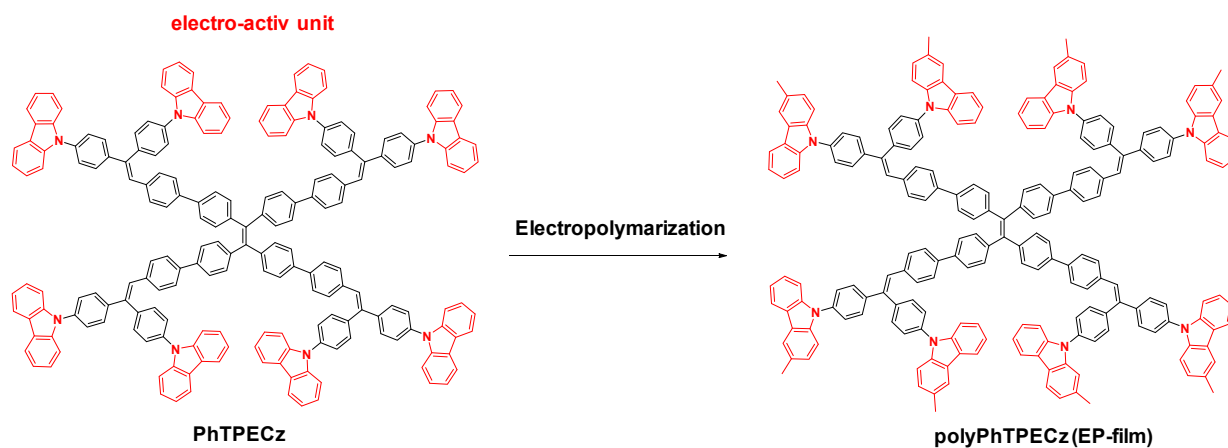
Figure 36. Structures of through-space conjugated polymers **P9–13**.

The effect of the super-amplification of emission by nanoaggregates of polymers in an aqueous medium upon the detection of TNP was proved by comparing the quenching constants in THF/water mixtures and THF. For example, the quenching constant of **P1** in the THF/water mixture ($f_w = 80$ vol%) was up to $552,000 \text{ M}^{-1}$, which is much higher than that in the THF solution ($78,200 \text{ M}^{-1}$).

3.2.2. AIE-Active Porous Conjugated Polymers

The integration of typical AIE luminogens into a porous organic network provides additional advantages for the detection of analytes of various natures, such as extended π -delocalization compared to a conjugated network of linear polymer sensors, which leads to efficient exciton migration. In addition, the porous structure of polymer sensors promotes the efficient diffusion of analytes, enabling specific molecular interactions within pores and allowing the design of sensors with highly sensitive and selective detection of analytes [55].

Special attention from scientists is drawn to porous polymer films used as sensors for volatile organic pollutant compounds, most often obtained in situ by electropolymerization (EP). For example, polymeric porous films (EP films) were obtained in situ by electropolymerization (EP) of a new luminescent AIE-active monomer, **PhTPECz**, consisting of terphenylethylene units as the central core and eight electroactive carbazole fragments (Scheme 5, Figure 37) [56]. Based on the results of transmission electron microscopy, it was shown that for two possible twist conformations, the micropores of the resulting films were ~ 1.2 and 2.9 nm. The sensing performance of these EP films was optimized by controlling the thin-film thickness by adjusting the electrochemical parameters.



Scheme 5. Schematic diagram of electropolymerization to form EP film (red carbazole connected to ext carbazole unit).

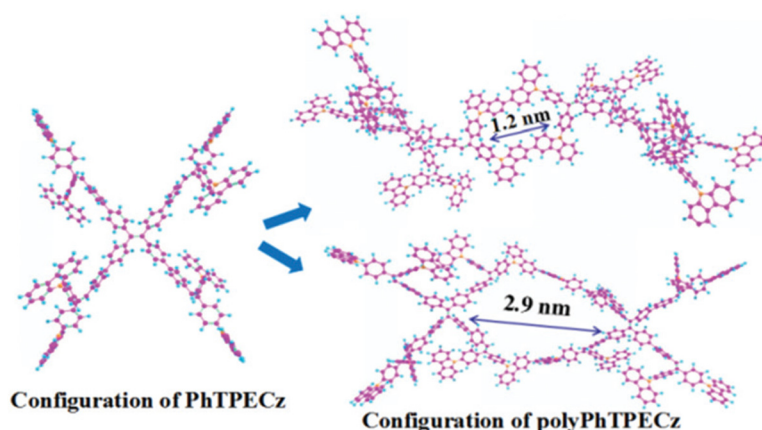


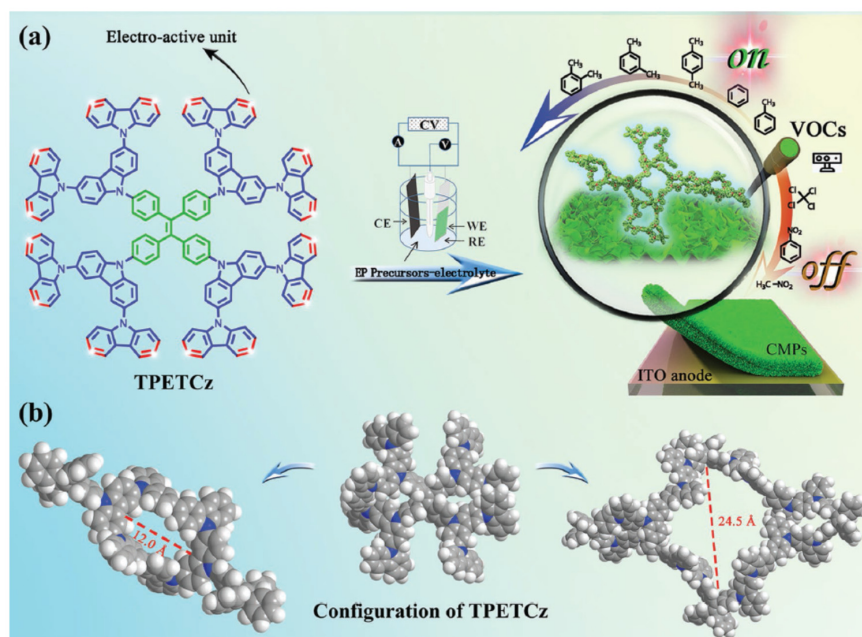
Figure 37. PhTPECz and polyPhTPECz (optimized structures) and diameter of pores in polyTPECz. Reproduced with permission from reference [56]. Copyright © Royal Society of Chemistry 2021.

Thus, due to the bright yellow-green fluorescence and crosslinked porous texture, the films showed excellent sensory properties with the possibility of their repeated use in the processing of various NACs, namely, TNP, DNP, NP, TNT, NT, and NB. Thus, due to the bright yellow-green fluorescence and porous texture, the films showed excellent sensory properties with the possibility of their repeated use in the processing of various NACs, namely, TNP, DNP, NP, TNT, NT, and NB. For sensing TNP, the LOD of the **polyPhTPECz** EP films was 3.8 nM, and the K_{SV} was calculated to be $1.63 \times 10^5 \text{ M}^{-1}$ in an aqueous solution. Additionally, 73% of the fluorescence emission of the film was quenched within 180 s when exposed to TNP vapor. The fluorescence-quenching mechanism for TNP was a combination of electron transfer and resonance energy transfer.

Similarly, a porous polymeric EP film with a high specific surface area for analyte diffusion and pore diameters of 1.2 and 2.45 nm in two possible configurations was constructed and studied based on a new dendrimer characterized by its central tetraphenylethylene “core” with an aggregation-induced emission effect and its highly electroactive “branches” (Scheme 6) [57]. Films have been shown to exhibit an on-off fluorescence response to 18 types of volatile organic compounds (VOCs). Significantly, a 2D sensing array was established through **CMP** films and their spin-coated monomer films, and 18 types of VOC vapors were precisely distinguished by linear discriminant analysis.

Currently, conjugated mesoporous polymers/oligomers with pore sizes of 2 to 50 nm are attracting increasing attention as sensors due to their high surface area and porosity, low density, high stability, tunable pores and skeletons, and ease of functionalization, which leads to increased quantum yields and energy transfer efficiency for the ultra-sensitive detection of explosives [58].

Thus, AIEE-active mesoporous conjugated oligomers **CMO1** and **CMO2** have been developed (Figure 38) [59]. The integration of typical AIE building blocks, such as tetraphenylethylene and triphenylamine (TPA), into **CMO** scaffolds endowed them with AIEE characteristics. Namely, **CMOs** emit weakly in solution, while enhanced and strong emission is observed in the solid state. A 90% aggregated solution formed in a THF/water mixture showed the highest quantum yield for the oligomers and was used to detect TNP (Figure 39). The best results were shown by the **CMO1** oligomer, with K_{SV} of $2.6 \times 10^6 \text{ M}^{-1}$ for TNP and $2.3 \times 10^3 \text{ M}^{-1}$ for TNT.



Scheme 6. (a) Formation of EP film through electropolymerization; (b) optimized structures of TPETCz and the diameters of their pores. Reproduced with permission from reference [57]. Copyright © Wiley 2020.

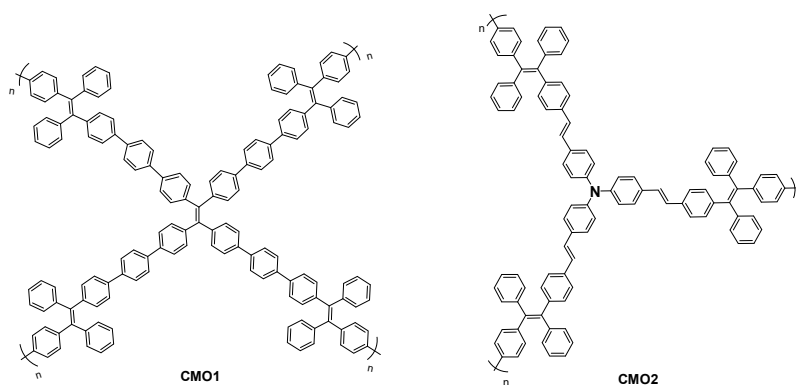


Figure 38. Structures of AIEE-active CMO1 and CMO2.

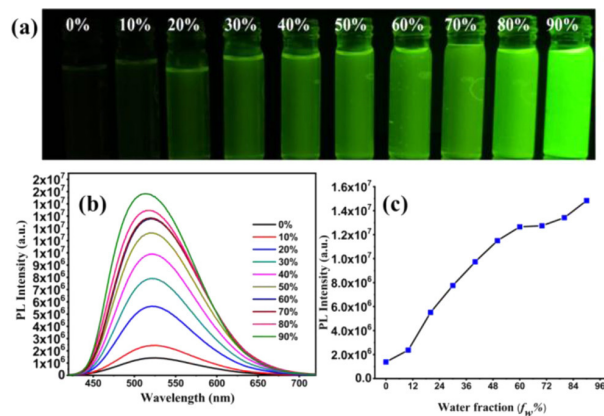


Figure 39. (a) Photos of CMO1 in mixtures of THF–water solution under UV light. (b) PL spectra of CMO1 in THF–water mixtures; (c) changes in PL intensity of CMO1 with variations in water fraction. Reproduced with permission from reference [59]. Copyright © ACS Publications 2020.

Pesticide detection with fluorescent porous organic polymers is a new technology developed in 2018 [60]. Thus, two hyper-crosslinked fluorescent porous polymers, **PAN-TPE-1** and **PAN-TPE-2**, were synthesized via the polycondensation reaction of two AIE-active aromatic tetraaldehydes with pores ranging from micropores (1.4–1.9 nm) to mesopores (3.8–26.2 nm) (Figure 40) [61]. The obtained porous polymer sensors showed high fluorescence sensitivity to trace amounts of pesticides in the aquatic environment, as well as excellent discrimination of imidacloprid (IDP) from other pesticides with a value of K_{SV} of $53,745 \text{ M}^{-1}$ and a LOD of 28 ppb for **PAN-TPE-1**, which is far lower than the WHO-allowed residue limit in common fruits and vegetables.

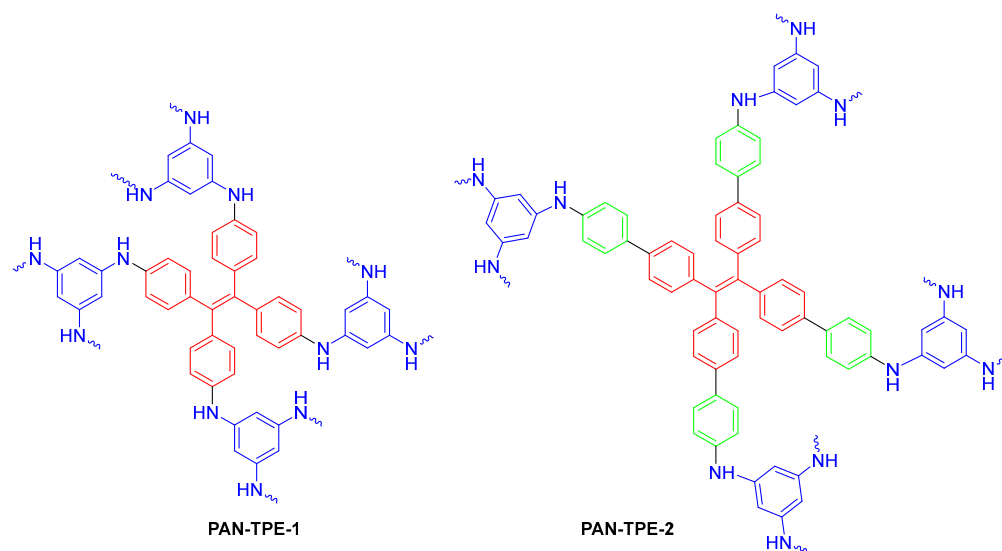
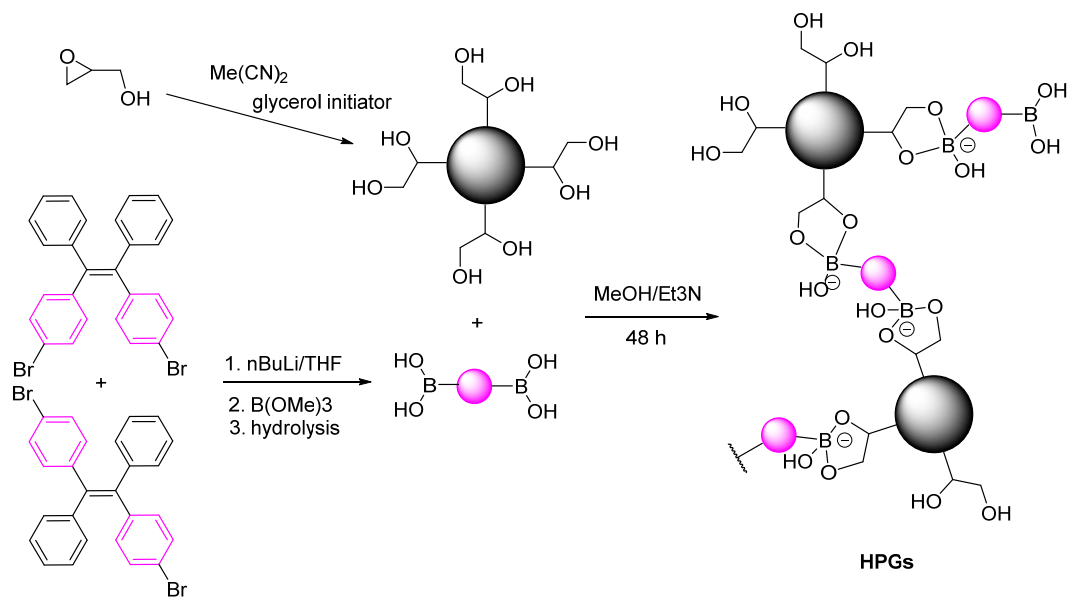


Figure 40. Structures of AIE-active fluorescent polymers.

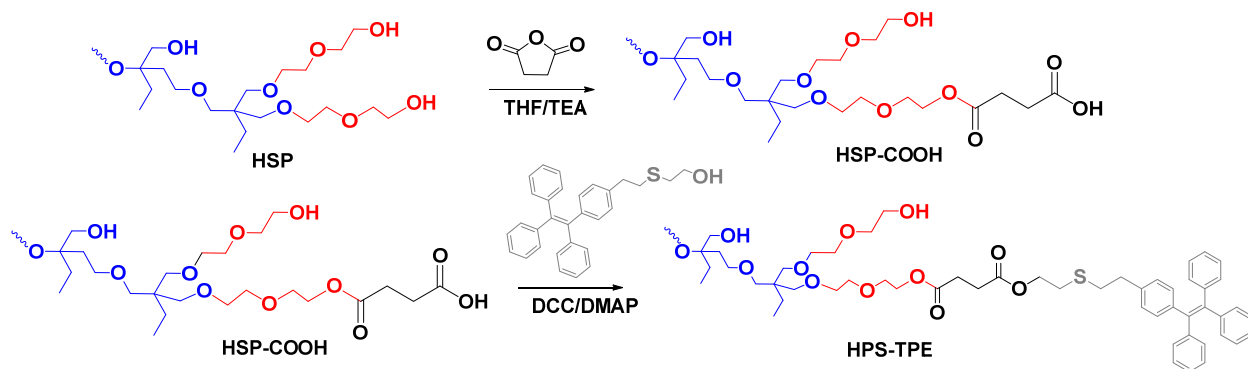
3.2.3. AIE-Active Hyperbranched Conjugated Polymers

AIE-active hyperbranched conjugated polymers are mainly used for the high-sensitivity detection of TNP in aqueous media. This is due not only to the fact that polymer nanoaggregates in an aqueous system have a high fluorescent quantum efficiency due to AIE characteristics but also to the fact that a loose packing of spherical structures forms a large number of intermolecular holes that can bind a larger number of TNP molecules, which leads to higher detection sensitivity [62]. For example, N. Kalva et al. used aggregation-induced emission (AIE)-active hyperbranched polyglycidols (**HPGs**) to design a solid-state sensor for detecting nitroaromatic explosives. The tetraphenylethylene moieties were conjugated to the periphery of **HPGs** in a single step using dynamic boronate ester crosslinkers (Scheme 7) [63]. According to dynamic light scattering and transmission electron microscopic analyses, the self-assembled nanosized aggregates were stable in a THF/H₂O mixture. The fluorescence of the aggregates was quenched dramatically by different NACs, including nitromethane, 4-nitrophenol, 4-nitrotoluene, 2,6-dinitrophenol, and 2,4,6-trinitrophenol. The nanoaggregates showed remarkable sensitivity to TNP, with a Stern–Volmer constant (K_{SV}) of $2.27 \times 10^4 \text{ M}^{-1}$ and a LOD of 40 ppb.

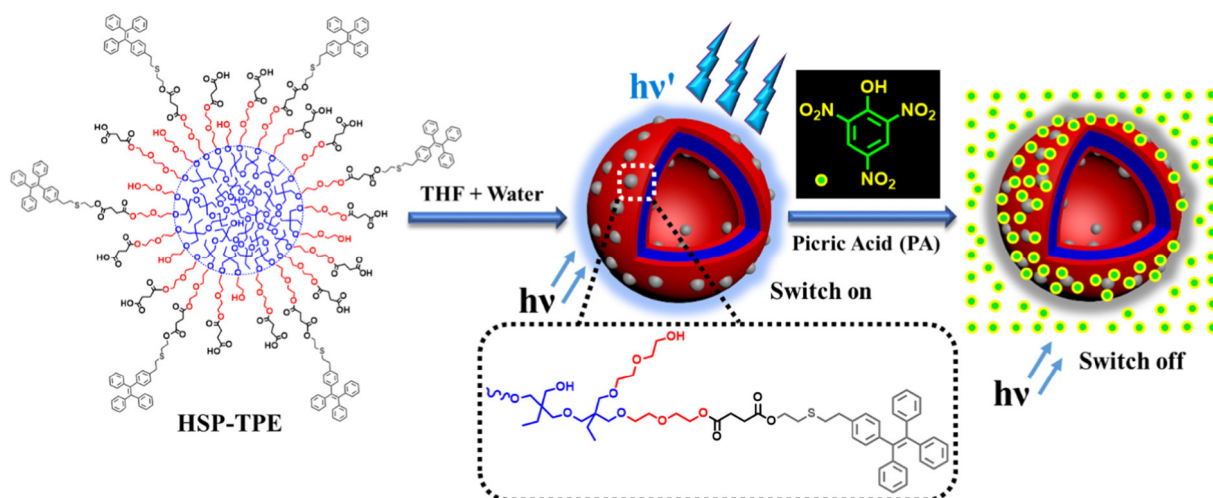


Scheme 7. Synthesis of nanosized AIE-active **HPG-TPE** aggregates that exhibit high sensitivity for the detection of nitroaromatic explosives.

F. Nabeel et al. reported a hyperbranched **HPS-TPE** polymer prepared through the esterification reaction of poly(3-ethyl-3-oxetanemethanol)-star-poly(ethylene oxide) (**HSP-COOH**) with **TPE**-containing thioethanol (i.e., 2-((4-(1,2,2-triphenylvinyl)phenethyl)thio)ethanol (**TPE-OH**) with high yields (Scheme 8) [62]. In an aqueous solution, the copolymer self-assembles to form aggregates. The aggregates display maximum photoluminescence (PL) in a THF/water (3:7 *v/v*) mixture. The introduction of **TPE** units into the polymer made it a highly sensitive AIE probe for picric acid with a detection limit as low as 20 ppb and a quenching constant of $2.4 \times 10^4 \text{ M}^{-1}$ (Scheme 9).

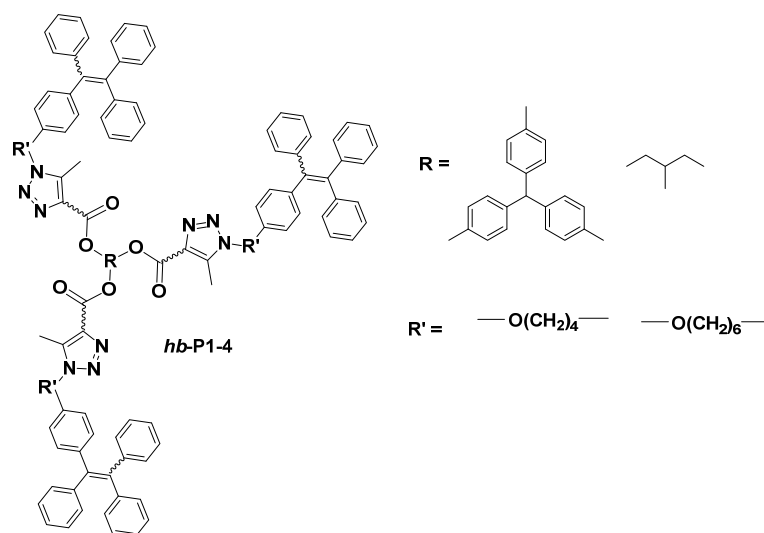


Scheme 8. The synthesis of **HPS-TPE** via esterification reaction from **TPE-OH** and **HSP-COOH** produced by carboxylation of **HSP**.



Scheme 9. Diagram of copolymer **HSP-TPE** self-assembly and sensing behavior aggregating toward TNF. In **HPS-TPE**, the blue, red, and gray colors represent the hydrophobic core, hydrophilic arms, and the probe, respectively. Reproduced with permission from reference [62]. Copyright © Elsevier 2020.

In 2020, four hyperbranched poly(methyltriazolylcarboxylate)s (**hb-P1–4**) with high molecular weights (M_w up to 2.4×10^4) and regioregularities (up to 83.9%) were obtained via a click polymerization reaction of alkyne monomers with tetraphenylethene-containing diazides (Scheme 10) [64]. The obtained **hb-P1–4** were characterized by good solubility, film-forming ability, and thermal stability. Their nanoaggregates ($f_w = 90\%$ in a mixture of THF/water) were studied as chemosensors for the detection of TNF in an aqueous solution. In particular, the Stern–Volmer plots of **hb-P1–4** were almost linearly correlated with the TNP concentration below $20 \mu\text{g mL}^{-1}$, with K_{SV} of 14,290, 14,300, 24,670, and $11,900 \text{ M}^{-1}$, respectively.



Scheme 10. Synthesis of **hb-P1–4** by click polymerizations of tributynoates **1** and diazides **2**.

3.3. Donor–Acceptor Architecture of Conjugated Polymers

For conjugated polymer sensors, the introduction of electron-donor groups is thought to enhance the interaction between electron-rich polymers and electron-deficient explosives, resulting in higher sensitivity in both the gas phase and solution, so most of them are based on donor-only structures [65–67]. Various conjugated polymers have been extensively

studied as thin-film sensor materials due to their extremely high sensitivity, which can be explained based on the molecular wire effect [68]. Owing to the PET fluorescence-quenching process, the main disadvantage of CP-based sensors is the problem of selectivity in a complex environment containing various electron acceptors. For example, discrimination between TNT and PA is still a challenge because both of them are extremely strong electron acceptors. In practical applications, selectivity is critical to successful detection, so a lot of effort has been put into this area.

Thus, Wang et al. synthesized the donor–acceptor polymer **P14** and two donor-only polymers **P15** and **P16** to study the dependence of sensitivity and selectivity in the detection of explosives on the structure of the polymer [69]. It was expected that the donor–acceptor structure of the polymer would first lead to a significant intrachain charge transfer from donor groups (diethylamine phenyl) to acceptor groups (2,1,3-benzothiadiazole, BT) and to the appearance of a dipole moment. Second, the LUMO would also mainly localize on the BT units, as occurs in the case of many D-A polymers [70].

According to the authors, because PA can easily form a negatively charged anion in an aqueous solution, an electrostatic repulsion interaction between the BT unit and PA will block the efficient electron transfer from the LUMO of **P14** to PA, as shown in Figure 41, which will not happen in the case of TNT. Therefore, **P14** can selectively detect TNT instead of PA in an aqueous solution. On the other hand, the reference polymers **P15** and **P16** with only donor groups should behave like most CP sensors with higher selectivity toward PA. Although the emission of polymers in the dissolved state was very weak, centrifuged films, due to the AIE activity of the polymers, showed bright emission and were investigated as sensors for detecting a mixture of picric acid and TNT. The **P14** sensor film selectively detected TNT instead of TNP in an aqueous solution with a K_{SV} of $1.2 \times 10^5 \text{ M}^{-1}$. The **P16** sensor film selectively detected TNP with a K_{SV} of $2.8 \times 10^4 \text{ M}^{-1}$ and a LOD of 2 ppb. In addition, it was also shown that the emission of **P14** and **P16** films can be effectively quenched by TNT and DNT vapors. These quenching effects of both TNT and TNP on **P14** and **P16** films were found to be reversible.

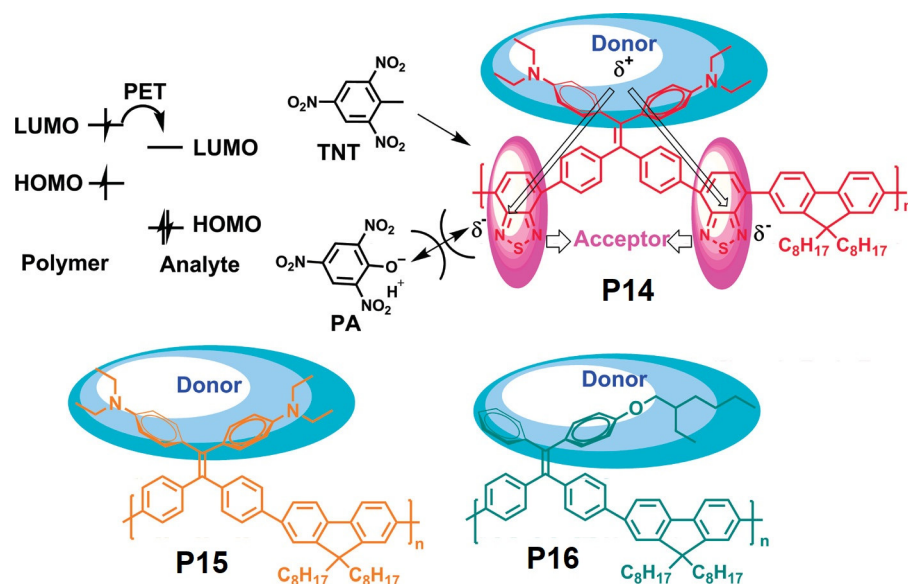


Figure 41. **P14–P16** electron transfer fluorescence quenching process and structures. Reproduced with permission from reference [69]. Copyright © ACS Publications 2011.

In another study, four D-A-type conjugated copolymers, **P17–20**, based on isoindigo as an acceptor unit with four different triphenylamine (TPA) donor derivatives were prepared (Figure 42) [71]. Quenching the emission of the **P17** sensor upon the addition of picric acid gave rise to a new emission peak, whereas this was not observed when quenching with TNT. The appearance of this new emission peak means that **P17** not only detects TNT and

TNP but also selectively detects TNP. The authors suggested that, on the one hand, the addition of TNP results in the protonation of the TPA group, which leads to the quenching of the emission of the sensor; on the other hand, it is likely that a complex with the polymer is formed, which generates a new emission peak and chemical shifts.

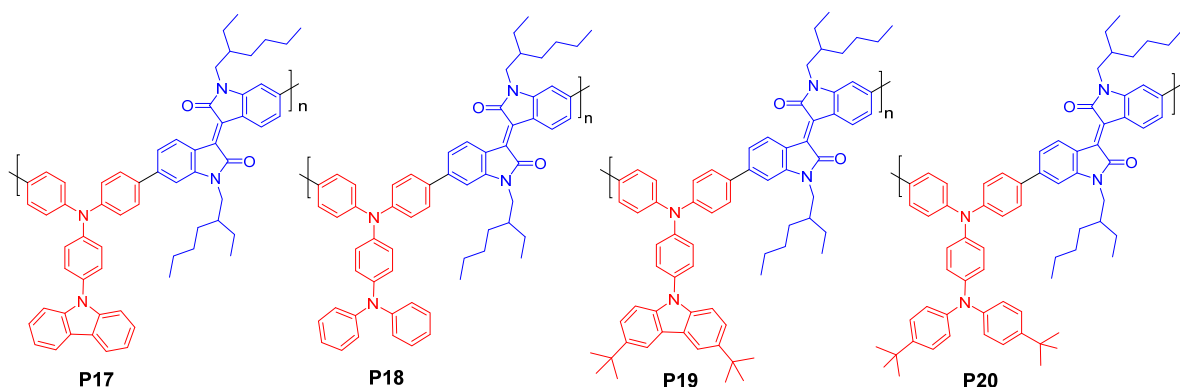


Figure 42. Structures of donor–acceptor conjugated polymers P17–P20.

Similar research was published in 2021. Thus, six donor–acceptor conjugated polymers were developed based on triarylamine derivatives as donor units with an isoindigo derivative or benzothiadiazole as acceptor units (Figure 43) [72]. These polymers are characterized by good solubility, film-forming properties in common organic solvents, and high luminescence quantum efficiency (up to 42.9%). In addition to showing electrochromic and photoelectric sensor properties, the films also proved to be highly sensitive probes for the detection of 2,4,6-trinitrophenol ($K_{SV} = 45,790 \text{ M}^{-1}$) and can meet the requirements of multifunctional materials.

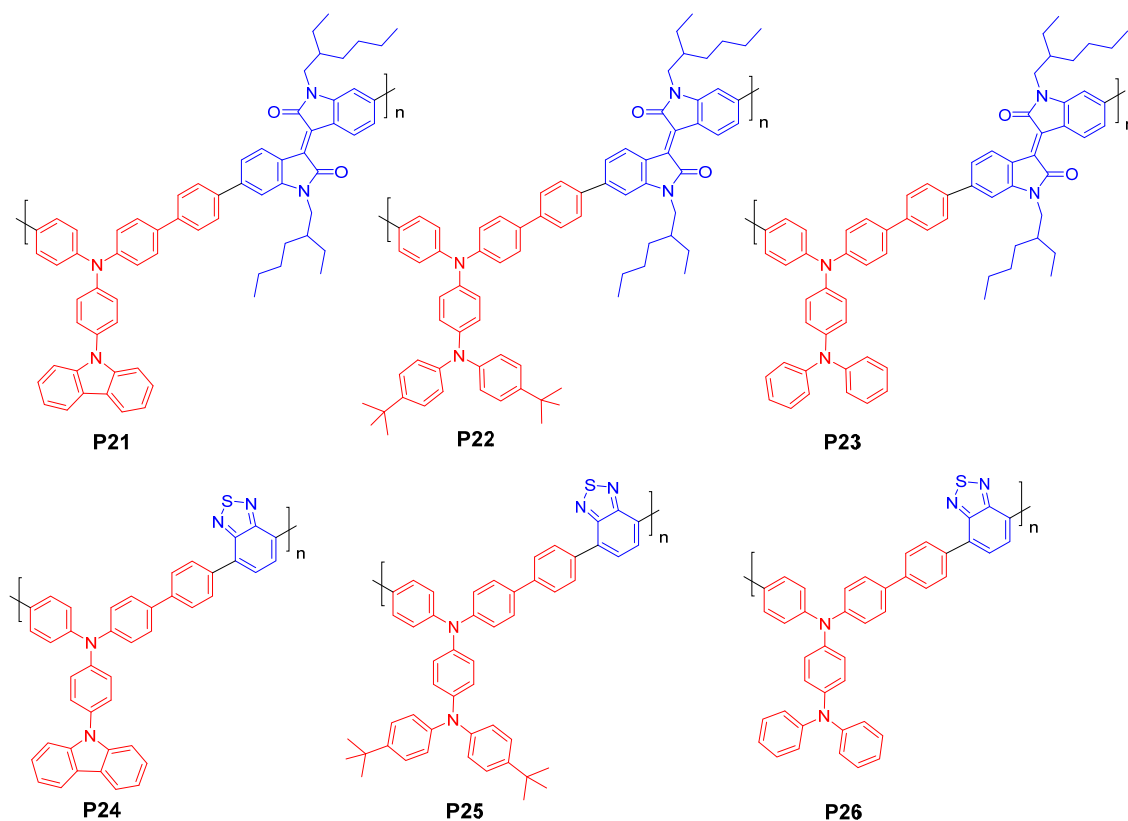
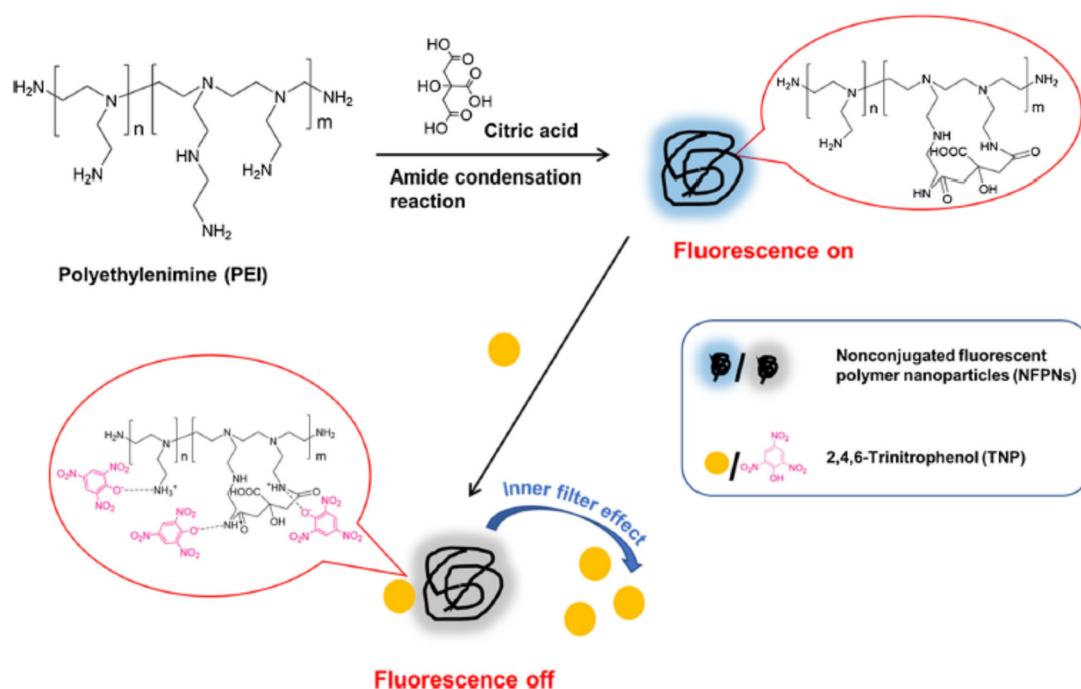


Figure 43. Structures of donor–acceptor conjugated polymers P21–P26.

3.4. Polymer Sensors Based on Cluster Luminogens

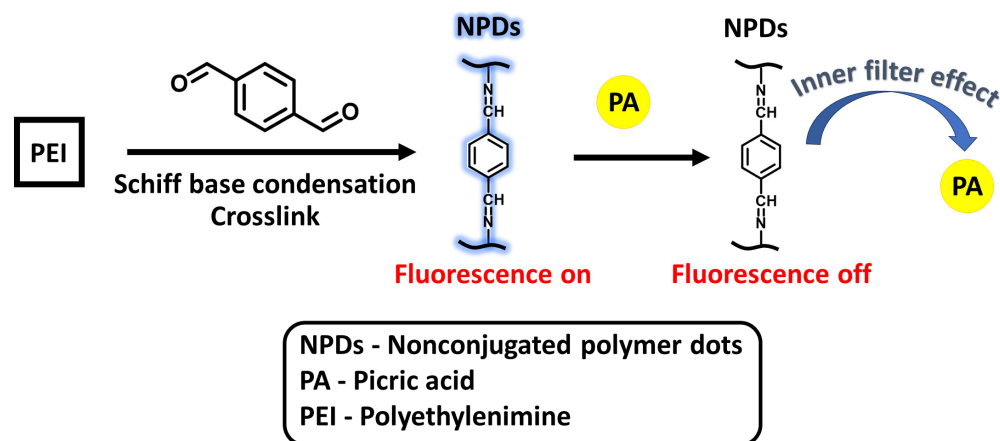
In some cases, polymers are constructed from nonconjugated monomeric structures by using C-C, C-O, or C-N bonds in polymers to form aggregates or solid forms, which exhibit strong photoluminescence due to so-called “clusterization-triggered emission” [73]. Based on the theory of through-space conjugation (TSC), arising from $n-\sigma^*$, $n-\pi^*$, and $\pi-\pi^*$ orbital overlaps, as well as hydrogen bonding and other weak interactions, the effect of clusterization-triggered emission (CTE effect) can be applied for various applications, for example, in the areas of process monitoring, structural visualization, sensors, and probes [74]. In particular, due to the high content of n - or π -electrons, polymers based on clusteroluminogens are considered promising new candidates for the detection of nitro-explosives.

For example, very recently, water-soluble fluorescent nonconjugated polymer nanoparticles (NFPNs) containing numerous n -electrons were prepared from branched polyethylenimine (PEI) and citric acid through an amide condensation reaction in the aqueous phase (Scheme 11) [75]. Numerous active amino groups of polyethylenimine were linked by citric acid and formed the highly crosslinked NFPNs. The nanoparticles exhibited stable bright fluorescence, which was quenched dramatically in the presence of trace concentrations of PA. Thus, in an aqueous solution, upon excitation at 360 nm, ca. 40% of the emission of NFPNs at 450 nm was quenched upon the addition of PA, while in the presence of other interfering species/quenchers, no noticeable fluorescence changes were observed. The authors ascribed such selectivity to the inner-filter effect (IFE) and the formation of self-assembled non-fluorescent Meisenheimer complexes between PA and NFPN side groups on the surface. The calibration plot of $\log(F_0/F)$ vs. PA concentration shows a linear relationship ($R^2 = 0.999$) for PA concentrations in the range of 0.5–150 μM . The detection limit for PA was 0.7 μM . The assay was successfully used to determine PA in spiked lake-water samples, and the recoveries were 96.6–102.7%.



Scheme 11. Synthesis of fluorescent polymer nanoparticles (NFPNs) from branched polyethylenimine (PEI) and citric acid through an amide condensation reaction and the quenching mechanism of NFPN emission by TNP. Reproduced with permission from reference [75]. Copyright © Springer Nature 2020.

In a similar manner, nonconjugated polymer dots (NPDs) were prepared from PEI and 1,4-phthalaldehyde by means of the formation of Schiff bases in combination with self-assembly (Scheme 12) [76]. These NPDs have been successfully used as novel, fast, and sensitive fluorescent probes for PA detection. Thus, NPD fluorescence was effectively quenched by PA via the inner-filter effect (IFE) because the absorption spectrum of the analyte and the excitation spectrum of NPDs overlapped. The proposed method gave a high degree of precision, good accuracy, and good sensitivity when used to quantitatively analyze PA in water samples. The PA recoveries (101.63–103.15%) and relative standard deviations (2.07–2.16%) were acceptable.



Scheme 12. Schematic diagram of the method used to fabricate NPD nanoprobe for determining PA using an on-off method.

3.5. Iptycene-Based Fluorescent Conjugated Polymer Sensors

Iptycene-based conjugated polymer sensors represent a unique combination of two concepts: the concept of the amplified fluorescent conjugated polymer, the so-called “molecular wire” [77], and the concept of interstitial space (free volume) around the molecules of iptycenes, giving them the ability to form supramolecular architectures with high porosity [78].

Common polymers, such as polyethylene and polypropylene, are electrical insulators, as they do not have free charge carriers in their backbones. However, *trans*-polyacetylene showed electrical conductivity, which gave rise to conjugated polymers (CPs) as semiconductive materials with promising properties from an applied point of view [79]. CPs include a wide range of structural classes: *trans*-polyacetylenes, poly(*p*-phenylene)s, poly(*p*-phenylene-vinylene)s, poly(phenylene-ethynylene)s (PPE), poly(*p*-phenylene-sulfide)s, polypyrroles, polythiophenes, poly(3,4-ethylenedioxythiophene)s, polyanilines, and polyfluorenes [79], some of which are fluorescent, which determines their use as sensors as well [80].

Such a possibility was demonstrated for the first time by Zhou and Swager in 1995 using CP PPE cyclophanic receptor systems and paraquat as a fluorescence quencher, and the “molecular wire” model was proposed [81,82].

In this model, as the authors suggested, receptor units are “wired in series” throughout the fluorescent conjugated polymer, forming a polyreceptor system, which operates on the principle of “*unus pro omnibus, omnes pro uno*” (“one for all, all for one”), making the whole polymer behave as a single molecule. Upon excitation, facile energy migration across the polymer backbone occurs, sampling multiple receptor sites and inducing emission. However, this fluorescence would be significantly quenched if the exciton encounters even a single receptor site occupied by a quencher (Figure 44A). Such a situation, in which a few receptor sites occupied by quencher molecules lead to the almost complete quenching of the whole polymer, is called the amplification of the signal, and such systems were

named amplifying fluorescent polymers (AFPs). Classical monoreceptor sensors, typical for isolated small fluorophore molecules, do not have signal amplification like this; thus, the degree of their fluorescence quenching is proportional to the number of receptor sites occupied by the quencher (Figure 44B). Therefore, a higher concentration of the quencher is required for a monoreceptor system to obtain a degree of fluorescence quenching equal to that of the AFP polyreceptor system.

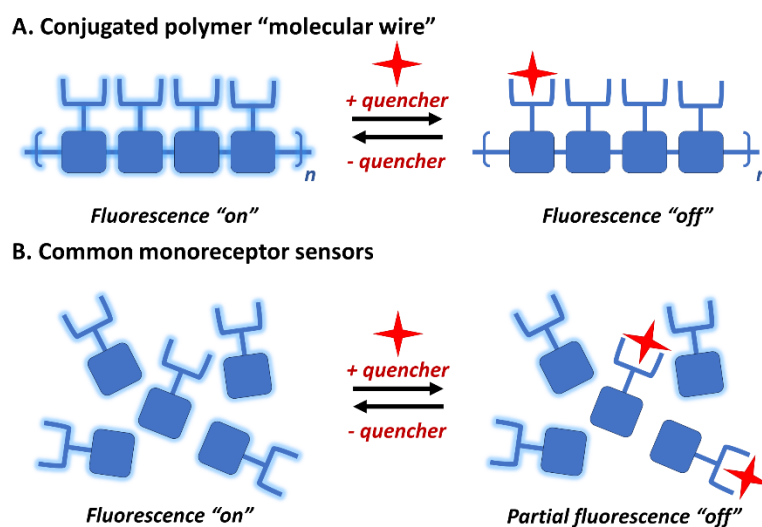


Figure 44. Difference between “molecular wire” polyreceptor system (A) and common monoreceptor one (B).

Nevertheless, as one might guess, “molecular wire” AFP systems have their own limitations related to molecular weight (M_n). Indeed, it was shown that the degree of signal amplification increased at low M_n as the diffusion length of the excitation outnumbers the length of the molecule, and then it becomes insensitive at M_n above $\sim 65,000$ – $100,000$, where the size of the polymer exceeds the diffusion length of the excitation [80–82]. Given that the latter is determined by the excited-state lifetime and the excitation’s diffusion rate, to gain the maximum signal amplification degree, a combination of long-lived excitation states, excitations with high mobilities, high-efficiency energy transfer, and high molecular weight is required. For example, it was shown that in molecular structures in which energy transfer is hindered, like in meta-conjugated substituted PPE, the ability to amplify fluorescence quenching is decreased [82].

Another similar case is the lowered sensitivity of AFPs in solution due to the isolation of polymeric chains from each other. It causes excitons to walk in a one-dimensional way, which is ineffective because excitons revisit the same receptor sites several times as a result. Also, in the solution state, the competitive solvation of AFPs and quencher molecules and their rates of diffusion should be taken into account as additional limitations. In addition, carrying out fluorescence-quenching experiments in the solution state requires meticulous solution preparation and the usage of toxic solvents [80].

As a one-time solution to the above-mentioned problems, the usage of AFP sensors in the form of films instead of solutions was proposed. This allows the sample preparation stage to be eliminated, as the film is a ready-to-use sensor device, which is particularly convenient for operators in field conditions. Also, there was hope that the limitations imposed by the diffusion rate, which is linked to the process of sensor and quencher solvation, would be reduced. But the most important advantage of films over solutions lies in their two- or three-dimensional structure. It eliminates the one-sided walking behavior of excitons, which is obligatory in the solution state, and allows hopping from one chain to nearby ones. Such multidimensionality of potential routes decreases the possibility of the

exciton revisiting the same receptor sites and increases the likelihood of it meeting a site occupied by a quencher, which further advances the amplification of the signal [78,83].

For example, in poly(*p*-phenylene ethynylene) thin films prepared by Langmuir–Blodgett deposition, an increase in energy transfer efficiency accompanying an increase in the number of layers up to 16 layers was observed. The phenomenological model used for the evaluation of energy transfer efficiency revealed a high rate of energy transport between different layers ($>6 \times 10^{11} \text{ s}^{-1}$) and a diffusion length exceeding 100 Å in the Z-direction [5].

But just as solution-state AFP sensor usage has its own problems and limitations, the same can be said for the solid-state one: (1) The planar geometry of the above-mentioned polymers favors π -stacking interactions and results in aggregation. (2) Such interactions, in turn, create local energy minima on the potential energy surface of the film. With the addition of intra- and interchain exciton migration, a large amount of the initial excitation energy is funneled to aggregation sites in AFP thin films. Also, these low-energy trap sites restrict the extent of exciton migration [80]. (3) Aggregation is accompanied by the well-known phenomenon called “aggregation-caused quenching” (ACQ) [84], expressed as a lower fluorescence intensity compared to the same polymer in the non-aggregated state. (4) Weak emission, in turn, means the low sensitivity of the sensor polymer, as higher concentrations of the quencher are required to give a reliable response.

Despite the advantages of such systems for enhanced fluorescence-quenching efficiency, the initial CP sensors lacked the visualization of recognition events and selectivity.

To overcome the listed disadvantages and pitfalls of classical CP-AFP sensors, especially the films, and to increase their selectivity, the introduction of sterically bulky pendants into the structure was suggested. Triptycene-containing polymers have been known since 1968 [85]; thus, in 1998, Yang and Swager designed new CP-AFP sensors but based on a pentiptycene moiety (IP1–3) (Figure 45) [65,66].

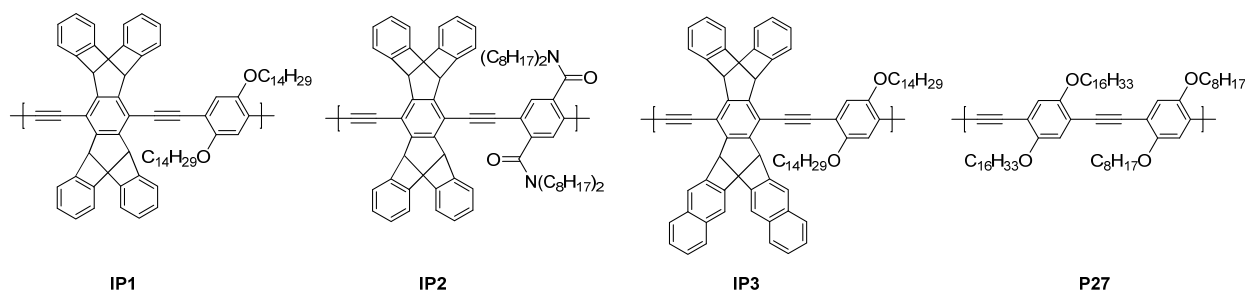


Figure 45. Structures of Yang and Swager’s original iptycene-based conjugated polymers.

Iptycene turned out to be the most attractive candidate, as it has a unique three-dimensional structure and properties. The dihedral angles between the aromatic rings of its bicyclo [2.2.2]octatriene bridgehead system are equal to 120 °C, resulting in a rigid three-bladed geometry (Figure 46A), which hampers π -stacking and other intra- and intermolecular interactions and makes molecules resistant to aggregation [86]. This results in (1) higher fluorescence intensity and quantum yields, as ACQ does not happen (with iptycene-based IP1–3 having greater fluorescence quantum yields compared to P27 in the solid state); (2) improved solubility in organic solvents (as IP1 is ~100-fold more soluble than P27 in chloroform); (3) higher spectroscopy stability and reproducibility; (4) the enhanced stability of the polymer films to thermal actions, solvent treatment, photobleaching, and degradation, since the enthalpic driving force for the reorganization of the polymer chains is smaller when there is no direct contact [66]; (5) increased energy transfer efficiency through polymer layers due to the prevention of energy waste upon exciton migration [80].

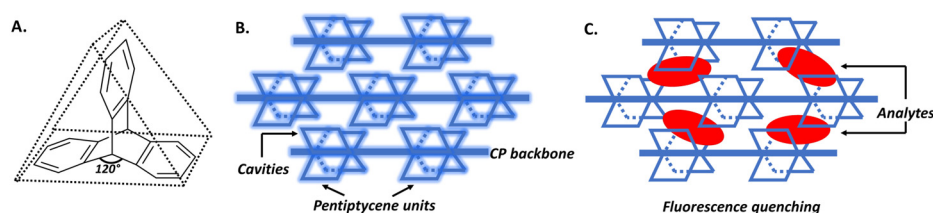


Figure 46. Internal free volume and dihedral angles of iptycene (A); concept of “sponge”-like porous structure of iptycene-based polymers (B) and their fluorescence quenching after contact with analytes (C).

Furthermore, such voluminous pendants stack up in the polymer film in such a way that voids are formed, named “internal free volume” (Figure 46A). Consequently, it increases the porosity of the film, turning it into a kind of “sponge” (Figure 46B). The cavities in the polymeric “sponge” serve as molecular-scale channels, which facilitate the penetration of analytes and their adjustment to receptor sites (Figure 46C).

It is also worth mentioning that the clefts and cavities of iptycenes afford a venue and direct the course for supramolecular interactions and additionally enable size-based selectivity in some cases [87].

Also, as for selectivity, iptycenes are electron-rich, and therefore, in the presence of electron-deficient analytes (e.g., nitroaromatic explosives, their precursors, and their derivatives), the fluorescence quenching of iptycene-based CP-AFPs occurs due to noncovalent interactions, i.e., photoinduced electron transfer (PET) [66].

Based on the above, first, CP-AFP pentiptycene-based sensors IP1–3 (planar electron-rich polymer 4 was synthesized as a reference compound) were developed by Yang and Swager in 1998, as was mentioned earlier, and their sensory response to electron-acceptor compounds—nitroaromatic ones and quinones—were studied. Structure-activity relationships were investigated to understand what it takes to create effective and sensitive fluorescence “turn-off” sensors for the detection of explosives and some other analytes [65,67].

Fluorescence-quenching experiments in the solid state, specifically in films, showed that quenching depends on the analyte diffusion rate, which, in turn, correlates with sensor-analyte binding interactions, the vapor pressure of the analyte, and the film thickness. For nitroaromatic quenchers, the relationship between the film thickness and quenching efficiency was inversely proportional (Figure 47A); in thin films (25 Å), a greater quenching efficiency was obtained compared to thick (200 Å) ones (70% and 30% at 60 s for TNT, respectively). This happens because of the strong binding interactions between the sensor and nitroaromatic compounds, which slow down the diffusion of the latter through the film. For quinones (namely, duroquinone (DQ)), the opposite was observed because of weaker interactions (Figure 47B) [65,66]. And the dependence of the sensory response on the vapor pressure of the analyte manifests itself in the following: DNT, having a higher vapor pressure than TNT (18:1), caused more pronounced and faster fluorescence quenching (80% vs. 30% after 10 s in thin films, respectively).

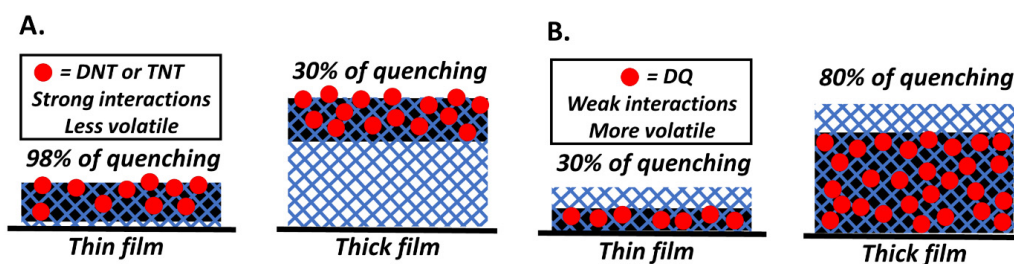


Figure 47. Dependence of quenching efficiency on film thickness and analyte nature (nitroaromatic compounds (A) or duroquinone (B)).

Now, if you think about it, the dependence of the quenching efficiency of CP-AFP sensors on the analyte diffusion rate runs somewhat counter to the concept of the “molecular wire”, as the latter should not depend on the analyte diffusion rate so much. If the “molecular wire” model were completely correct, then the occupation of receptor sites on the surface by the quencher should be enough for rapid, substantial fluorescence quenching. Indeed, in one of the later studies, a time-resolved quartz crystal microbalance with in situ fluorescence measurements confirmed that the fluorescence-quenching efficiency is mainly related to analyte diffusion, not exciton diffusion, as in real-time sensing, the diffusion of the vapor of the analyte–quencher into the film is driven by the swelling kinetics of the latter [88]. Thus, according to these findings, optimizing and improving analyte penetration should be one of the priorities when designing future sensors operating in the solid state. However, regardless of the real mechanism behind high quenching efficiency—the “molecular wire” or diffusion-dependent one—iptycene-based CP-AFP sensors proved themselves effective and promising for detecting nitro-containing substances, especially their vapors.

By virtue of the initial studies of iptycene-based polymer sensors carried out by Yang and Swager, several ways to improve sensitivity can be distinguished: (1) increasing the electron richness of the sensor, making it more “appealing” to electron-acceptor substances (for example, the electron-withdrawing character of amide substituents in polymer **IP2** leads to its decrease, which results in a reduction in sensor sensitivity to nitroaromatics [66]); (2) tuning the porosity or configuration (size/shape) of 3D cavities; (3) increasing the excited-state lifetime, which expands the range of through-bond exciton migration; (4) tuning sensor–analyte binding interactions (not too strong, not too weak); (5) increasing the fluorescence quantum yield via exciplex formation (due to excited energy delocalization) or the aggregation-induced emission (AIE) phenomenon [89], which also elevates the interchain exciton transport simultaneously.

Since isolated fused polycyclic aromatics have rigid structures and symmetrically forbidden/weakly allowed transitions, instead of “classic” PPE pentiptycene-containing polymers **IP1–3**, the dibenzochrysene-based π -conjugated analog **IP5** was created for the extension of the excited-state lifetime. As was supposed, due to the structural modification made, improved sensitivity toward TNT was observed [90].

The introduction of chiral alkyloxy side chains into PPEs gave polymer **IP6**, which aggregates into a 3D helical grid structure with longer exciton diffusion and conjugation lengths. Films of **IP6** exhibited a rapid and substantial sensory response: exposure to 10 ppb of TNT vapor led to 75% fluorescence quenching in 10 s. Moreover, the quenching efficiency of the **IP6** film depended very little on its thickness. These results indicated a great improvement in sensitivity and performance compared to **IP1–3** films [91].

Similar to **IP6**, but having pendant hexafluoro-2-propanol (HFIP) groups instead of alkyloxy side chains, derivatives **IP7–8** were synthesized (Figure 48) [92]. It was found that the introduction of strongly hydrogen-bond-donating pendants such as HFIP is more effective in terms of the detection of hydrogen-bond-accepting analytes (e.g., pyridine and 2,4-dichloropyrimidine) compared to weak hydrogen-bonding but strongly electron-deficient ones such as DNT (only 20–28% fluorescence quenching was observed upon exposure to DNT). So, it can be concluded that this modification strategy showed itself to not be successful in the design of sensitive sensory materials for the detection of explosives and their derivatives.

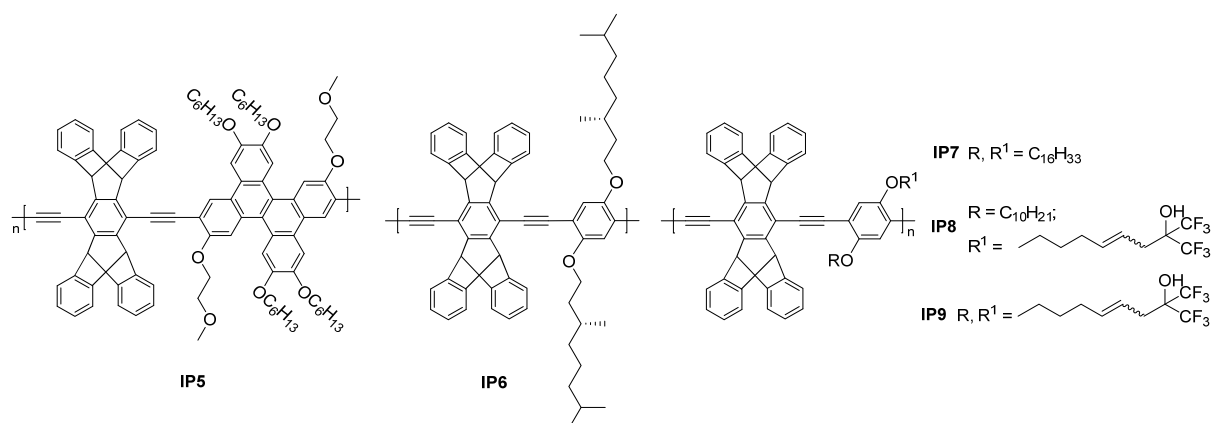


Figure 48. Structures of iptycene-based conjugated polymers (IP5–IP9).

As was mentioned earlier, tuning the size/shape of 3D cavities, as well as binding interactions, should also be taken into account while designing new sensory materials. Thus, novel all-iptycene-based poly(*p*-phenylenebutadiynylene)s (PPD) IP9–11 were synthesized (polymer IP12, similar to “classic” PPE polymers IP1–3, was obtained as the model compound) (Figure 49) [67]. A crucial point of such a structural modification lies in the fact that every *p*-phenylene unit within the conjugated backbone is built into the iptycene structure as the core unit in such a way that it lies at the bottom of the three-dimensional rigid “nest”. Consequently, direct “face-to-face” interactions between nitroaromatic molecules and these *p*-phenylene units are restricted, which is fundamentally different from the above-mentioned open-structure iptycene-based polymers IP1–8.

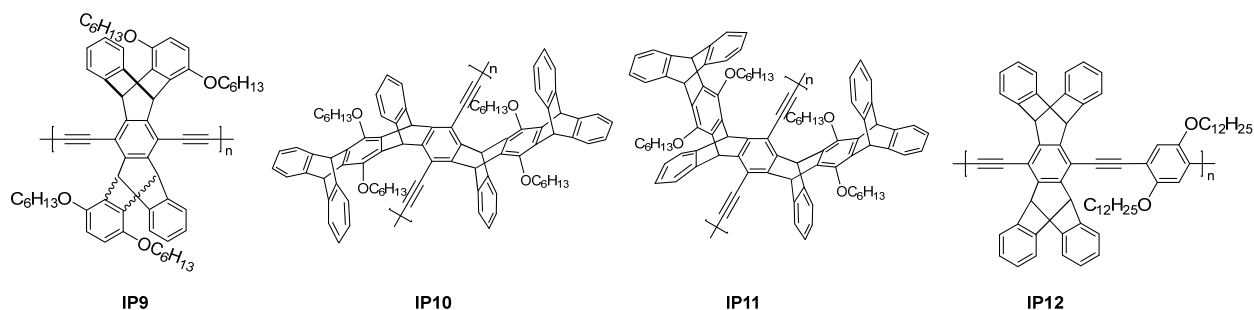


Figure 49. Structures of iptycene-based conjugated polymers IP9–IP12.

To evaluate the sensory properties of the obtained PPD polymers IP9–11, fluorescence-quenching experiments were carried out in the presence of nitroaromatic substances (DNT, TNT, *p*-nitrotoluene, and benzophenone) both in solution (in CHCl₃) and in the solid state. Interestingly, among the four polymers, IP10 exhibited the highest sensitivity: the Stern–Volmer static quenching constant values varied within 21–185 M^{−1} (for IP9 and IP11, they varied within 13–166 M^{−1} and 1–64 M^{−1}, respectively; for IP12, the quenching constant for DNT was equal to 26 M^{−1}). For all polymers, the greatest sensory response was obtained in the presence of TNT, which can probably be attributed to the largest number of electron-withdrawing nitro-groups in its structure among all involved in the quenching experiment’s nitroaromatic compounds. Considering that IP10 and IP11 have similar electronic properties, the difference in their sensitivity can be attributed to the influence of the stereo-configurations of the iptycene moieties.

However, in the solid state, the opposite behavior was observed: films of PPDs IP9–11 showed a much slower response to the presence of DNT and TNT compared to PPE IP12. Moreover, the fluorescence recovery rate after the cessation of contact with the vapor of the quencher was slow for IP9 and took an extremely long time for IP10–11, indicating almost

irreversible binding between iptycene cores and nitroaromatic molecules, which hinders the exit of the quencher from the cavity of the sensor.

In summary, two conclusions can be drawn: first, different factors play a role in sensing electron-deficient compounds by PPD sensor polymers in solution and in the solid state; second, tuning the quencher's binding degree should be very fine and weighted, as too strong a retention of the analyte hampers its diffusion, which, in turn, negatively affects the sensor sensitivity. It is also especially important if the aim is to design recoverable sensory materials.

Another interesting design attempt is the creation of sensory polymers **13–14** (Figure 50) with greater photoreduction abilities for the detection of the taggant 2,3-dimethyl-2,3-dinitrobutane (DMNB), which is quite hard to detect due to its reduction potential of approximately -1.7 V and three-dimensional structure, eliminating the possibility of direct π -stacking with the sensor film [93]. The idea was to introduce amines into the structure, whose π -donation would reduce the ground-state oxidation potential. However, it turned out that it also lowers the band gap, simultaneously increasing the excited-state oxidation potential. Only the polymer **IP13** film gave a sensory response to DMNB, and it was very weak—around 4–5%.

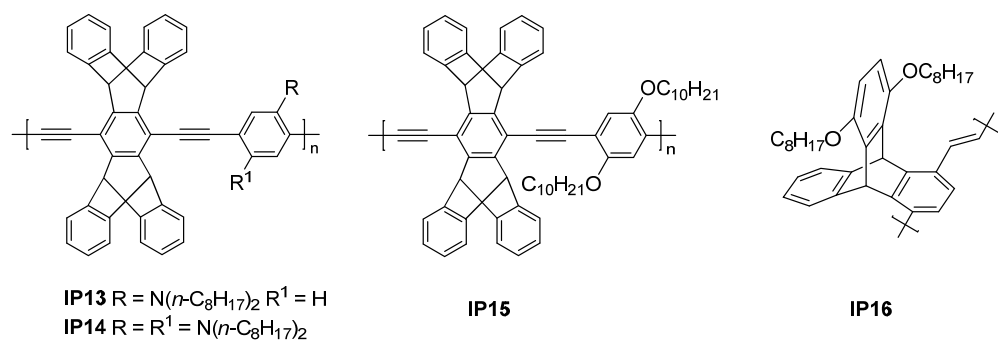


Figure 50. Structures of iptycene-based conjugated polymers **IP13–IP16**.

It is worth mentioning that triptycene was also used in CP-AFPs as an aggregation-preventing unit, as well as an electron donor for electron-deficient compounds, such as explosives, despite the fact that triptycene is less effective than pentiptycene in the alleviation of ACQ [94].

The classic PPE polymer **IP15** was obtained together with the triptycene-based poly(phenylenevinylene) (PPV) one, **IP16**, both of which exhibited multiphoton-excited fluorescence that was sensitive to the presence of TNT (Figure 50) [95]. To compare their sensory abilities, two-photon- and three-photon-excited-fluorescence-quenching measurements were carried out by microtitration in solution. The pentiptycene-based polymer **IP15** showed a larger degree of two- and three-photon-excited-fluorescence quenching than the triptycene-based (**IP16**) one (quenching factor of ~ 5 vs. ~ 1.2 at millimolar concentrations, respectively). The results may indirectly indicate that pentiptycene is a more preferable unit for CP-AFP sensors than the triptycene one.

Another two triptycene-based PPVs—**IP17** and its derivative **IP18**, having O-alkyl-donating substituents—may serve as examples of the influence of structural modifications on sensory abilities (Figure 51) [96]. Electron-donor substituents lead to an increase in the energy of the highest occupied molecular orbital, with a subsequent decrease in the oxidation potential of polymer **IP18**. Also, they add bulkiness to the already-voluminous triptycene moiety, reducing the tendency to aggregate and increasing the overall electron richness of polymer **IP18**. Indeed, more pronounced fluorescence quenching in the solid state in the presence of DNT was observed for polymer **IP18** than for its analog **IP17**—55% vs. 37% after 60 s, respectively. Another advantage of polymer **IP18** is that it can be easily reactivated. The Stern–Volmer quenching constants, measured in solution, were equal to

12.8 M^{-1} and 28.4 M^{-1} for **IP17** and **IP18**, respectively, which is in accordance with the previously mentioned constant values for **IP9–12**.

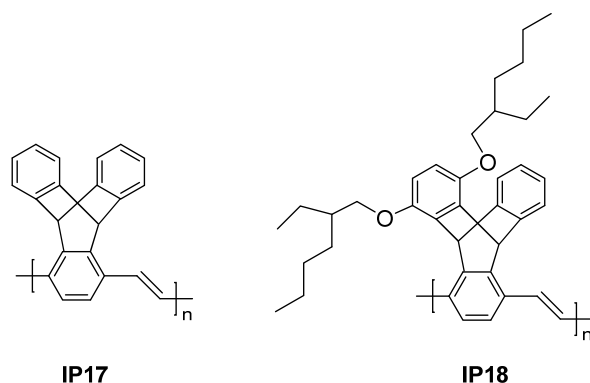


Figure 51. Structures of iptycene-based conjugated polymers **IP17–IP18**.

Other examples of using triptycene moieties for the creation of sensory materials are azobenzene-functionalized polymers **IP19–20** for the detection of picric acid (PA) (Figure 52) [97]. Facile interactions (hydrogen bonding, π – π , or dipole–dipole ones) of polymers **IP19–20** with PA were suggested due to the electron-rich character of the polymer backbones and the presence of nitrogen-rich azo ($-\text{N}=\text{N}-$) linkages in the polymer frameworks. Indeed, fluorescence quenching amounted to 78% for **IP19** and 57% for **IP20**, and the values of Stern–Volmer quenching constants varied within $(2.4\text{--}5.3) \times 10^5 \text{ M}^{-1}$, which are several orders of magnitude higher than those obtained for any of the above-mentioned polymers, indicating the high sensitivity of the obtained polymers to PA. Thus, the applied strategy of structural modification proved to be successful.

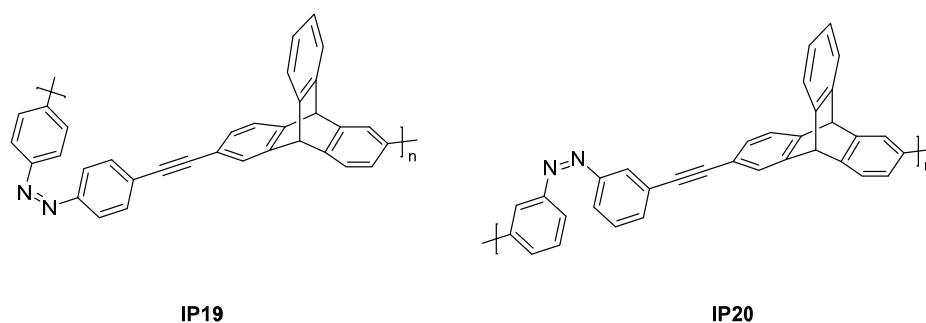


Figure 52. Structures of iptycene-based conjugated polymers **IP19–IP20**.

The peculiar compilation of design strategies for polymers **IP5** and **IP18**, namely, the incorporation of fused polycyclic aromatics and O-alkyl-donating substituents, yielded polymer **IP21**, in which the structure's triphenylene core was integrated (Figure 53) [98]. It allowed an increase in bulkiness and electron-donating propensity at the same time. This, in turn, increased selectivity, since triphenylene has three-fold symmetric sites, which are complementary to the positive charges on TNT and DNT, and sensitivity to nitroaromatic explosives. Polymer **IP21** exhibited improved sensitivity to TNT vapor.

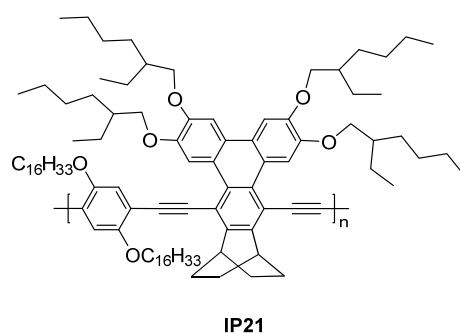


Figure 53. Structure of iptycene-based conjugated polymer **IP21**.

An unusual pentiptycene-based PPE sensor polymer, **IP22**, having cholesteryl ester substituents, was designed (Figure 54) [99]. Bulky pendant cholesteryl ester groups act as an additional measure to prevent aggregation and increase the porosity of the polymer film. In the solid state, fluorescence quenching of 51% after 60 s exposure to DNT vapor was observed for the thin film (2 nm). Undercoating with 7.5–8.5 nm thick APTES and blending with a non-fluorescent polymer added 18.5% (with 20 s exposure) and 18.7% (with 5 min exposure) to the fluorescence intensity decrease, respectively. Thus, polymer **IP22** has shown itself to be relatively efficient for the detection of DNT and capable of improvement.

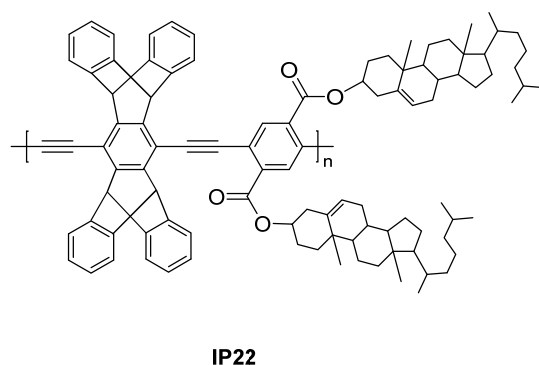


Figure 54. Structure of iptycene-based conjugated polymer **IP22**.

The outstanding photophysical properties of pyrene, for example, its high fluorescence quantum yield combined with long-lived excited states, electron-rich nature, and sensitivity to microenvironmental changes, are well known, which is why pyrene has a long history of being used as a basic and classic unit for the creation of sensitive sensory materials for the detection of explosives [100]. Thus, pentiptycene-based CPs **IP23–25**, containing pyrene or a *t*-butyl-substituted derivative in the main chain, were created (Figure 55) [101]. It can be said that the same design strategies were applied in this case as for polymer **IP5**, having dibenzochrysene units, and polymer **IP21**, containing a triphenylene core with bulky substituents. Polymer films of **IP23–25** were able to detect TNT in both the vapor and aqueous states, which confirms the effectiveness and feasibility of the chosen design strategies. It should be said that polymer **IP25**, having mono *t*-butyl-substituted pyrene, showed the best performance, which tells us about the need for balance in bulkiness. Fluorescence quenching of the **IP25** polymer film by TNT vapor was equal to 60.4% and 90% after 10 s and 30 s of exposure, respectively, which is higher than those exhibited by previously mentioned polymer sensors. Also, fluorescence quenching of 69.8% was observed for the **IP25** polymer film within 60 s of immersion in an aqueous solution of TNT (50 M). Moreover, sensor films of polymers **IP23–25** are recoverable after usage.

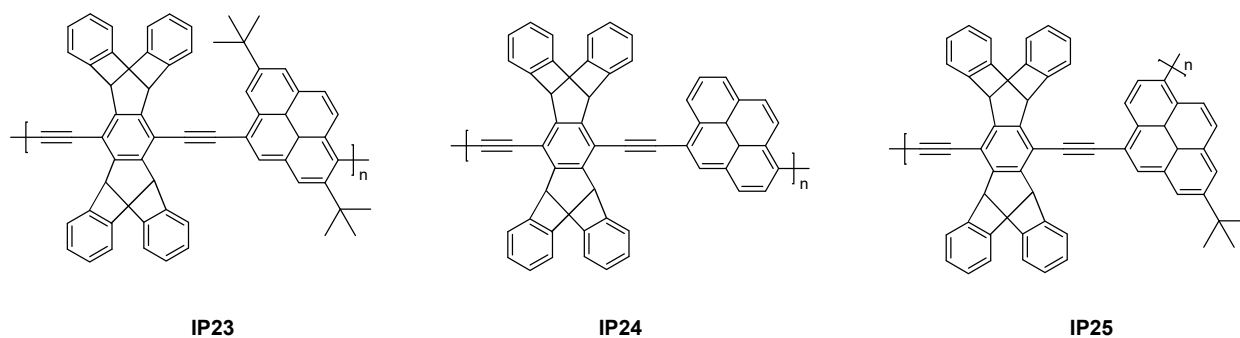


Figure 55. Structures of ipitycene-based conjugated polymers IP23–IP25.

Series of poly(aryleneethynylene)s (PAEs) based on electron-rich dialkylated 3,4-propylenedioxythiophenes (ProDOT) and pentiptycene polymers **IP26–28** were synthesized as sensors for the detection of the explosive TNT (“classic” PPE polymer **IP28** was obtained as a model compound) (Figure 56) [102]. The fluorescence quantum yields of **IP26–27** are higher than those for wholly ProDOT-based PAE polymers due to the pentiptycene unit’s incorporation but lower than the yields of fully PAE polymers and PPE polymer **IP28**, thanks to the presence of sulfur, inducing the heavy-atom effect. However, the sensitivity of **IP26–27** to the presence of TNT in CHCl_3 turned out to be on par with that of polymer **IP28** despite the lower quantum yields of the former. It is worth mentioning that a later organic composite combining poly 3-hexylthiophene, Cu (II) tetraphenylporphyrin, and **IP27** was produced and able to detect vapors of such explosives as 1,3,5-trinitro-1,3,5-triazacyclohexane (RDX), TNT, and dinitrobenzene by measuring the saturation current and conductance as the key parameters representing molecular the recognition event [103].

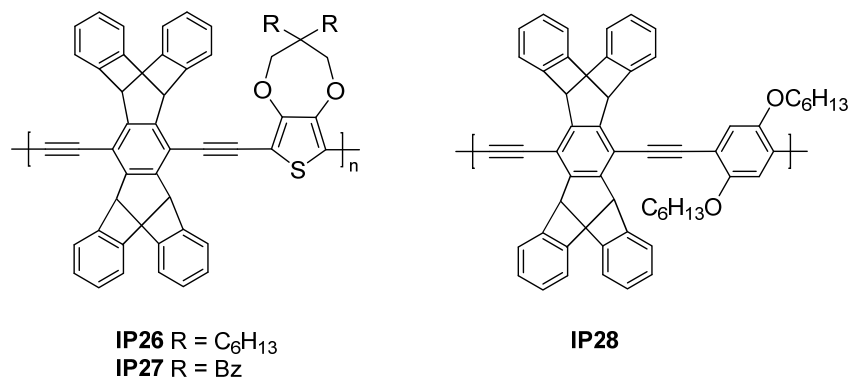
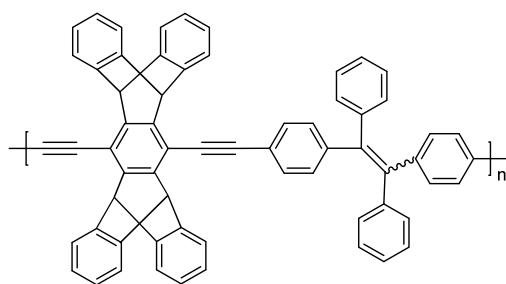


Figure 56. Structures of ipitycene-based conjugated polymers IP26–IP28.

Since tetraphenylethene (TPE)-based polymers are aggregation-induced emission (AIE)-active, a versatile and sensitive pentiptycene-based TPE-containing sensor polymer, **IP29**, capable of detecting explosives (PA and dinitrotoluene) both in solution and in air was created (Figure 57) [104]. In aqueous organic media (in a H_2O –THF mixture (9:1 (vol. %)) to be more precise), it forms highly emissive and sensitive nanoaggregates that detect nitroaromatic explosives at ppb levels: fluorescence quenching was equal to 24% with a PA concentration of 4.36×10^{-8} M and reached over 98% with a PA concentration of 4.71×10^{-6} M. In the solid state, 70% of the fluorescence of the thin film (4 nm) was quenched by DNT vapor after 30 s, whereas for the thick film (80 nm), quenching was only 37%; thus, thickness-dependent behavior of quenching was observed, which agrees with the previous data for model polymers **IP1–3**.



IP29

Figure 57. Structure of iptycene-based conjugated polymer IP29.

3.6. Pyrene-Containing Excimer-Based Polymer Sensors

It was mentioned earlier that pyrene has unique photophysical properties, which is why it has found widespread use in the design of sensory materials. The excimer emission of pyrene is of particular interest, as it is very sensitive to microenvironmental conditions such as temperature, pressure, or pH [105]; thus, sensors in which the formation of pyrene excimers takes place are highly desirable.

Many pyrene-based sensors have been created, including small-molecule ones [100,106] and polymer films [105], but the latter have advantages, as they are cheap, user-friendly, convenient to use on-site, reusable, usually organic-solvent-free (which is more eco-friendly), and, ideally, easy to prepare. There are several types of pyrene-containing polymer materials based on the type of pyrene introduction into the polymer structure: thin film with covalently bonded pyrene pendants [105] and physically encapsulated pyrene molecules in non-porous or porous materials [107,108]. Each type has its own advantages and disadvantages.

The production of thin polymer films with covalently attached pyrene or its derivative pendants usually prevents leakage and decreases excimer emission decay; however, it can result in weak excimer emission. Also, the covalent bonding of pyrene molecules is time-consuming, tedious, and costly and usually yields low amounts of the target product. On the other hand, they are preferable for the detection of analytes in solutions. Poor excimer emission can also be observed in the case of the physical encapsulation of pyrene molecules in non-porous films. Moreover, the dense polymer matrix hinders the diffusion of the analyte, reducing the sensitivity of the material. To reduce this effect, very thin films can be prepared, but they have low fluorescence intensity, which makes results obtained with their usage unreliable and unrepeatable. To enhance excimer formation and facilitate analyte diffusion through the polymer, a non-porous type of polymer can be designed, but the leakage issue must be kept in mind. In addition, it should be mentioned that the physical entrapment of the polymer in either non-porous or porous materials can lead to inhomogeneity and reduce the stability of the material, lowering its performance and the reproducibility of the results.

Despite the above-listed issues, design strategies have been polished over the years to keep only the positive properties of different materials while eliminating the negative ones, which allowed the production of effective sensory materials suitable for particular types of analytes/application fields. Several interesting examples are discussed below.

Beyazkılıç et al. prepared sensory mesoporous thin films via a facile template-free sol-gel method based on organically modified silica (ormosil) with entrapped pyrene molecules for the detection of nitroaromatic compounds, including explosive ones (Figure 58) [109]. The advantages of this material are its cheapness, its simplicity, and the lack of a need for any chemical modifications of pyrene. Also, porosity facilitates analyte penetration, which is especially useful for the detection of analytes in the form of vapor. Moreover, pyrene excimer emission was observed. Its intensity was higher in a porous film than in its non-porous counterpart, which is expected, as it is well known that pores promote excimer formation [110]. Furthermore, in porous films, it was stable for at least 2 months,

whereas in non-porous films, pyrene excimer emission decayed within 2 h. The solid-state fluorescence-quenching efficiency of pyrene excimer emission by DNT, TNT, and nitrobenzene was equal to 39.2, 31.5, and 16.2% after 30 s of exposure, respectively. These results are lower than those obtained for iptycene-based polymer films; however, this quenching can be observed by the naked eye under a UV lamp, which is convenient for no-instrument, fast, on-site analyte detection. Other analytes (toluene, ammonium nitrate, benzene, benzoic acid, sodium hydroxide, 3,4-dihydroxybenzoic acid, methanol) caused no sensory response, which testifies in favor of film selectivity. Also, it is worth mentioning that the obtained sensory films can be recovered and used again at least five times by just immersing them in water.

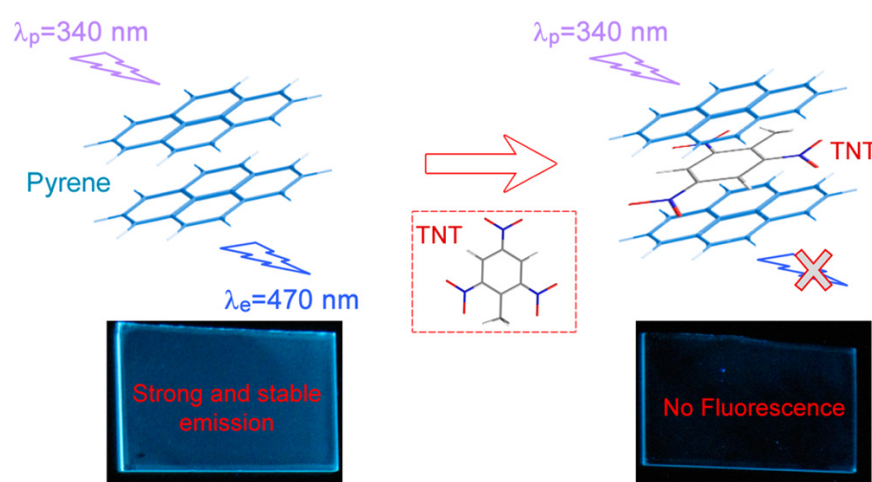


Figure 58. Schematic illustration of fluorescence-quenching-based TNT sensing with pyrene molecules. Reproduced with permission from reference [109]. Copyright © ACS Publications 2014.

Another intrinsic example of pyrene-based porous sensory material is the self-assembled 3D nanoporous pyrene–polystyrene (**Py-PS**) film, which was prepared via the simple single dip coating of PS and Py solutions (Figure 59A) [111]. The authors managed to fine-tune its sensitivity by fine-tuning the morphology and by optimizing the degree of pyrene doping into the polymer matrix (via varying the pyrene–styrene molar ratios), which affects the electronic properties. The best-sensing film quenched the pyrene excimer emission intensity by 60% and 90% after 6 min and 30 min of exposure to saturated DNT vapor (Figure 59B); thus, the produced film is pretty sensitive. Also, the selectivity of the film was additionally proven by the absence of fluorescence quenching in the presence of other analytes, such as 3,5-dinitroaniline, perfume, chloranil, urea, ammonium nitrate, and sodium nitrite (Figure 59C).

As seen in the above-mentioned examples of iptycene- and pyrene-based porous films, this type of material is more suitable for the detection of analytes in the vapor state. However, for detection in an aqueous matrix, it was concluded by Sun et al. that sensors in the form of nanofibers are preferable, as nanofibers are cost-effective, having high porosity and a large surface area of approximately 1–2 orders of magnitude higher than those of continuous thin films, enhancing their sensitivity and response time, and it is also possible to produce fibers with low polymer concentrations and, in turn, small diameters, which are favorable for fluorescence sensing [112]. Thus, pyrene–polyethersulfone (**Py-PES**) nanofibers were prepared under optimized conditions via the electrospinning technique using mixed solvents (Figure 60A). **Py-PES** nanofibers proved themselves to be highly sensitive, as pronounced excimer emission quenching was observed in the presence of explosives, such as TNT, DNT, and 1,3,5-trinitroperhydro-1,3,5-triazine (RDX), in aqueous solutions (Figure 60B,C). The Stern–Volmer quenching constants were calculated to be $1.80 \times 10^5 \text{ M}^{-1}$, $7.52 \times 10^4 \text{ M}^{-1}$, and $3.26 \times 10^4 \text{ M}^{-1}$, respectively, with limits of detection of 23, 160, 400, and 980 nM, respectively. In addition, other analytes, namely, ethanol,

acetonitrile, benzonitrile, chlorobenzene, and toluene, caused almost no changes in fluorescence intensity. Moreover, the immersion of the **Py-PES** nanofiber film in water for 48 h also did not affect the fluorescence intensity, which indicates the absence of leakage. As in the case of the previously mentioned pyrene-based materials, the **Py-PES** film is reusable.

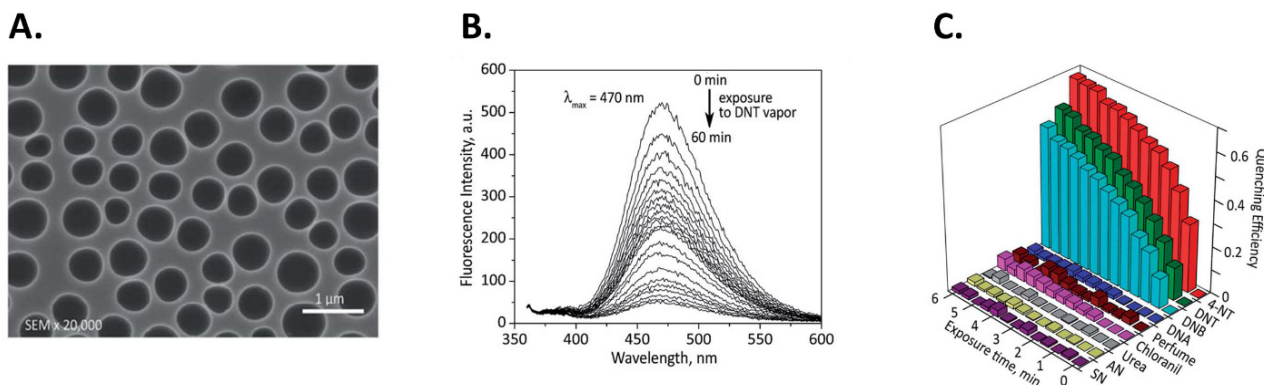


Figure 59. Nanoporous **Py-PS** film (SEM image) with an average pore size of ~ 400 nm (A); fluorescence intensity upon exposure to equilibrium DNT vapor (time-dependent) (B); fluorescence-quenching efficiency at the Py excimer peak upon exposure of the nanoporous **Py-PS** film (3D) to saturated vapors of various analytes (C). Reproduced with permission from reference [111]. Copyright © Royal Society of Chemistry 2014.

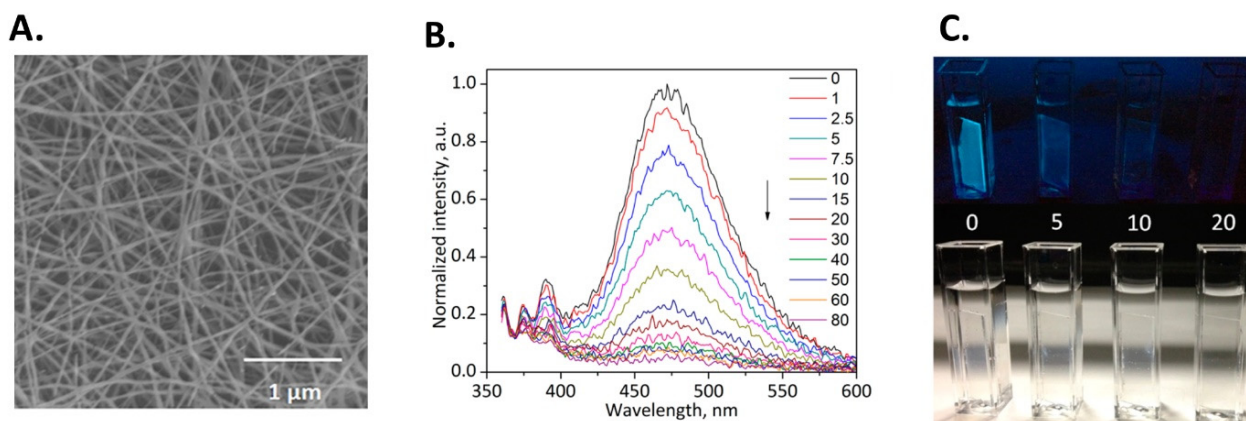


Figure 60. Nanofibrous **Py-PES** (SEM image) (A); fluorescence quenching (concentration-dependent) of **Py-PES** nanofiber film during addition of different concentrations (μM) of TNT in deionized water (B); photos of **Py-PES** fluorescent nanofiber films under UV light (254 nm, upper panel) and visible light (bottom panel) in the presence of various TNT concentrations (0, 5, 10, and 20 μM) (C). Reproduced with permission from reference [112]. Copyright © ACS Publications 2015.

Another example of sensory pyrene-based nanofiber-like material was reported by Guo et al. [113]. Novel flexible polyvinylpyrrolidone/pyrene/3-aminopropyltriethoxysilane/reduced graphene oxide (**PVP/pyrene/APTS/rGO**) nanonets (Figure 61A) were produced by using a one-step electrospinning method for the detection of explosives. Almost every component synergistically plays a role in enhancing the sensitivity of the final product. The need for pyrene usage in designing sensors for the detection of electron-acceptor substances, such as explosives (e.g., TNT, DNT), is clear. APTS was chosen, as aromatic electron-deficient compounds can be absorbed by electron-rich amino groups of organic amines via the formation of charge-transfer complexes between amino groups and the aromatic rings. rGO serves as a charge transport bridge between pyrene and TNT to facilitate the fluorescence quenching of the former. Also, rGO can interact with TNT through co-facial π - π stacking, inducing efficient long-range energy migration (Figure 61C).

As so many steps were taken to improve the performance of the sensory material, the high sensitivity of PVP/pyrene/APTS/rGO nanonets was not surprising, since this was expected. For example, the fluorescence-quenching (via excimer emission quenching) efficiency was 81% and 89% after 540 s of exposure to TNT and DNT vapors, respectively (Figure 61B). A sensory response to NO₂, NaNO₃, PA, and *para*-nitro toluene was also observed: the quenching efficiency was up to 53%, 18%, 34%, and 18% within 540 s of exposure, which speaks in favor of nanonets' sensitivity to TNT and DNT.

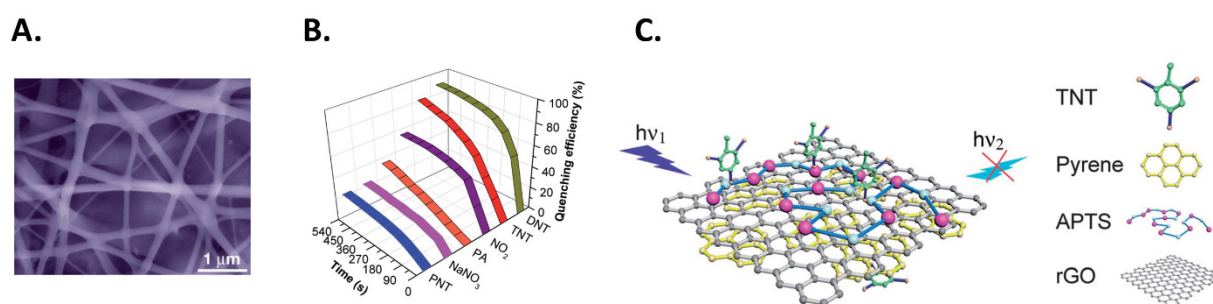


Figure 61. PVP/pyrene/APTS/rGO nanonets (SEM image) (A); quenching efficiencies of PVP/pyrene/APTS/rGO nanonets upon exposure to DNT, TNT, PA, NaNO₃, and PNT subsaturated vapors and NO₂ (50 ppb) at room temperature with respect to time (B); fluorescence-quenching mechanistic pathway of PVP/pyrene/APTS/rGO nanonets toward TNT (C). Reproduced with permission from reference [113]. Copyright © Royal Society of Chemistry 2014.

Unusual sensory fluorescent film-forming polymeric ionic liquids (PILs) containing pyrene or anthracene moieties were made via the solution polycondensation of 3,3'-diaminobenzidine and 5-*tert*-butyl isophthalic acid in polyphosphoric acid (Figure 62) [114]. The produced films showed intense excimer emission and moderate solution-state and high solid-state sensitivity (for ~12 μm thin film) to common nitroaromatic compounds. In DMSO, the fluorescence intensity was reduced by 70%, 60%, and 46% in the presence of PA, TNT, and nitrobenzene, respectively, in the case of the pyrene-based material ([DPyDBzPBI-BuI][Br]), and for the anthracene-based one ([DAnDBzPBI-BuI][Br]), fluorescence quenching was a little bit lower—55%, 53%, and 44%, respectively—which can be attributed to the lower electron richness and the tendency toward excimer formation of the latter. The Stern–Volmer quenching constants varied within $(1.78\text{--}4.15) \times 10^4 \text{ M}^{-1}$ for [DPyDBzPBI-BuI][Br] and $(1.59\text{--}2.03) \times 10^4 \text{ M}^{-1}$ for [DAnDBzPBI-BuI][Br]. However, the excimer emission of the [DPyDBzPBI-BuI][Br] film was reduced by 87%, 76.8%, and 71.6% quenching after 500 s exposure to nitrobenzene, TNT, and PA, respectively, and 80.3%, 73.5%, and 67.5% of the fluorescence intensity of the [DAnDBzPBI-BuI][Br] film was quenched by nitrobenzene, TNT, and PA, respectively. It should be noted that for thick films (~40 μm), a decrease in sensitivity was observed: fluorescence was quenched only by 11% and 30% after 50 s and 300 s of exposure to nitrobenzene, respectively, but this phenomenon is not unusual. Both films possess selectivity, as they showed no sensory response to benzoquinone, toluene, THF, or NaNO₃. An additional benefit is that the films can be renewed by washing with methanol after usage.

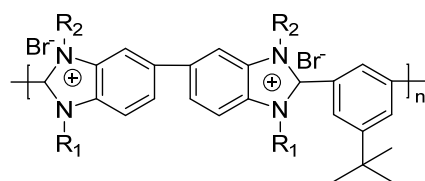


Figure 62. Structure of polymeric ionic liquids (PILs) made from polybenzimidazole (PBI-BuI).

Though “classic” thin polymeric films with covalently attached fluorophores have their own disadvantages, as was mentioned above, this type of material can still be useful if designed correctly and can find its own application field. One such example is Gupta and Lee’s thin polymeric film with pyrene pendants synthesized via the free radical copolymerization of dimethylacrylamide (DMA), benzophenone acrylamide (BPAM), and glycidyl methacrylate (GMA) with a feed ratio of 95:1:4 (Figure 63) [33]. The final product—[*p*(DMA-co-BPAM-co-GMA)]—was initially designed for the sensitive and selective detection of PA. Both pyrene units and their attachment to tertiary amine groups provided a fluorescence “turn-off” sensory response to the presence of PA, and its separation from other analytes (DNTs, nitrophenols, dimethylnitrobenzene, 4-nitrotoluene, various anions and cations, etc.) by electrostatic interactions between the positively charged polymer and picrate in water and crosslinkable benzophenone moieties requires immobilizing the film onto quartz slides. The proximity of pyrene moieties throughout the polymer backbone resulted in molecular aggregation and π – π stacking, which amplified fluorescence quenching by PA via an exciton-hopping process via intermolecular electronic coupling, facilitating long-range exciton diffusion. The limit of detection for PA was as small as 11.4 atto-grams (10^{-14} M), and the Stern–Volmer quenching constant was determined to be 7.75×10^4 in water. Also, the recovery of fluorescence was possible for the polymer by washing it with just water, which is pretty convenient.

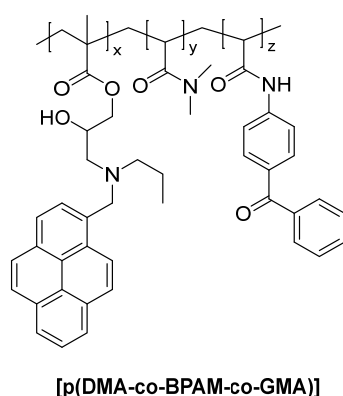


Figure 63. Structure of [*p*(DMA-co-BPAM-co-GMA)].

3.7. Optical Sensors Based on Porous Fluorescent Polymers: The Molecular Imprinting Technique

Molecularly imprinted polymers (MIPs) have received widespread attention due to the creation of selective artificial recognition cavities [115]. As probes, molecularly imprinted polymers are synthesized by the copolymerization of functional monomers and crosslinking agents in the presence of matrix molecules, which can be either explosives or their non-explosive structural analogs. By removing such matrices from the polymer substrate, cavities are created, resulting in the selective and accurate detection of explosives [116]. Despite the variety of different synthesis methods, there are currently no commercially available MIP sensors. Due to the change in the conformation of the binding sites during the drying of the polymer, MIP sensors are described in the literature only for detecting explosives in solution [116].

The infusion of carbon dots (CDs) with MIPs has been widely applied because of the high sensitivity of CDs and the high selectivity of MIPs [117]. A facile strategy to immobilize amino-carbon dots (CDs) onto mesoporous structured imprinted polymers for the highly sensitive and selective detection of TNT was developed, and a mesoporous structured sensor, M-MIPs@CDs, was obtained [118]. The selective sensing of TNT was guaranteed by the molecular imprinting technique and improved by two methods. One involved using mesoporous silica as an imprinting matrix, and the other entailed using fluorescent amino-CDs directly as a “functional monomer”. The thus-obtained sensory material exhibited excellent selectivity and sensitivity toward TNT, with a detection limit

of 17 nM. The recycling process was sustainable for 10 cycles without an obvious efficiency decrease. The feasibility of the developed method with real samples was successfully evaluated through the analysis of TNT in soil and water samples, with satisfactory recoveries of 88.6–95.7%.

In another example, a fluorometric sensor based on nitrogen-passivated carbon dots infused with a molecularly imprinted polymer (**N-CDs@MIP**) *via* a reverse microemulsion technique using 3-aminopropyltriethoxysilane (APTES) as a functional monomer, tetraethoxysilane (TEOS) as a crosslinker, and PA as a template was published (Figure 64) [119]. The removal of template molecules leads to the formation of a molecularly imprinted layer, and the **N-CDs@MIP** fluorescence response was quenched by PA. The developed fluorescence probe shows a fine linear range from 0.5 to 2.5 nM with a detection limit of 0.15 nM. The synthesized fluorescent probe was used to analyze PA in regular tap- and lake-water samples.

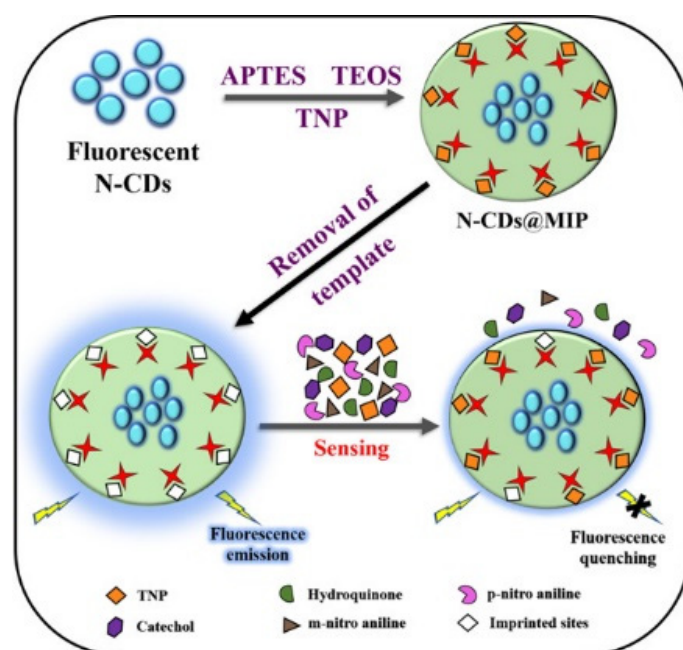


Figure 64. Schematic diagram of the fluorometric sensor **N-CDs@MIP** and quenching mechanism of the **N-CDs@MIP** emission by TNP. Reproduced with permission from reference [119]. Copyright © ACS Publications 2022.

The influence of the nature/amount of the crosslinker, as well as the template–monomer ratio, on the fluorescence intensity and sensitivity of two fluorescent polymers, 7-hydroxy-4-methylcoumarin acrylate (HMC) and 2,6-bis-acrylamidopyridine (BAP), was studied by Apodaca and co-authors [120]. Ethylene glycol dimethacrylate (EGDMA), trimethylolpropane trimethacrylate (TRIM), and divinyl benzene (DV55) were used as crosslinkers. The target analytes were 1,4-dinitrotoluene (DNT), trinitrotoluene (TNT), and *N*-methyl-3-cyano-4-methoxy-2-pyridone (ricinine, neutral alkaloid). It was established that **HMC-MIP** displayed a fluorescence-quenching effect, whereas the binding of the template to **BAP-MIP** yielded an enhancement of the fluorescent signal. In addition, the **MIP** formulation incorporating 20 mmol EGDMA yields an **MIP** with an obvious change in the fluorescence response for the detection of chemical warfare agents. Such a formulation exhibits the potential of detecting TNT in the μM concentration range. The resulting imprinted polymers were assumed to possess structural rigidity brought about by the interaction of BAP and HMC with the target analyte, allowing the **MIP** to respond via a change in the fluorescence signal intensity upon binding to ricinine (an analog of ricin), DNT, TNT, and other analytes.

The imprinted-polymer-functionalized optical sensor **MIP-NP** based on ethylene glycol dimethacrylate (EGDMA) for hypersensitive and selective water pollutants in aqueous media, with a dynamic detection range of 10^{-12} – 10^{-4} M measured using a concatenated microfiber interferometer technique, was developed (Figure 65) [121]. In the present detection system, **COM** was used for the generation and retention of stable interference patterns, while the MIP was used as a receiving agent for 4-nitrophenol (4-NP). The sensitivity of the proposed sensor was measured at 6.14×10^{11} nm/M with a LOD of 1.628 fM.

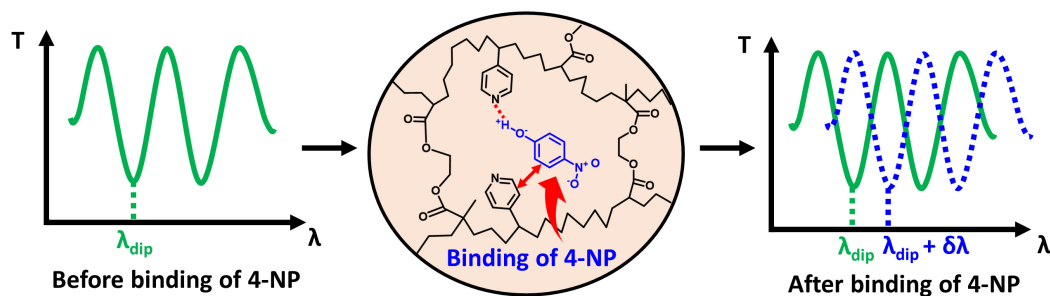


Figure 65. Schematic representation of working principle of the proposed sensor **MIP-NP**.

3.8. Optical Sensors Based on Fluorescent Polymers Containing Macrocycles

Conjugated macrocycle polymers, as a combination of extended π -conjugated polymers with macrocycles, are an emerging class of organic porous materials [122]. Conjugated macrocycle polymers synthesized by integrating macrocycles such as crown ethers, porphyrins, phthalocyanines, pillararenes, calixarene, and others demonstrate many flexible modular design possibilities for specific structures and functions, particularly for the detection of nitro-containing analytes.

A “three-components” supramolecular assembly composed of 2,2′:6′,2′′-terpyridine attached pillar[5]arene **P5A1**, a guest molecule containing 1,2,3-triazole-bearing CN-terminated alkyl chain **G**, and Zn^{2+} was fabricated (Figure 66) [123]. A supramolecular organo-gel was formed with a concentration of components amounting to 1 M, which acted as a sensor probe for nitrobenzene-based explosives. In particular, the limit of detection for picric acid was determined to be 1.66×10^{-4} M, with a fluorescent-quenching efficiency of 83.7%.

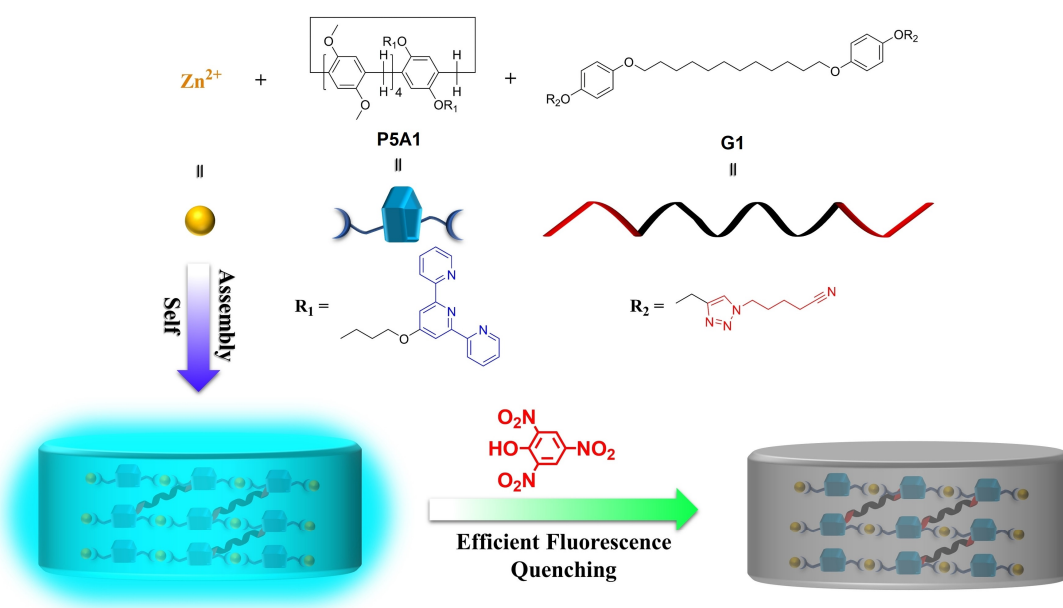


Figure 66. Schematic diagram of supramolecular organo-gel fabrication and picric acid sensing. Reproduced with permission from reference [123]. Copyright © Wiley 2021.

A linear supramolecular polymer obtained via the substitution reaction of the hydrazide groups on pillar[5]arene derivative **P5A2** with terephthaloylchloride (TPC) was used to construct a sensor for detecting nitro-explosives. Then, a supramolecular polymer network was successfully constructed via the introduction of a neutral guest **G** through pillar[5]arene-based host–guest interactions (Figure 67) [124]. The fluorescence intensity of the resulting film decreased dramatically upon the addition of nitro-compound explosives *o*-DNB and *p*-DNB. The limits of detection (LODs) of the probe for *o*-DNB and *p*-DNB were determined to be 7.90×10^{-7} M and 4.40×10^{-7} M, respectively.

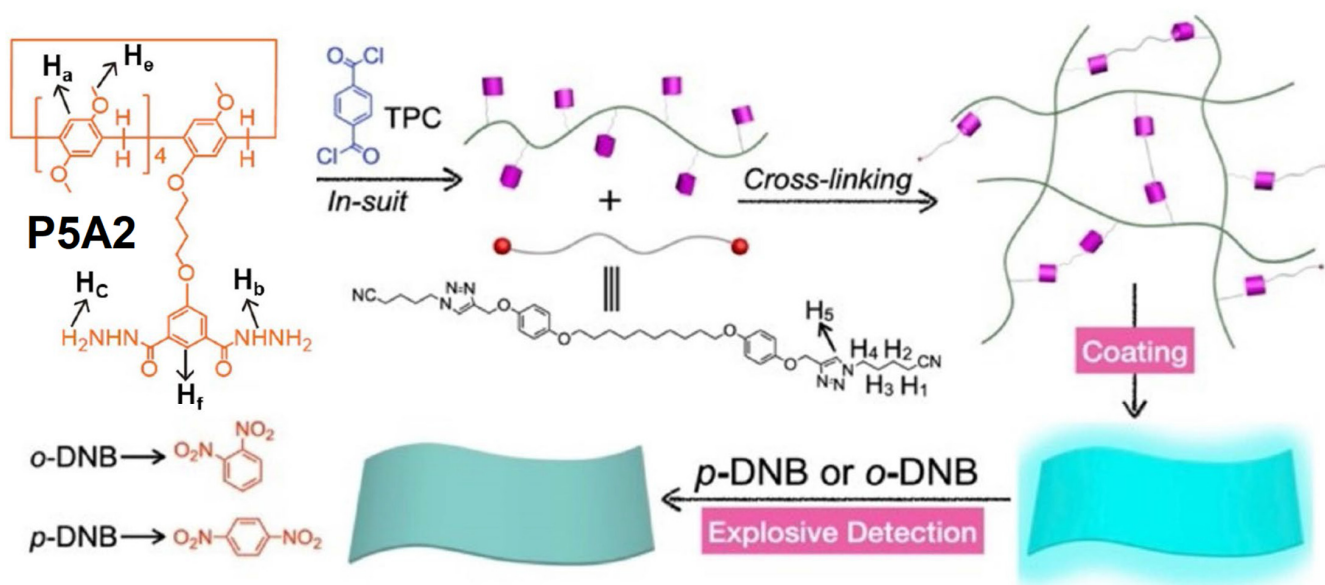


Figure 67. Pillar[5]arene-containing polymer structure and a neutral guest **G** bearing two cyano sites and two triazole sites. Schematic representation of crosslinked supramolecular polymer network formation with the property of explosive detection. Reproduced with permission from reference [124]. Copyright © Springer Nature 2022.

The concept behind the assembly of calix[4]arenes with a carbazole-containing conjugated polymer (**CALIXPPE-CBZs**) [125] was used to construct a new conjugated calix[4]arene-containing polymer, **CALIX-p-PPE**, which had a *p*-phenylene ethynylene-type main chain [126]. Five sensory materials were studied for the detection of non-volatile nitroaliphatic liquid nitromethane (NM) and the explosive taggant 2,3-dimethyl-2,3-dinitrobutane (DMNB) in the vapor phase: two **CALIXPPE-CBZs** (Figure 68A), which differed in the structural arrangement of the diethynyl substitution (3,6- or 2,7-) pattern on the carbazole units; two non-calixarene-based polymers, **TBP-PPECBZs** (Figure 68B), with the same polymer backbone; and a **CALIX-p-PPE** (Figure 68C) [127].

Experimental studies and theoretical calculations confirmed the hypothesis that the calixarene hosts were the unique differentiating elements responsible for the overall enhanced sensing in the solid state. The most sensitive and selective polymers in the detection of NB and DMNB were carbazole-containing calix[4]arene-based **CPs** (**CALIX-PPE-CBZs**), which was ascribed to cooperativity effects developed between the calix[4]arene hosts and the phenylene ethynylene–carbazolyne main chains. In particular, the **CALIX-PPE-3,6-CBZ** film was the best sensory material for NM and DMNB and reached around 60% quenching efficiency after only 10 s of exposure.

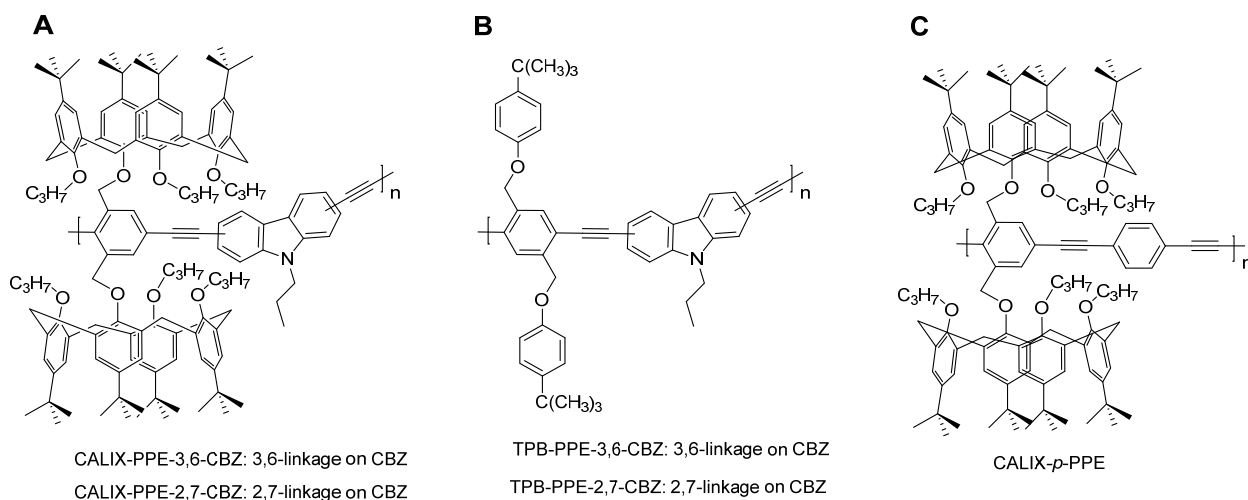


Figure 68. (A) Molecular structures of poly([2,5-bis-[5,11,17,23-tetrakis(1,1-dimethylethyl)-25-(oxymethyl)-26,27,28-tripropyloxycalix[4]arene]-p-phenylene]ethynylene-alt-3,6 or 2,7-carbazolyleneethynylene) (CALIX-PPE-CBZs); (B) poly[2,5-bis(p-tert-butylphenoxy)methyl]-p-phenylene]ethynylene-alt-3,6 or 2,7-carbazolyleneethynylene (TBP-PPE-CBZs); (C) poly([2,5-bis-[5,11,17,23-tetrakis(1,1-dimethylethyl)-25-(oxymethyl)-26,27,28-tripropyloxycalix[4]arene]-p-phenylene]ethynylene-p-phenylene ethynylene) (CALIX-*p*-PPE).

Recently, the same authors published studies of past research on the best calix[4]arene-containing phenylene-alt-ethynylene-carbazolylene polymers (Calix-PPE-CBZs) for the detection of nitroaromatic explosive compounds in solution and in the vapor phase. Both fluorophores exhibit high sensitivity and selectivity for NAC detection. The quenching efficiencies in solution, assessed through static Stern–Volmer constants K_{SV} , follow the order picric acid (PA) \gg 2,4,6-trinitrotoluene (TNT) > 2,4-dinitrotoluene > (2,4-DNT) > nitrobenzene (NB) [128].

A novel kind of flexible 5,10,15,20-tetrakis(4-aminophenyl)porphyrin (TAPP)-doped polymer optical fiber (PPOF) for the rapid and accurate detection of trace 2,4-dinitrotoluene (DNT) in vapor was reported by Gu and co-authors [129]. When the PPOF was pumped with green laser light, the TAPP molecules were excited, and subsequently, the emitted fluorescence was transmitted along the PPOF and recorded by a spectrometer (Figure 69). It was experimentally demonstrated that the limit of detection and response time of the proposed PPOF could reach around 120 ppb and 3 min, with a fluorescence quenching efficiency of 80.5%.

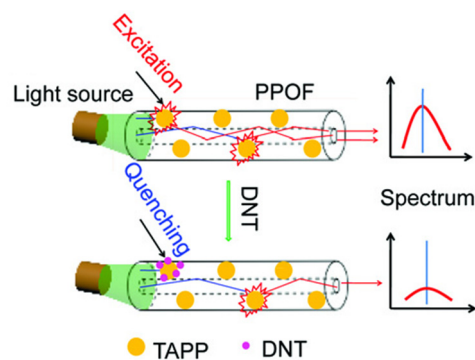


Figure 69. Schematic representation of the PPOF sensor's working principle for monitoring DNT vapor. Reproduced with permission from reference [129]. Copyright © Royal Society of Chemistry 2020.

3.9. Paper-Based Sensors

In view of sustainability and green concepts, paper-based electronics [130] and sensorics seem attractive for practical applications. Below, the most representative examples of paper-supported chemosensors for the detection of explosives are described.

Most paper-supported chemosensors are based on tri- or tetraphenylene fluorophores. Thus, Feng and co-authors [131] reported tetraphenylene **3a–c**-impregnated AIE sensory materials for the detection of methyl-substituted nitro-explosives (Figure 70). These materials exhibited a “Turn-off” response to TNT at a concentration as low as 1.0×10^{-13} M with a LOD of 0.2^{-4} ppb. The best response, with a LOD of $0.45 \text{ pg} \times \text{cm}^{-3}$, was observed for chemosensor **3a** (Figure 71), while chemosensors **3b–c** exhibited lower sensitivity.

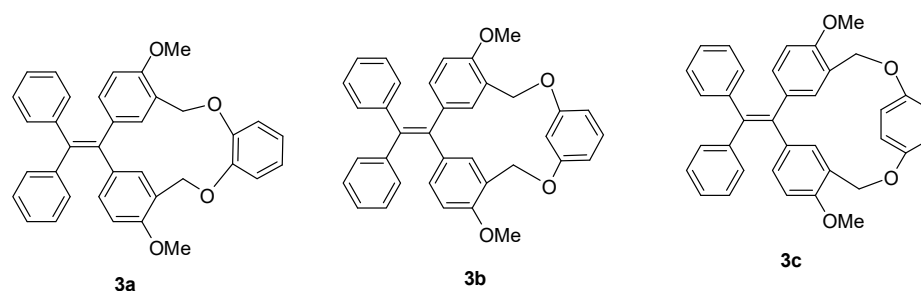


Figure 70. TPE-based chemosensors **3a–c**.

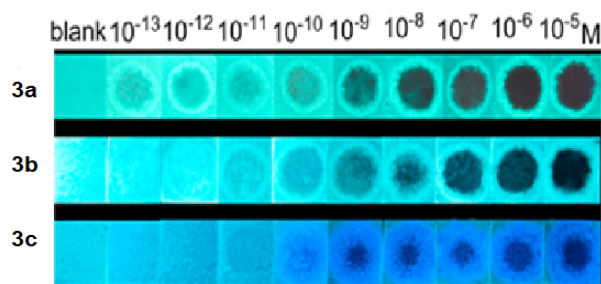


Figure 71. Chemosensor **3a–c**-impregnated paper strips in presence of different concentrations of TNT under UV light (365 nm). Reproduced with permission from reference [131]. Copyright © ACS Publications 2014.

In Section 3.2.3, hyperbranched polyglycidols, as highly fluorescent AIE fluorophores/chemosensors, are reported (Scheme 7) [63]. In aqueous solutions, these chemosensors formed nanoaggregates and exhibited a strong response to PA, with a K_{sv} of $2.27 \times 10^4 \text{ M}^{-1}$ and a LOD of 40 ppb. When impregnated on the surfaces of paper strips, these chemosensors exhibited the intensive quenching of blue fluorescence in response to the presence of PA (0 to $10 \text{ } \mu\text{M}$) (Figure 72).

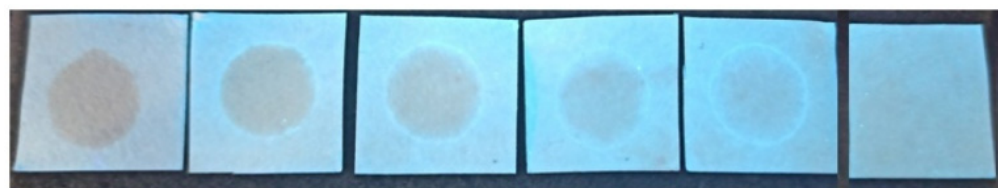


Figure 72. Chemosensor **2**-impregnated paper strips in presence of different concentrations of PA (up to $10 \text{ } \mu\text{M}$) under UV light (365 nm). Reproduced with permission from reference [63]. Copyright © Elsevier 2021.

Zhou and co-authors reported poly(triphenyl)- and poly(tetraphenyl) ethene polymers **P27–28** (Figure 73) as sensory materials for the “turn-off” detection of nitro-explosives [132]. As the first step, polymer films were fabricated from chemosensor **P27** by using drop coating (film thickness of $5.51 \pm 0.36 \mu\text{m}$), spin coating (film thickness of $2.00 \pm 0.24 \mu\text{m}$), and electrospinning (film thickness of $1.61 \pm 0.06 \mu\text{m}$) and from the electrospun chemosensor **P27** (film thickness $1.54 \pm 0.16 \mu\text{m}$). Due to the larger contact surface (S_{BET} value of $120 \text{ m}^2 \text{ g}^{-1}$ for the electrospun film of chemosensor **P27** vs. $S_{\text{BET}} = 6 \text{ m}^2 \text{ g}^{-1}$ for the drop-casted film), after exposure to DNT vapor, fluorescence quenching of 68% in 2 min and 75% in 4 min was observed, while for TNT, 35% fluorescence quenching in 4.0 min and 69% in 20 min was detected. To extend the practical application, paper strips were fabricated from the polymer more responsive to nitro-explosives, polymer **P28**, by means of fabricating a suspension of nanoparticles, followed by their deposition on paper strips with a polymer surface concentration as low as $1.0 \mu\text{g cm}^{-2}$. And these strips were effective in detecting various nitro-compounds at a scale less than 1 ng (Figure 74).

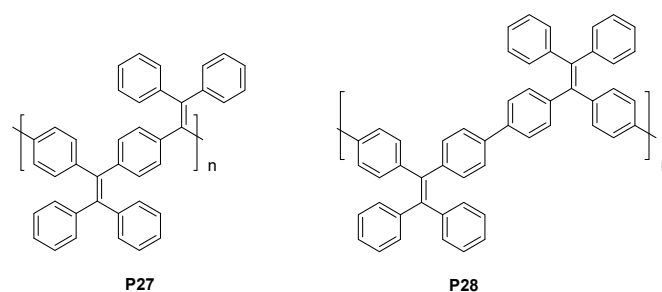


Figure 73. Structures of poly(triphenyl)- and poly(tetraphenyl) ethene polymers **P27–28**.

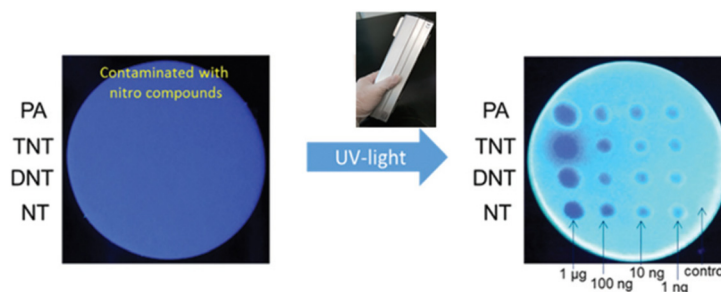


Figure 74. Detection limit of the paper sensor **P27** for nitro-compounds (PA, TNT, DNT, and NT). The images of the paper sensor are under UV light radiation (365 nm). Reproduced with permission from reference [132]. Copyright © Royal Society of Chemistry 2016.

Wang and co-authors reported [133] di-, tri-, and tetraphenylethylen-based polymers **P29–31** (Figure 75). According to the obtained results, the porosity of the obtained polymer strongly depends on the substitution degree of ethylene. Thus, compared with polymer **P29** ($S_{\text{BET}} = 603 \text{ m}^2 \text{ g}^{-1}$, total pore volume $V_{\text{total}} = 1.01 \text{ cm}^3 \text{ g}^{-1}$, micropore surface area $S_{\text{micro}} = 60 \text{ m}^2 \text{ g}^{-1}$, micropore volume $V_{\text{micro}} = 0.02 \text{ cm}^3$, $V_{\text{micro}}/V_{\text{total}} = 0/02$), polymers **P30** and **P31** exhibited enhanced porosities, with S_{BET} of 747 (**P30**) and $848 \text{ m}^2 \text{ g}^{-1}$ (**P31**), V_{total} of 1.50 (**P30**) and $0.86 \text{ cm}^3 \text{ g}^{-1}$ (**P29**), and higher microporous properties, with S_{micro} of up to $451 \text{ m}^2 \text{ g}^{-1}$ (**P31**) and V_{micro} of $0.21 \text{ cm}^3 \text{ g}^{-1}$ (**P31**). In an ethanol solution, polymer **P30** exhibited dramatic fluorescence quenching, with Stern–Volmer constants (K_{sv}) of 494 M^{-1} (NT), 1930 M^{-1} (DNT), $21,980 \text{ M}^{-1}$ (TNT), 638 M^{-1} (NP), 2100 M^{-1} (DNP), and $24,140 \text{ M}^{-1}$ (PA).

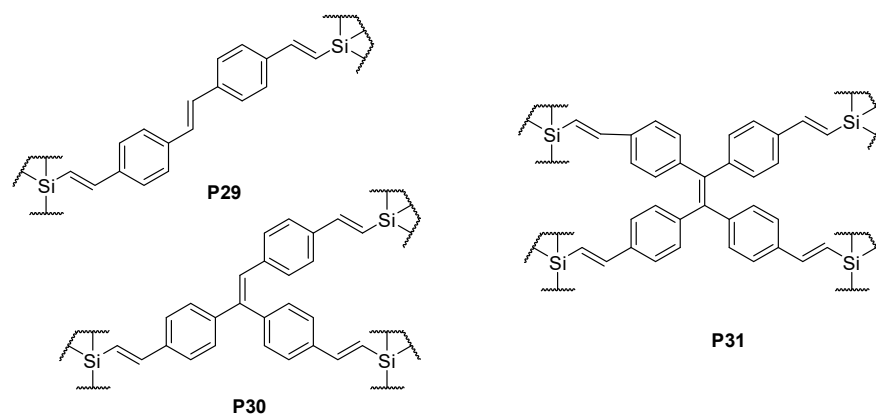


Figure 75. Structures of di-, tri- and tetraphenylene-based polymers **P29–31**.

As the next step, a fluorescent paper sensor was fabricated by means of the simple vacuum filtration of a **P30** dispersion in ethanol, followed by washing and natural drying (Figure 76). The resultant paper sensor was found to be sensitive to explosives in the solution, solid, and vapor phases, with a rapid response time of <10 s, by visually observing the fluorescence-quenching phenomenon. Moreover, this paper sensor was more sensitive to NT ($K_{sv} = 578 \text{ M}^{-1}$, LOD 57.3), DNT ($K_{sv} = 3260 \text{ M}^{-1}$, LOD = 43.39), and DNP ($K_{sv} = 3630 \text{ M}^{-1}$, LOD = 40.84), and it was fully recyclable with a desirable fluorescence recovery ratio, which was higher than 75% after 10 cycles of detection and recycling.

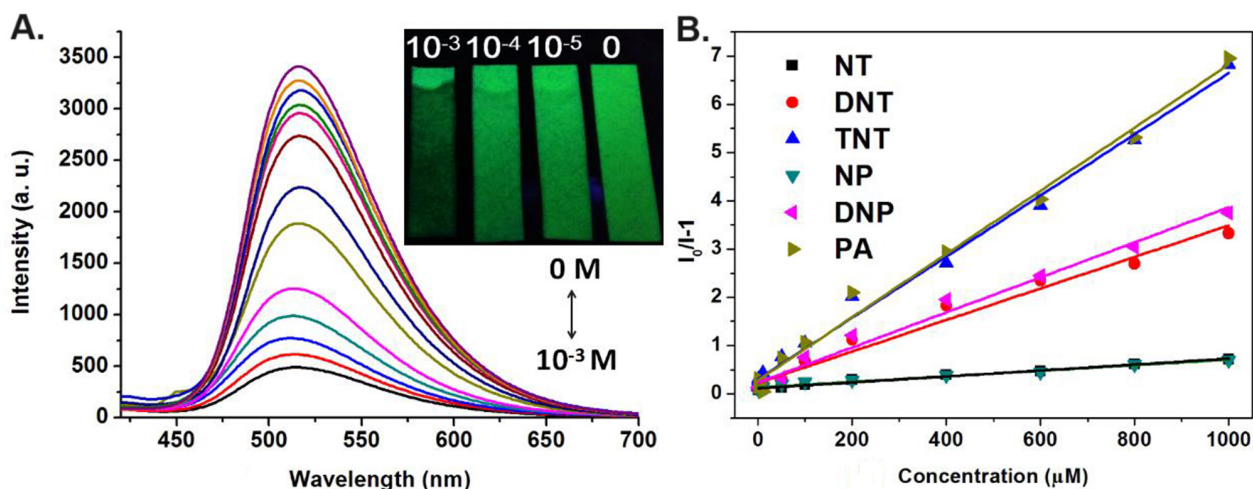


Figure 76. (A) Fluorescence-quenching spectra of paper sensors based on polymer **P30** with different concentrations of PA ($0\text{--}1 \times 10^{-3} \text{ mol/L}$) ($\lambda_{ex} = 365 \text{ nm}$); inset: photos of paper sensors under UV light (365 nm); (B) Stern–Volmer plots for paper sensors in the presence of NT, DNT, TNT, NB, DNP, and PA. Reproduced with permission from reference [133]. Copyright © Elsevier 2018.

Liang and co-authors reported a paper-supported sensory material based on spirofluorene-9,9'-xantene **4** (Figure 77) that was highly fluorescent in the solid state [134]. This sensory material exhibited a quantitative fluorescence “Turn-off” response to PA in solution with a low detection limit of up to 0.12 nmol/cm^2 (the response was analyzed by means of the variation in fluorescent images in grayscale). Simplicity and reliability, as well as good thermal stability at temperatures up to $100 \text{ }^\circ\text{C}$, are the most attractive features of the reported material.

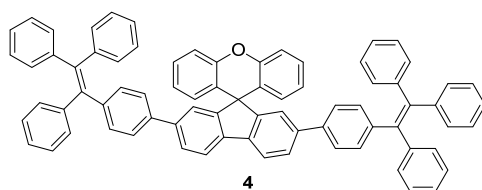


Figure 77. Structure of spirofluorene-9,9'-xantene **4**.

A separate group of sensors for nitroanalytes immobilized on paper carriers comprises polyacrylates containing fluorescent end groups. Thus, Ming Hui Chua and colleagues described a number of polymers containing AIE-active fragments of 3,6-bis(1,2,2-triphenylvinyl)carbazole **P32** and bis(4-(1,2,2-triphenylvinyl)phenyl)amine **P33** linked to the polymer backbone via a flexible alkyl chain (Figure 78) [50]. Paper sensors were also made for the solid-state detection of explosives.

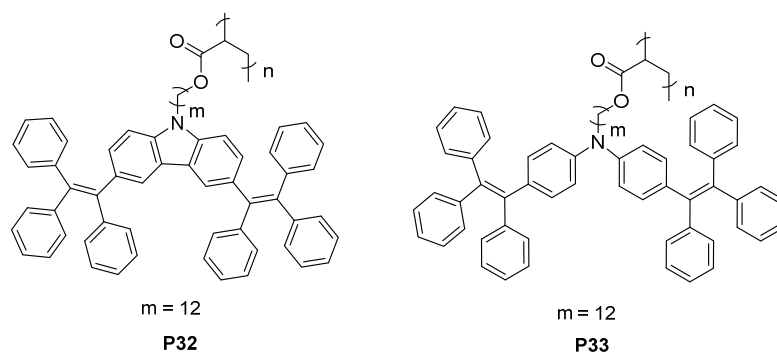


Figure 78. Polymers containing AIE-active fragments of 3,6-bis(1,2,2-triphenylvinyl)carbazole **P32** and bis(4-(1,2,2-triphenylvinyl)phenyl)amine **P33**.

Polymers **P32** and **P33** exhibited good performance for the detection of TNT with a LOD of 10^{-4} M, which was, however, lower than that for PA and 4-NT (Figure 79).

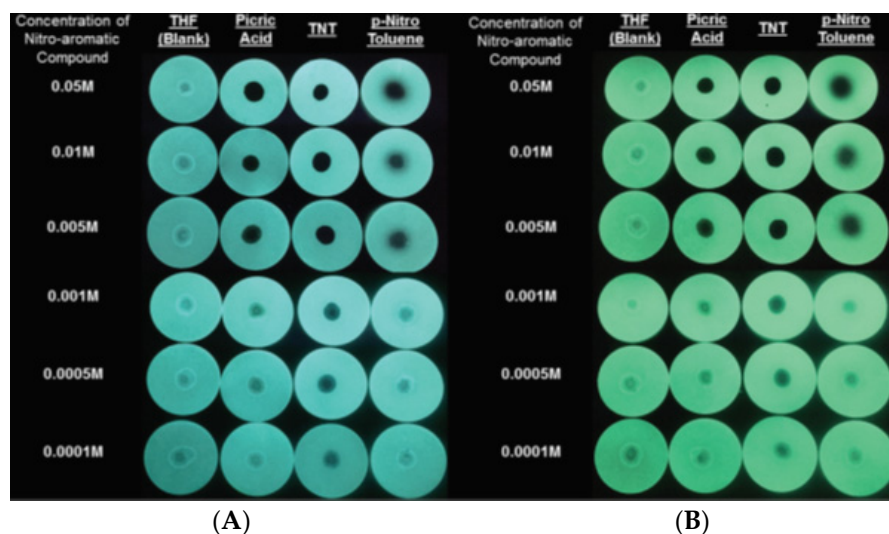


Figure 79. Fluorescence quenching of polymer-coated filter paper (A) **P32** and (B) **P33** at different concentrations of picric acid, TNT, and *p*-nitrotoluene. Reproduced with permission from reference [50]. Copyright © Wiley 2017.

The authors also studied the ability of the above-mentioned paper-based sensors to detect dispersions of nitro-explosives in air (dust) by means of the direct contact of a nitro-explosive-contaminated gloved finger with the surface of polymer-coated filter paper probes. Fluorescence quenching was observed for coated filter paper probes **P32** and **P33** when exposed to a UV lamp (365 nm), as shown in Figure 80. At the same time, mechanical action on the sensor in the absence of nitro-explosive dust does not lead to the quenching of its fluorescence.

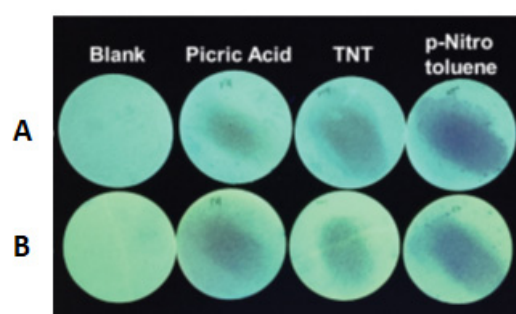


Figure 80. Fluorescence quenching of polymer-coated filter paper (A) **P32** and (B) **P33** with the dust of nitroaromatic explosives. Reproduced with permission from reference [50]. Copyright © Wiley 2017.

Another polyacrylate-based polymer, **P34**, was reported by Lu and co-authors (Figure 81) [135]. The paper-based sensory material was prepared by means of the direct impregnation of filter paper with a solution of **P34**. According to the authors, due to the presence of pyrene moieties and oxygen groups, the obtained paper-based material would provide both a good driving force for the transport of NACs inside the material and good interaction contact with pyrene moieties via π - π stacking to result in dramatic fluorescence quenching (Figure 82a).

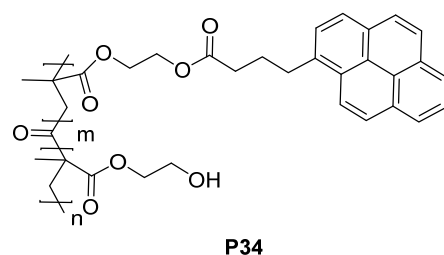


Figure 81. Polyacrylate-based polymer **P34**.

Upon the treatment of a paper sensor with a solution of NACs, a “turn-off” response was observed after 5 s (in the case of TNT) or longer periods (in the case of DNT and NB) (Figure 82c). These results show that the developed paper sensors provide a much faster fluorescence response than their counterparts on quartz plates. It was also shown that the change in fluorescence was recorded by test strips at TNT concentrations up to 1 ppm (Figure 82d).

In addition to organic solutions, the ability of the test strips to detect NACs in water was also demonstrated (Figure 83). Again, the best results were observed for TNT.

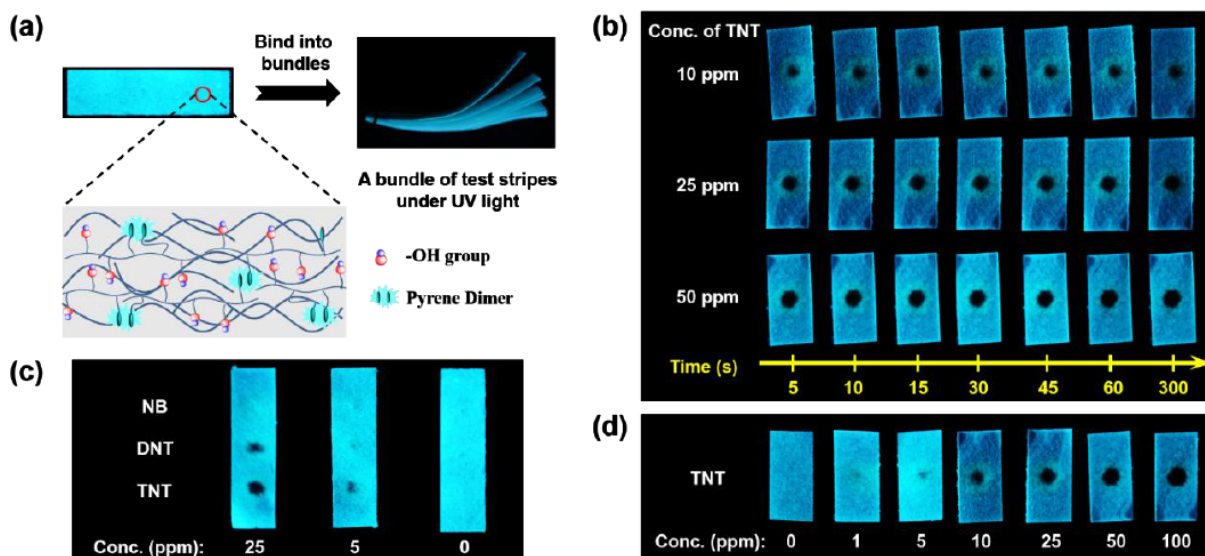


Figure 82. (a) Photographs of test strips based on polymer 8 on cellulose paper substrates taken in UV light at a wavelength of 365 nm, as well as their schematic representation; (b) fluorescence photographs of paper sensors based on polymer P34 at various durations (5~300 s) after adding 5 µL of aqueous solutions of various concentrations to these paper sensors at room temperature; (c) comparison of fluorescence quenching of sensors based on polymer P34 under the action of TNT, DNT, and NB; (d) fluorescence quenching of sensors based on polymer P34 caused by aqueous solutions of TNT at various concentrations. Reproduced with permission from reference [135]. Copyright © ACS Publications 2017.

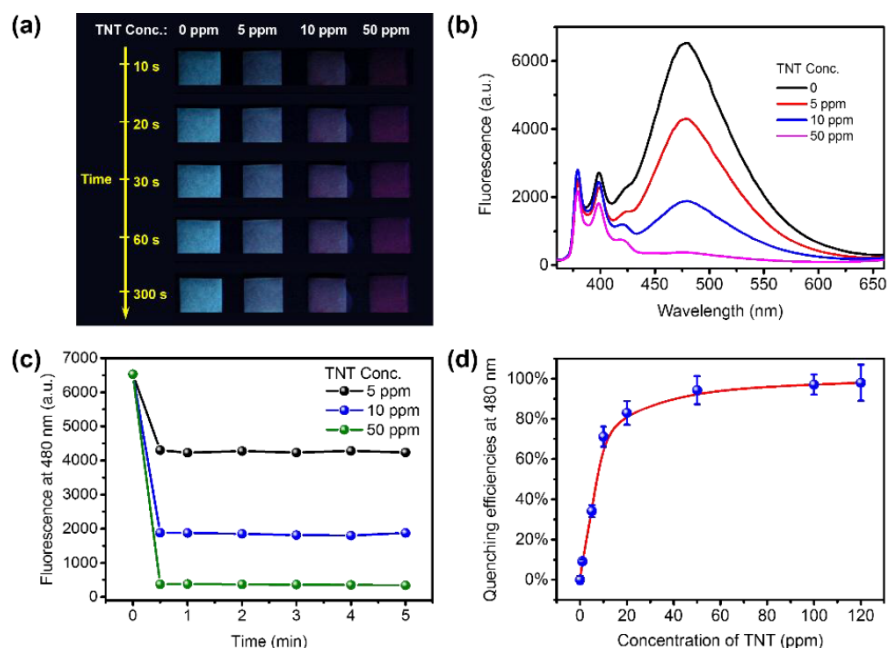


Figure 83. (a) Photographs of fluorescence quenching of paper sensors based on polymer P34 for various durations (10~300 s) after the test paper was immersed in aqueous solutions of TNT at various concentrations at room temperature; (b) fluorescent titration spectra of paper sensors based on sensor 8 after treatment with aqueous solutions of TNT at various concentrations; (c) profiles of radiation intensity of paper sensors based on polymer P34 as a function of time in the presence of TNT at various concentrations (5, 10, and 50 ppm); (d) extinguishing efficiency values of paper sensors at 480 nm as a function of TNT concentration in the range from 0 to 120 ppm. Reproduced with permission from reference [135]. Copyright © ACS Publications 2017.

In 2022, the pyrene-based porous aromatic polymer **P35** was reported (Figure 84) [136].

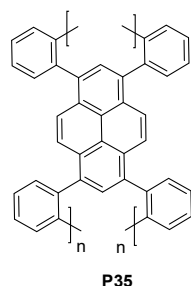


Figure 84. Pyrene-based porous aromatic polymer **P35**.

P35 exhibited strong blue fluorescence with a quantum yield of 18.31%, as well as excellent light and heat resistance. Due to the high-lying LUMO level, polymer **P35** exhibited a strong “turn-off” response to common NACs, with a detection limit (LOD) $\approx 1.47 \times 10^{-5}$ M. When impregnated with **P35**, the paper-based sensor exhibited a visual response to nitrobenzene vapor within 10 s (Figure 85A), as well as nitrobenzene-contaminated dust (Figure 85B) and nitrobenzene solutions (Figure 85C).

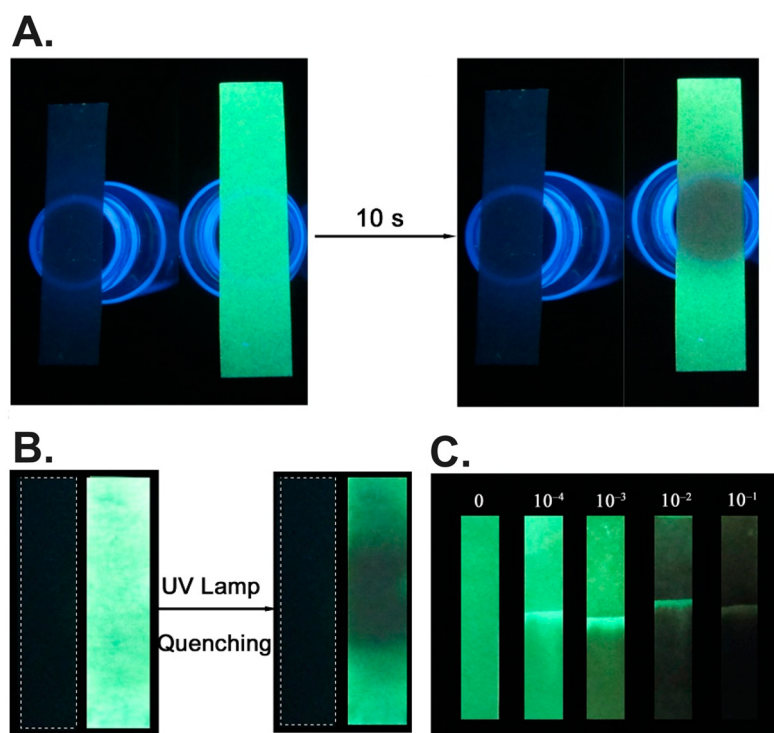


Figure 85. (A) Fluorescence photo of indicator paper with polymer **P35** after contact with gaseous nitrobenzene; (B) upon detection of nitrobenzene in the form of dust; (C) in the presence of various concentrations of liquid nitrobenzene. Reproduced with permission from reference [136]. Copyright © MDPI 2022.

Hussain and co-authors reported benzo[ghi]perylene- and coronene-based excimer probes for the selective sensing of NACs [137]. These two compounds are polyaromatic hydrocarbons (PAHs) and tend to form excimers/nanoaggregates, which was observed in an ethanol/water (1:4) mixture. In fluorescence spectra, monomer–excimer dual emissions were detected. As the next step, fluorescent paper strips were prepared by means of impregnating filter paper with solutions of the above-mentioned PAHs. As a result, the thus-obtained materials exhibited strong excimer quenching upon the addition of a drop of

a PA solution at various concentrations (Figure 86). According to the authors, the observed detection range for PA varied from 0.1 to 120 μM PA (22.9 ppb–27.5 ppm). In addition, the authors tested for the presence of a response to non-explosive compounds, such as volatile organic solvents, including aromatics (toluene, xylene, and ethylbenzene), as well as acids and bases. As a result, it was shown that the fluorescence of the strips remained unchanged, which demonstrates the high selectivity of this test system for foreign substances.

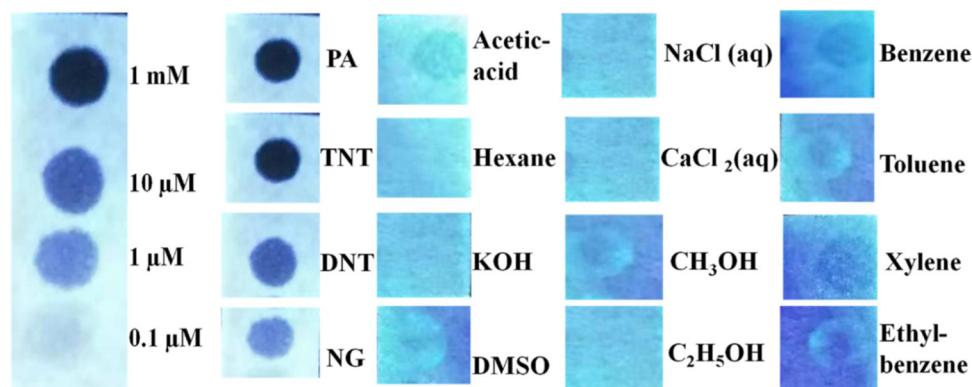


Figure 86. PA detection down to 0.1 μM with fluorescent paper strips (left) and strip selectivity for interfering compounds. Reproduced with permission from reference [137]. Copyright © Elsevier 2020.

We reported a series of pyrene derivatives 5–8, as well as micelle-like aggregates/preaggregates 9–10 obtained from 7 by means of the introduction of surface-active hydrophilic “heads” onto the periphery of lipophilic “tails” (Figure 87) [138]. As a result, in aqueous solutions at a concentration of 10^{-5} M, the formation of highly fluorescent micelle-like aggregates/preaggregates was observed.

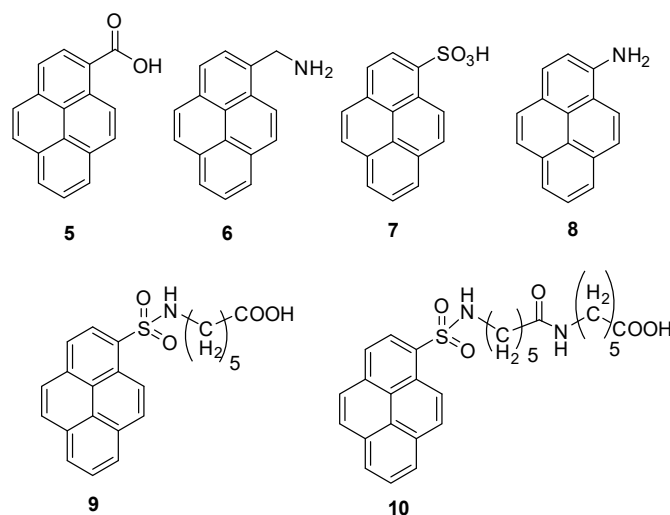


Figure 87. Pyrene derivatives 5–8 and micelle-like aggregates/preaggregates 9–10.

For all of the chemosensors, in the presence of NACs, improved fluorescence quenching was achieved with Stern–Volmer quenching constants close to 10^5 M^{-1} and a detection limit of only 182 ppb, and the most hydrophilic probes, 9–10, showed a higher response to 2,4-DNT than to TNT. As the next step, paper strips impregnated with 10^{-5} M solutions of 5–10 were fabricated. These paper strips were capable of the “turn-off” fluorescence detection of TNT, 2,4-DNT, and other nitro-explosives at a level of 50 ppb in water for 10 s (Figure 88).

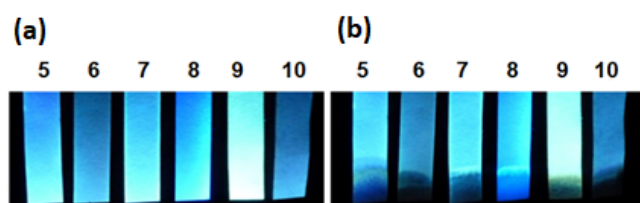


Figure 88. (a) Paper strips impregnated with aqueous solutions of sensors 5–10 in UV light; (b) the same paper strips after brief contact (10 s) with a solution of TNT in water (50 ppb) under UV light. Reproduced with permission from reference [138]. Copyright © Wiley 2016.

In addition to PAHs, a significant number of examples of paper sensors for nitro-analytes based on fluorophores bearing residues of nitrogen-containing heterocycles are described in the literature. Thus, a group of researchers from India reported a polymer cationic sensor, poly(3,3'-((2-phenyl-9H-fluorene-9,9-diyl)bis(hexane-6, 1-diyl))bis(1-methyl-1H-imidazol-3-yl)bromide), **P36**, for the subsequent preparation of nanoparticles (Figure 89) [38].

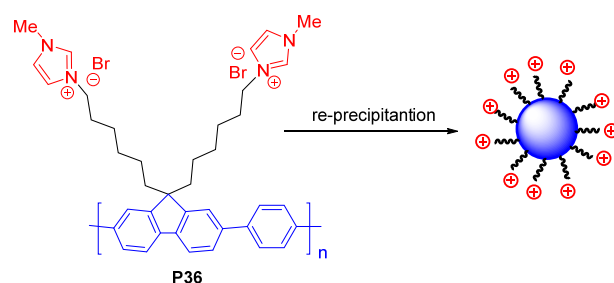


Figure 89. Structure of newly synthesized polymer **P36** and its corresponding nanoparticles.

The authors described experiments on the detection of PC vapor with the contact method using fluorescent paper strips based on the obtained polymer, **P36** (Figure 90). The ability of the sample to detect PC in vapor with a concentration up to 10^{-11} M and a detection limit of 22.9 fg/cm^2 was shown, which makes it one of the best indicators among the sensors described in the literature. The authors attributed the observed oversensitivity mechanism of the PA detection probe to the “molecular wire effect” and electrostatic interactions, combined with PET and possibly RET mechanisms.

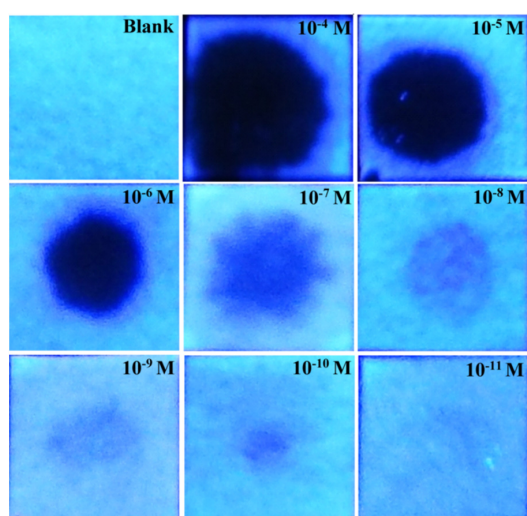


Figure 90. Photos of fluorescent test strips based on polyelectrolyte **P36** in UV light after adding $10 \mu\text{L}$ of various concentrations of PA. Reproduced with permission from reference [38]. Copyright © ACS Publications 2015.

Mao Xia Guo et al. reported a representative of the class of luminescent organometallic gels based on a complex of trivalent aluminum with 4-[2,2':6',2''-terpyridine]-4'-ylbenzoic acid (Figure 91) [139].

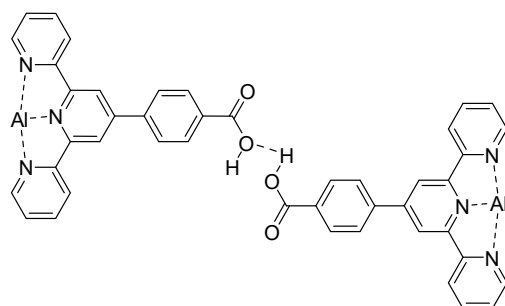


Figure 91. Complex of trivalent aluminum with 4-[2,2':6',2''-terpyridine]-4'-ylbenzoic acid.

The authors reported the ability of the complex to selectively recognize hydroxyl nitroaromatic compounds, including those in mixtures with other analytes that do not contain OH groups. The quenching of the fluorescence of test paper sensors based on the complex at 467 nm by PA solutions with different concentrations is described. As shown in Figure 92, the fluorescence intensity of the test paper gradually decreased with an increase in the concentration of teardrop-shaped PA from 10^{-5} M.

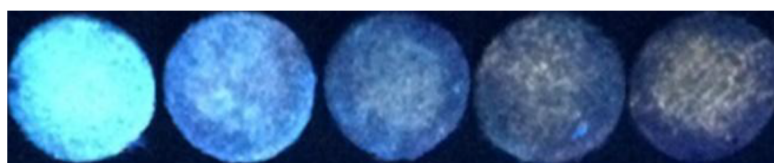


Figure 92. Paper-based sensory material for recognition of PA in solutions with varying concentrations (from left to right): control sample; 1.0×10^{-5} ; 5.0×10^{-5} ; 1.0×10^{-4} ; 2.0×10^{-4} M ($\lambda_{\text{ex}} = 365$ nm). Reproduced with permission from [139]. Copyright © Elsevier 2017.

Guo and colleagues described the copolymer **P37** based on *N*-hexylcarbazole and tetraphenylsilane for the detection of nitroaromatic compounds (Figure 93) [140]. In addition to fluorescent and sensory properties, among the advantages of the polymer, the authors emphasize the high glass transition temperature and good thermal stability of the resulting copolymer.

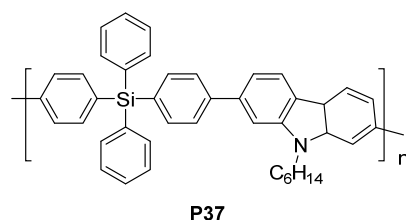


Figure 93. Copolymer **P37** based on *N*-hexylcarbazole and tetraphenylsilane.

For potential in-field applications, **P37**-copolymer-based paper strips were fabricated for experiments on the detection of PA in solutions and vapors. According to Figure 94, with an increase in the concentration of PA in solution up to 1000 $\mu\text{g/mL}$, the progressive quenching of the fluorescence of the sample is observed. However, it is noted that apparent quenching is unambiguously recognizable at a concentration of 0.01 $\mu\text{g/mL}$ PA in solution. In addition, the quenching of the image emission under the influence of TNP vapor for 25 min is shown.

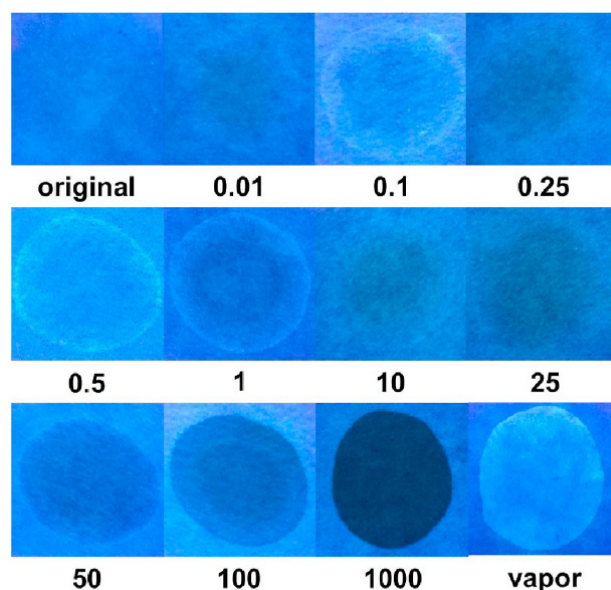


Figure 94. Paper strips based on copolymer before and after contact with THF solution (concentrations: 0.01, 0.1, 0.25, 0.5, 1, 10, 25, 50, 100, and 1000 $\mu\text{g}/\text{mL}$) and after storage over THF vapor for 25 min at 365 nm excitation. Reproduced with permission from reference [140]. Copyright © Elsevier 2021.

In 2016, a fluorescent complex of Al^{3+} and bis(8-hydroxyquinoline) (**Bhq-AI**) was prepared and applied for the detection of PA (TNP) [141]. In a formamide solution, this complex formed a suspension with an emission peak at 519 nm upon excitation at 388 nm. In the presence of TNP (90.9 μM), the fluorescence intensity of **Bhq-AI** was reduced by 83.1%. As the next step, the paper-based sensor was prepared by means of the impregnation of filter paper with a solution of **Bhq-AI**, and it was shown that the quenching of the sensor emission was noticeable at a concentration of 2 μM TNP (Figure 95).

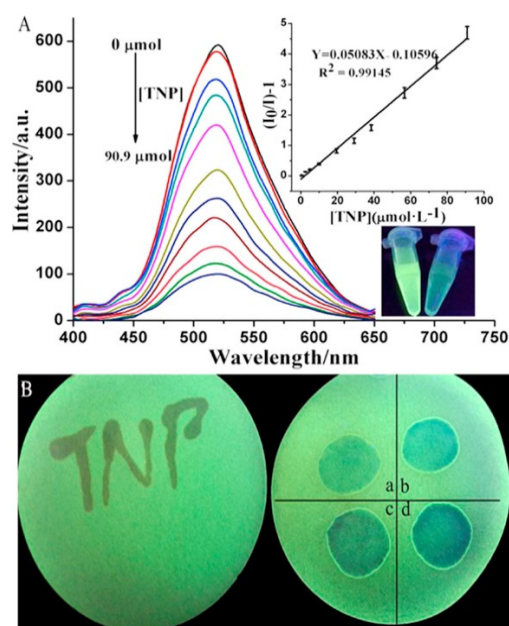


Figure 95. (A) Fluorescence quenching of the suspension of **Bhq-AI** in the presence of TNP; (B) fluorescence quenching of paper-based material upon deposition of TNP at various concentrations. Reproduced with permission from reference [141]. Copyright © Elsevier 2016.

A Canadian–Egyptian research team [142] developed a fluorescent organometallic framework based on zeolitic imidazole (ZIF-8) doped with fluorescent 8-hydroxyquinoline zinc (ZnQ) (Figure 96). In comparison with the fluorescence of ZnQ at ~ 420 nm, the resulting ZnQ@ZIF-8 exhibited red-shifted emission at ~ 520 nm due to the encapsulation of ZnQ guests inside the ZIF-8 matrix. As the next step, a paper-based sensor was prepared.

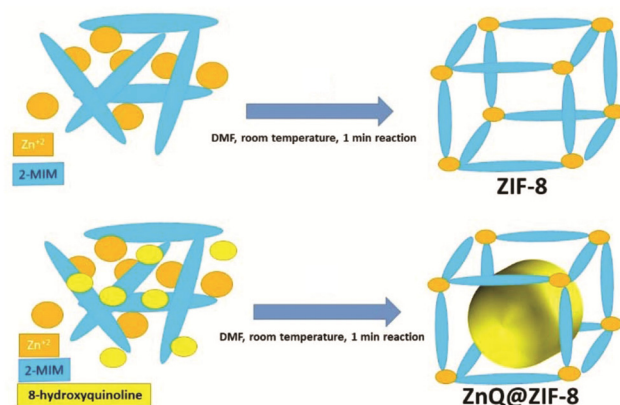


Figure 96. Schematic diagram illustrating the strategy of the in situ encapsulation of ZnQ guest in ZIF-8 voids. Reproduced with permission from reference [142]. Copyright © Royal Society of Chemistry 2020.

When applying various concentrations of TNT, the authors observed a visible color change from ivory to light red in about one minute, indicating an interaction between TNT and ZnQ@ZIF-8, as shown in Figure 97A.

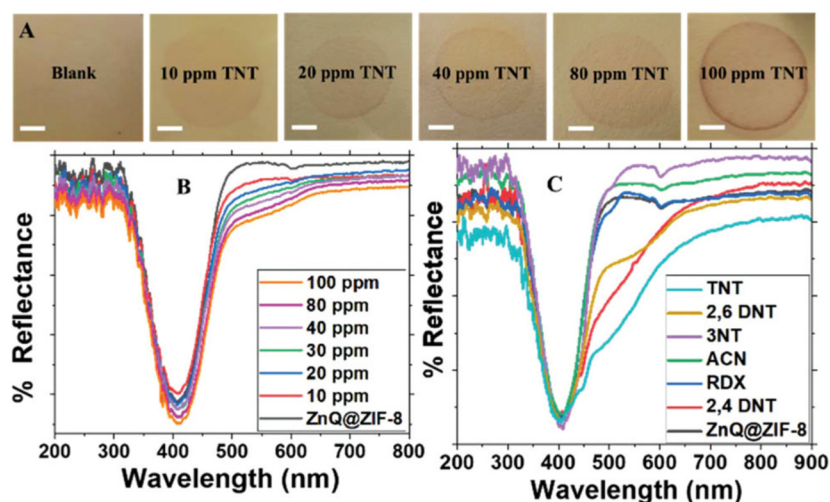


Figure 97. (A) Images of a paper sensor coated with ZnQ@ZIF-8 in contact with solutions of TNT at various concentrations; (B) UV–visible reflectance spectra as a function of TNT concentration; (C) UV–visible reflectance spectra in contact with various nitroaromatic compounds. Reproduced with permission from reference [142]. Copyright © Royal Society of Chemistry 2020.

This interaction proceeds between the electron-deficient aromatic nucleus of TNT and the electron-rich ZnQ@ZIF-8 fragments, which contribute to the formation of a donor–acceptor electron transfer mechanism, which, consequently, causes a color change in the visible range. It is noted that the lowest concentration of TNT that causes a visible color change observed by the naked eye is 3 ppm. As shown in Figure 98B, as the concentration of TNT increases, the absorption of light with a wavelength of about 500 nm increases, resulting in a color change in the visible region. However, UV–visible reflectance mea-

measurements also showed no interaction after the addition of TNT, RDX, and ACN at low concentrations (1000 ppm), as shown in Figure 98C.

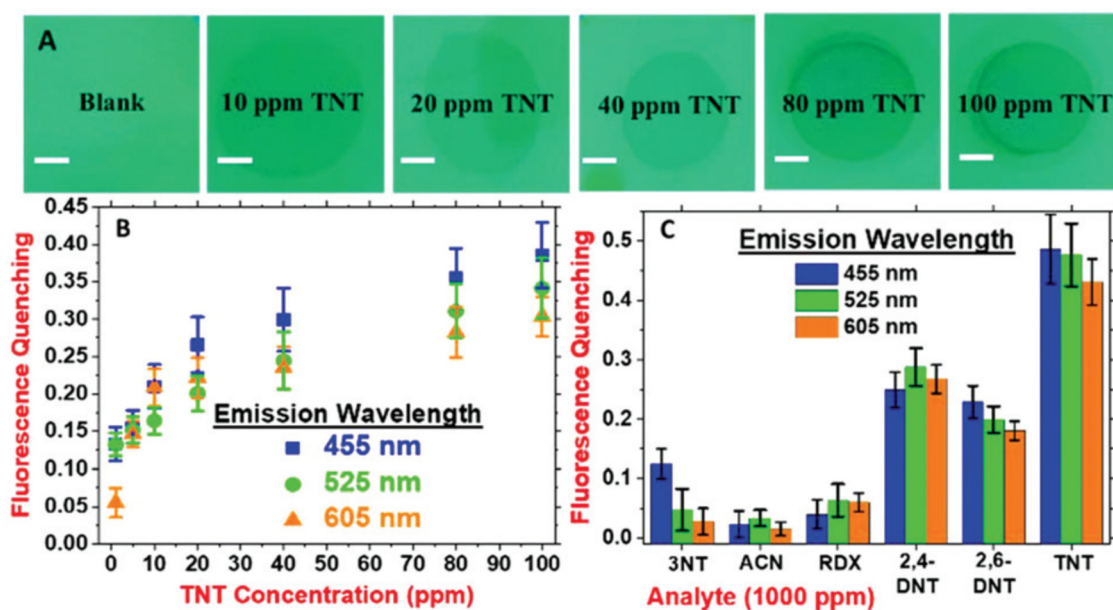


Figure 98. (A) Images of paper sensor coated with ZnQ@ZIF-8 as a function of TNT concentration under UV irradiation ($\lambda_{\text{ex}} = 365 \text{ nm}$); (B) fluorescence quenching at various wavelengths ($\lambda_{\text{em}} = 455 \text{ nm}$, 525 nm , and 605 nm) for a sensor coated with ZnQ@ZIF-8 depending on the TNT concentration from 1 to 100 ppm; (C) fluorescence quenching at different wavelengths ($\lambda_{\text{em}} = 455 \text{ nm}$, 525 nm , and 605 nm) for a ZnQ@ZIF-8-coated sensor upon contact with various nitroaromatic compounds. Reproduced with permission from reference [142]. Copyright © Royal Society of Chemistry 2020.

When exposed to TNT on a paper sensor coated with ZnQ@ZIF-8, fluorescence quenching is also observed upon irradiation with portable UV light ($\lambda_{\text{ex}} = 365 \text{ nm}$) (Figure 98A). A decrease in bluish-green fluorescence was noted as the concentration of TNT increased from 10 to 100 ppm. The fluorescence intensities at different radiation wavelengths ($\lambda_{\text{em}} = 455 \text{ nm}$, 525 nm , and 605 nm) obtained using a fluorescent microscope are shown in Figure 96b. It was noted that the maximum quenching of fluorescence always occurs in the blue emission mode at 455 nm.

The authors also found that the bluish-green fluorescence intensity was not significantly affected by the addition of other nitroaromatic compounds, including TNT, RDX, and ACN, as shown in Figure 98C. However, some changes in fluorescence quenching were noted with the addition of 2,4-DNT and 2,6-DNT, which means that high concentrations of TNT by-products are also detected with this paper sensor. This fact indirectly confirms the emission-quenching mechanism of the described nanomaterial.

In 2021, a Schiff-base-functionalized graphene quantum dot nanocomposite PA sensor (**Schiff-GQD**) was reported (Figure 99) [143]. According to the authors, the fluorescence quantum yield of Schiff-GQD increased to as high as 11.63% (due to the AIE effect), which was higher than that of graphene oxide quantum dots (N-GQDs) (2.71%) and seven times higher than that of triphenylamino-substituted thiophene-2-carbaldehyde (1.51%). As the next step, an electrospun material, Schiff-GQD/PVA, was prepared, and the obtained material exhibited up to 82.5% at a PA concentration of $2.5 \times 10^{-4} \text{ M}$.

More importantly, paper-based Schiff-GQD sensor materials were fabricated using a self-assembly method for the visual detection of PA by immobilization on filter paper (Figure 100a).

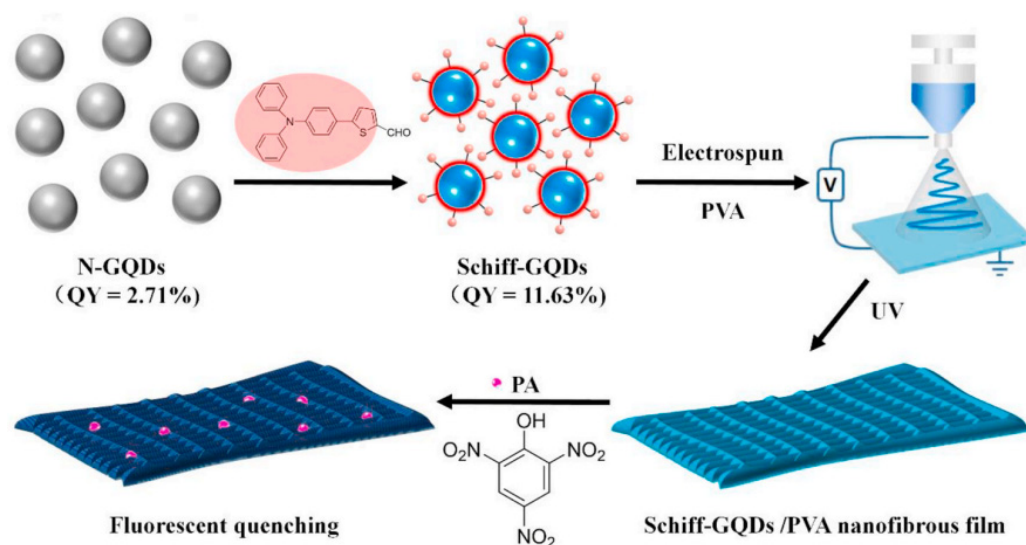


Figure 99. Schematic illustration of the sensitive detection of PA based on Schiff-GQDs. Reproduced with permission from reference [143]. Copyright © Elsevier 2021.

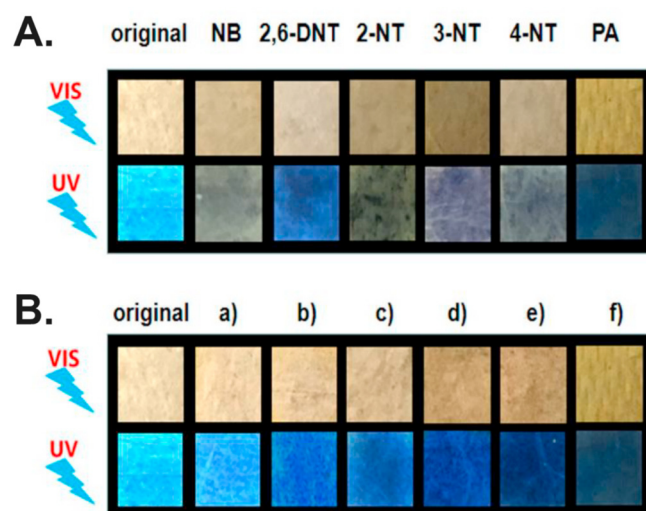


Figure 100. (a A) Visual matrix image of paper-based materials before and after the addition of explosives; (B) test strips based on sensor for visual determination of various concentrations of PA: initial 0 M, (a) 1.0×10^{-6} M, (b) 5.0×10^{-6} M, (c) 1.0×10^{-5} M, (d) 1×10^{-4} M, (e) 2×10^{-4} M, and (f) 4.4×10^{-4} M in visible and 365 nm UV illumination. Reproduced with permission from reference [143]. Copyright © Elsevier 2021.

After contact with various PACs, the test paper showed various color changes, and in the presence of PA, intensive fluorescence and color changes were observed (Figure 100B). As the PA concentration gradually increases, the concentration of the fluorescent indicator paper gradually decreases. The color changes significantly under the influence of UV radiation, and the limit of detection, visible to the naked eye, reaches 11.45 ng/cm^2 .

In rare cases, paper-based matrices can be doped with inorganic luminophores. Thus, in research by a Canadian–German team [144], a paper sensor based on luminescent silicon nanocrystals was reported. For improved selectivity, the surface was functionalized with dodecyl groups, which are sensitive to solutions of nitroanalytes, including RDX and PETN. The results of the experiments (Figure 101) described by the authors show that the sample is more effective at a concentration of 0.01 mM nitroanalytes, while no visible differences in the response were observed for any concentrations of RDX and PETN. In the case of DNT,

however, a sharp increase in quenching is observed in the region surrounding the initial compound spot.

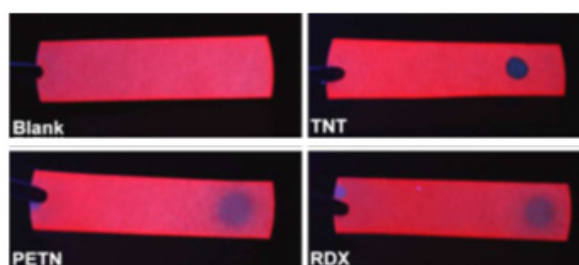


Figure 101. Photographs of luminescent silicon-nanomaterial-coated filter paper under a handheld UV lamp in the presence of solutions of various nitro-explosives. Reproduced with permission from reference [144]. Copyright © Royal Society of Chemistry 2014.

4. Conclusions and Future Perspectives

In the face of growing terroristic threats, one can see an intense interest in improving explosive detection. Of the many detection methods, fluorescence-based methods and materials are among the most promising tools for the detection of (nitro-)explosives due to their high sensitivity and selectivity, fast response time, simplicity, portability, and, in most cases, low cost. Therefore, fluorescence-based sensory materials can be easily and effectively integrated into sensing devices for remote (nitro-)explosive detection, for instance, the well-known Fido explosive detector [145], as well as other types of “electronic noses” [146,147]. In addition, some simpler devices and approaches can be introduced, for instance, mobile-phone-based explosive detection systems [148] or computer-vision-based algorithms [149].

Indeed, fluorescence-based conjugated polymers provide a fast and intensive response and good selectivity and sensitivity to the most common nitro-explosives, such as TNT, DNT, and PA, while in the case of aliphatic nitro-explosives, such as PETN, RDX, and others, these materials exhibit a low or no sensory response. The synthetic preparation of such polymers always requires multi-step synthesis, starting from specially designed monomers, and these issues make the mass production of sensory materials based on the above-mentioned polymers complicated and expensive. Another serious issue is the low durability and low thermo- and photostability of polymers. Finally, in the case of the detection of explosives in the vapor phase, the effectiveness of the sensory response depends strongly on the thickness of the polymer film and/or on the effective contact surface to provide efficient mass exchange. To overcome this issue, porous polymer materials can be introduced; for instance, iptycene-based or molecularly imprinted polymer-based aggregates or nanoparticles can be constructed, or electrospun materials can be used [150,151].

In terms of the mechanical properties of polymers, the impregnation of commercially available polymers with single-molecule sensors [152,153] or sensor arrays [154] or bio-/naturally occurring polymer-based materials can be used [155] as a way to increase the selectivity and sensory response of the polymer materials.

In the case of semiconductive organic polymers, bi-modular sensors for explosive detection can be designed, and these materials can detect explosives in dual modes. In this case, in addition to fluorescence “turn-off” detection, these polymers also show changes in electrochemical properties in the presence of explosives [156]. This results in improved sensing reliability, sensitivity, or selectivity due to the integration of two independent sensing technologies into one sensory material.

Fluorescence “turn-off” (fluorescence quenching) via PET, FRET, the “molecular wire” effect, or even the inner-filter effect is a common and the most understood method for fluorescence-based explosive detection. In this regard, PAH-containing fluorophores may be introduced into the sensory material to provide an excimer/excimer-like-based photo-

luminescence response for explosive detection [157,158]. In addition, the introduction of AIE-genic groups can be used to develop materials for the selective and sensitive detection of some explosives [24]. Finally, there is great promise in developing sensing systems for the detection of nitro-explosives based on a “turn-on” detection mechanism, where nitro-analytes will interrupt/destroy the quenching process, which results in dramatic fluorescence enhancement [159].

Finally, more detailed data are needed for a better interpretation/prediction of explosive-sensing mechanisms and the correlation of the connection between the nature of the sensing material, including its physical and mechanical properties, and the nature of its sensory response and sensing performance. So far, most explosive-sensing materials are made empirically and/or by a method of trial and error. The main reasons for this are the absence of both systematic literature analysis and theoretical methods for the better prediction of electronic and sensing performance for the proper material design.

Author Contributions: Conceptualization, G.V.Z. and B.C.R.; data curation, W.K.A.A.-I., I.L.N., D.S.K., I.S.K., S.S., A.F.K., O.S.T. and L.K.S.; writing—original draft preparation, G.V.Z., W.K.A.A.-I., I.L.N., O.S.T., L.K.S., D.S.K., I.S.K., S.S., A.F.K. and B.C.R.; writing—review and editing, G.V.Z., W.K.A.A.-I., I.L.N., D.S.K., I.S.K., S.S., A.F.K. and B.C.R.; supervision, G.V.Z. and B.C.R.; project administration, G.V.Z. and B.C.R.; funding acquisition, G.V.Z. and B.C.R. All authors have read and agreed to the published version of the manuscript.

Funding: This research was funded by the Council for Grants of the President of the Russian Federation, Grant # NSh-1223.2022.1.3 (Sections 3.4 and 3.9); the Russian Science Foundation, Grant # 21-13-00304 (Section 2.2); the Russian Science Foundation, Grant # 23-13-00318 (Sections 3.2 and 3.3); and the Ministry of Science and Higher Education of the Russian Federation, Reference # 075-15-2022-1118, dated 29 June 2022 (all other sections).

Institutional Review Board Statement: Not applicable.

Informed Consent Statement: Not applicable.

Conflicts of Interest: The authors declare no conflict of interest.

Abbreviations

ACQ	Aggregation-caused quenching
AFP	Amplifying fluorescent polymers
AIE	Aggregation-induced emission
CD	Carbon dots
CP	Conjugated polymer
DNP	Dinitrophenol
DNT	Dinitrotoluene
FRET	Förster resonance energy transfer
K_{SV}	Stern–Volmer constant
LOD	Limits of detection
MIP	Molecularly imprinted polymer
NACs	Nitroaromatic compounds (nitroaromatics)
NB	Nitrobenzene
NT	Nitrotoluene
PA (or TNP)	Picric acid (or trinitrophenol)
PAH	Polycyclic aromatic hydrocarbon
PET	Photoinduced electron transfer
PETN	Pentaerythritol tetranitrate
RDX	Research Department eXplosive (hexagen)
RET	Resonance energy transfer
S_{BET}	Surface of a porous solid material calculated according to Brunauer–Emmett–Teller theory
TNT	Trinitrotoluene
TPE	Tetraphenylethene

References

1. Lazarowski, L.; Waggoner, L.P.; Krichbaum, S.; Singletary, M.; Haney, P.; Rogers, B.; Angle, C. Selecting Dogs for Explosives Detection: Behavioral Characteristics. *Front. Vet. Sci.* **2020**, *7*, 597. [CrossRef]
2. Sigler, N.M. The Theoretical Application and Comparison of the Olfactory Sensory Organs in Swine vs. Canines for Accelerant and Explosives Detection. Honors Theses 390. 2016. Available online: https://encompass.eku.edu/honors_theses/390 (accessed on 21 January 2017).
3. Webb, E.K.; Saccardo, C.C.; Poling, A.; Cox, C.; Fast, C.D. Rapidly training African giant pouched rats (*Cricetomys ansorgei*) with multiple targets for scent detection. *Behav. Process.* **2020**, *174*, 104085. [CrossRef] [PubMed]
4. Corcelli, A.; Lobasso, S.; Lopalco, P.; Dibattista, M.; Araneda, R.; Peterlin, Z.; Firestein, S. Detection of explosives by olfactory sensory neurons. *J. Hazard. Mater.* **2010**, *175*, 1096–1100. [CrossRef] [PubMed]
5. Hodgson, M. *Sniffer Bees: New Flying Squad in War against Terror Archived July 9, 2012, at the Wayback Machine*; The Independent: London, UK, 2006.
6. Trained Wasps May Be Used to Detect Bombs, Bugs, Bodies and More. *Science Daily*, 21 October 2005.
7. Detecting Explosives with Honeybees: Experts Develop Method to Train Air Force of Bomb-Sniffing Bees. *Science Daily*, 29 November 2006.
8. Hall, M. Scientists recruit wasps for war on terror. *USA Today*, 26 December 2005.
9. Saha, D.; Mehta, D.; Altan, E.; Chandak, R.; Traner, M.; Lo, R.; Gupta, P.; Singamaneni, S.; Chakrabartty, S.; Raman, B. Explosive sensing with insect-based biorobots. *Biosens. Bioelectron. X* **2020**, *6*, 100050. [CrossRef]
10. Yinon, J. Chapter 2—Detection of Explosives by Mass Spectrometry. In *Counterterrorist Detection Techniques of Explosives*; Springer: Berlin/Heidelberg, Germany, 2007; pp. 41–59. [CrossRef]
11. Eiceman, G.A.; Schmidt, H.; Cagan, A.A. Chapter 3—Explosives Detection Using Differential Mobility Spectrometry. In *Counterterrorist Detection Techniques of Explosives*; Springer: Berlin/Heidelberg, Germany, 2007; pp. 61–90. [CrossRef]
12. Wang, J. Chapter 4—Electrochemical Sensing of Explosives. In *Counterterrorist Detection Techniques of Explosives*; Springer: Berlin/Heidelberg, Germany, 2007; pp. 91–107. [CrossRef]
13. Senesac, L.; Thundat, T. Chapter 5—Explosive Vapor Detection Using Microcantilever Sensors. In *Counterterrorist Detection Techniques of Explosives*; Springer: Berlin/Heidelberg, Germany, 2007; pp. 109–130. [CrossRef]
14. Lanza, R.C. Chapter 6—Neutron Techniques for Detection of Explosives. In *Counterterrorist Detection Techniques of Explosives*; Springer: Berlin/Heidelberg, Germany, 2007; pp. 131–155. [CrossRef]
15. Miller, J.B. Chapter 7—Nuclear Quadrupole Resonance Detection of Explosives. In *Counterterrorist Detection Techniques of Explosives*; Springer: Berlin/Heidelberg, Germany, 2007; pp. 157–198. [CrossRef]
16. Harding, G.; Harding, A. Chapter 8—X-ray Diffraction Imaging for Explosives Detection. In *Counterterrorist Detection Techniques of Explosives*; Springer: Berlin/Heidelberg, Germany, 2007; pp. 199–235.
17. Sheen, D.M.; McMakin, D.L.; Hall, T.E. Chapter 9—Detection of Explosives by Millimeter-wave Imaging. In *Counterterrorist Detection Techniques of Explosives*; Springer: Berlin/Heidelberg, Germany, 2007; pp. 237–277.
18. Federici, J.F.; Gary, D.; Barat, R.; Michalopoulou, Z.-H. Chapter 11—Detection of Explosives by Terahertz Imaging. In *Counterterrorist Detection Techniques of Explosives*; Springer: Berlin/Heidelberg, Germany, 2007; pp. 323–366. [CrossRef]
19. Munson, C.A.; Gottfried, J.L.; De Lucia, F.C.; McNesby, K.L.; Miziolek, A.W. Chapter 10—Laser-based Detection Methods of Explosives. In *Counterterrorist Detection Techniques of Explosives*; Springer: Berlin/Heidelberg, Germany, 2007; pp. 279–321. [CrossRef]
20. Adegoke, O.; Nic Daeid, N. Colorimetric optical nanosensors for trace explosive detection using metal nanoparticles: Advances, pitfalls, and future perspective. *Emerg. Top. Life Sci.* **2021**, *5*, 367–379.
21. Almog, J.; Zitrin, S. Chapter 4—Colorimetric Detection of Explosives. In *Aspects of Explosives Detection*; Springer: Berlin/Heidelberg, Germany, 2009; pp. 41–58. [CrossRef]
22. Sun, X.; Wang, Y.; Lei, Y. Fluorescence based explosive detection: From mechanisms to sensory materials. *Chem. Soc. Rev.* **2015**, *44*, 8019–8061. [CrossRef] [PubMed]
23. Wu, X.; Tong, H.; Wang, L. Fluorescent Polymer Materials for Detection of Explosives. *Prog. Chem.* **2019**, *31*, 1509–1527.
24. Zhou, H.; Chua, M.H.; Tang, B.Z.; Xu, J. Aggregation-induced emission (AIE)-active polymers for explosive detection. *Polym. Chem.* **2019**, *10*, 3822–3840. [CrossRef]
25. Thomas, S.W., III; Swager, T.M. Chapter 10—Detection of Explosives Using Amplified Fluorescent Polymers. In *Aspects of Explosives Detection*; Springer: Berlin/Heidelberg, Germany, 2009; pp. 203–221. [CrossRef]
26. Batool, R.; Riaz, N.; Junaid, H.M.; Waseem, M.T.; Khan, Z.A.; Nawazish, S.; Farooq, U.; Yu, C.; Shahzad, S.A. Fluorene-Based Fluorometric and Colorimetric Conjugated Polymers for Sensitive Detection of 2,4,6-Trinitrophenol Explosive in Aqueous Medium. *ACS Omega* **2022**, *7*, 1057–1070. [CrossRef]
27. Giri, D.; Patra, S.K. 1,2,3-Triazolyl functionalized thiophene, carbazole and fluorene based A-alt-B type π -conjugated copolymers for the sensitive and selective detection of aqueous and vapor phase nitroaromatics (NACs). *J. Mater. Chem. C* **2020**, *8*, 14469–14480. [CrossRef]
28. Liu, G.; Abdurahman, A.; Zhang, Z.; Feng, Y.; Li, F.; Zhang, M. New three-component conjugated polymers and their application as super rapid-response fluorescent probe to DNT vapor. *Sensors Actuators B Chem.* **2019**, *296*, 126592. [CrossRef]

29. Nailwal, Y.; Devi, M.; Pal, S.K. Luminescent Conjugated Microporous Polymers for Selective Sensing and Ultrafast Detection of Picric Acid. *ACS Appl. Polym. Mater.* **2022**, *4*, 2648–2655. [[CrossRef](#)]
30. Mothika, V.S.; Raupke, A.; Brinkmann, K.O.; Riedl, T.; Brunklaus, G.; Scherf, U. Nanometer-Thick Conjugated Microporous Polymer Films for Selective and Sensitive Vapor-Phase TNT Detection. *ACS Appl. Nano Mater.* **2018**, *1*, 6483–6492. [[CrossRef](#)]
31. Gou, Z.; Zuo, Y.; Tian, M.; Lin, W. Siloxane-Based Nanoporous Polymers with Narrow Pore-size Distribution for Cell Imaging and Explosive Detection. *ACS Appl. Mater. Interfaces* **2018**, *10*, 28979–28991. [[CrossRef](#)]
32. Manna, A.; Das, M.; Mukherjee, S.; Das, S. All-in-One: Sensing, Adsorptive Removal, and Photocatalytic Degradation of Nitro-Explosive Contaminants by Microporous Polycarbazole Polymer. *Macromol. Rapid Commun.* **2021**, *42*, 2000469. [[CrossRef](#)]
33. Gupta, M.; Lee, H.-I. Recyclable Polymeric Thin Films for the Selective Detection and Separation of Picric Acid. *ACS Appl. Mater. Interfaces* **2018**, *10*, 41717–41723. [[CrossRef](#)] [[PubMed](#)]
34. Kumar, V.; Maiti, B.; Chini, M.K.; De, P.; Satapathi, S. Multimodal Fluorescent Polymer Sensor for Highly Sensitive Detection of Nitroaromatics. *Sci. Rep.* **2019**, *9*, 7269. [[CrossRef](#)]
35. Kumar, V.; Saini, S.K.; Choudhury, N.; Kumar, A.; Maiti, B.; De, P.; Kumar, M.; Satapathi, S. Highly Sensitive Detection of Nitro Compounds Using a Fluorescent Copolymer-Based FRET System. *ACS Appl. Polym. Mater.* **2021**, *3*, 4017–4026. [[CrossRef](#)]
36. Chen, X.; Hussain, S.; Abbas, A.; Hao, Y.; Malik, A.H.; Tian, X.; Song, H.; Gao, R. Conjugated polymer nanoparticles and their nano-hybrids as smart photoluminescent and photoresponsive material for biosensing, imaging, and theranostics. *Microchim. Acta* **2022**, *189*, 83. [[CrossRef](#)]
37. MacFarlane, L.R.; Shaikh, H.; Garcia-Hernandez, J.D.; Vespa, M.; Fukui, T.; Manners, I. Functional nanoparticles through π -conjugated polymer self-assembly. *Nat. Rev. Mater.* **2021**, *6*, 7–26. [[CrossRef](#)]
38. Malik, A.H.; Hussain, S.; Kalita, A.; Iyer, P.K. Conjugated Polymer Nanoparticles for the Amplified Detection of Nitro-explosive Picric Acid on Multiple Platforms. *ACS Appl. Mater. Interfaces* **2015**, *7*, 26968–26976. [[CrossRef](#)]
39. Ouyang, T.; Guo, X.; Cui, Q.; Zhang, W.; Dong, W.; Fei, T. Conjugated Polymer Nanoparticles Based on Anthracene and Tetraphenylethene for Nitroaromatics Detection in Aqueous Phase. *Chemosensors* **2022**, *10*, 366. [[CrossRef](#)]
40. Wang, T.; Zhang, N.; Bai, R.; Bao, Y. Aggregation-enhanced FRET-active conjugated polymer nanoparticles for picric acid sensing in aqueous solution. *J. Mater. Chem. C* **2018**, *6*, 266–270. [[CrossRef](#)]
41. Wu, X.; Hang, H.; Li, H.; Chen, Y.; Tong, H.; Wang, L. Water-dispersible hyperbranched conjugated polymer nanoparticles with sulfonate terminal groups for amplified fluorescence sensing of trace TNT in aqueous solution. *Mater. Chem. Front.* **2017**, *1*, 1875–1880. [[CrossRef](#)]
42. Luo, J.; Xie, Z.; Xie, Z.; Lam, J.W.Y.; Cheng, L.; Chen, H.; Qiu, C.; Kwok, H.S.; Zhan, X.; Liu, Y.; et al. Aggregation-induced emission of 1-methyl-1,2,3,4,5-pentaphenylsilole. *Chem. Commun.* **2001**, *18*, 1740–1741. [[CrossRef](#)] [[PubMed](#)]
43. Sanchez-Ruiz, A.; Sousa-Herves, A.; Barrilero, J.T.; Navarro, A.; Garcia-Martinez, J.C. Aggregation-induced emission properties in fully π -conjugated polymers, dendrimers, and oligomers. *Polymers* **2021**, *13*, 213. [[CrossRef](#)]
44. Hu, R.; Qin, A.; Tang, B.Z. AIE polymers: Synthesis and applications. *Prog. Polym. Sci.* **2020**, *100*, 101176. [[CrossRef](#)]
45. Malik, A.H.; Habib, F.; Qazi, M.J.; Ganayee, M.A.; Ahmad, Z.; Yatoo, M.A. A short review article on conjugated polymers. *J. Polym. Res.* **2023**, *30*, 115. [[CrossRef](#)]
46. Han, T.; Wang, X.; Wang, D.; Tang, B.Z. Functional Polymer Systems with Aggregation-Induced Emission and Stimuli Responses. *Top. Curr. Chem.* **2021**, *379*, 7. [[CrossRef](#)]
47. Chu, Z.; Fan, Z.; Zhang, X.; Tan, X.; Li, D.; Chen, G.; Zhao, Q. A Comparison of ACQ, AIE and AEE-Based Polymers Loaded on Polyurethane Foams as Sensors for Explosives Detection. *Sensors* **2018**, *18*, 1565. [[CrossRef](#)]
48. Qi, J.; Hu, X.; Dong, X.; Lu, Y.; Lu, H.; Zhao, W.; Wu, W. Towards more accurate bioimaging of drug nanocarriers: Turning aggregation-caused quenching into a useful tool. *Adv. Drug Deliv. Rev.* **2019**, *143*, 206–225. [[CrossRef](#)]
49. Aldred, M.P.; Li, C.; Zhang, G.-F.; Gong, W.-L.; Li, A.D.Q.; Dai, Y.; Ma, D.; Zhu, M.-Q. Fluorescence quenching and enhancement of vitrifiable oligofluorenes end-capped with tetraphenylethene. *J. Mater. Chem.* **2012**, *22*, 7515–7528. [[CrossRef](#)]
50. Chua, M.H.; Zhou, H.; Lin, T.T.; Wu, J.; Xu, J.W. Aggregation-induced emission active 3,6-bis(1,2,2-triphenylvinyl)carbazole and bis(4-(1,2,2-triphenylvinyl)phenyl)amine-based poly(acrylates) for explosive detection. *J. Polym. Sci. Part A Polym. Chem.* **2017**, *55*, 672–681. [[CrossRef](#)]
51. Huang, W.; Bender, M.; Seehafer, K.; Wacker, I.; Schroder, R.R.; Bunz, U.H.F. A Tetraphenylethene-Based Polymer Array Discriminates Nitroarenes. *Macromolecules* **2018**, *51*, 1345–1350. [[CrossRef](#)]
52. Zhuang, Y.; Yao, J.; Zhuang, Z.; Ni, C.; Yao, H.; Su, D.; Zhou, J.; Zhao, Z. AEE-active conjugated polymers based on di(naphthalen-2-yl)-1,2-diphenylethene for sensitive fluorescence detection of picric acid. *Dye. Pigment.* **2020**, *174*, 108041. [[CrossRef](#)]
53. Jiang, N.; Zhu, D.; Su, Z.; Bryce, M.R. Recent advances in oligomers/polymers with unconventional chromophores. *Mater. Chem. Front.* **2021**, *5*, 60–75. [[CrossRef](#)]
54. Zhang, Y.; Shen, P.; He, B.; Luo, W.; Zhao, Z.; Tang, B.Z. New fluorescent through-space conjugated polymers: Synthesis, optical properties and explosive detection. *Polym. Chem.* **2018**, *9*, 558–564. [[CrossRef](#)]
55. Bai, M.M.; Babu, H.V.; Lakshmi, V.; Rao, M.R. Structure–property–function relationship of fluorescent conjugated microporous polymers. *Mater. Chem. Front.* **2021**, *5*, 2506–2551. [[CrossRef](#)]
56. Hao, H.; Xu, C.; Luo, H.; Yang, J.; Liu, C.; Xu, B.; Shi, G.; Xing, X.; Chi, Z. An AIE luminogen-based electropolymerized film: An ultrasensitive fluorescent probe for TNP and Fe³⁺ in water. *Mater. Chem. Front.* **2021**, *5*, 492–499. [[CrossRef](#)]

57. Liu, H.; Wang, Y.; Mo, W.; Tang, H.; Cheng, Z.; Chen, Y.; Zhang, S.; Ma, H.; Li, B.; Li, X. Dendrimer-Based, High-Luminescence Conjugated Microporous Polymer Films for Highly Sensitive and Selective Volatile Organic Compound Sensor Arrays. *Adv. Funct. Mater.* **2020**, *30*, 1910275. [[CrossRef](#)]
58. Zhu, Y.; Xu, P.; Zhang, X.; Wu, D. Emerging porous organic polymers for biomedical applications. *Chem. Soc. Rev.* **2022**, *51*, 1377–1414. [[CrossRef](#)] [[PubMed](#)]
59. Sengottuvelu, D.; Kachwal, V.; Raichure, P.; Raghav, T.; Laskar, I.R. Aggregation-Induced Enhanced Emission (AIEE)-Active Conjugated Mesoporous Oligomers (CMOs) with Improved Quantum Yield and Low-Cost Detection of a Trace Amount of Nitroaromatic Explosives. *ACS Appl. Mater. Interfaces* **2020**, *12*, 31875–31886. [[CrossRef](#)]
60. Wang, S.; Li, H.; Huang, H.; Cao, X.; Chen, X.; Cao, D. Porous Organic Polymers as a Platform for Sensing Applications. *Chem. Soc. Rev.* **2022**, *51*, 2031–2080. [[CrossRef](#)]
61. Zhang, J.; Xue, F.; Wang, Z. AIE-Active Fluorescent Porous Polymers for Recognizable Detection of Imidacloprid and Structure–Property Relationship. *Chem. Mater.* **2022**, *34*, 10701–10710. [[CrossRef](#)]
62. Nabeel, F.; Rasheed, T.; Mahmood, M.F.; Khan, S.U.-D. Hyperbranched copolymer based photoluminescent vesicular probe conjugated with tetraphenylethene: Synthesis, aggregation-induced emission and explosive detection. *J. Mol. Liq.* **2020**, *308*, 113034. [[CrossRef](#)]
63. Kalva, N.; Tran, C.H.; Lee, M.W.; Augustine, R.; Lee, S.J.; Kim, I. Aggregation-induced emission-active hyperbranched polymers conjugated with tetraphenylethylene for nitroaromatic explosive detection. *Dye. Pigment.* **2021**, *194*, 109617. [[CrossRef](#)]
64. Lang, M.-N.; Chi, W.-W.; Han, T.; Zhao, Q.-Z.; Li, H.-K.; Tang, B.Z.; Li, Y.-F. Synthesis of functional hyperbranched poly(methyltriazolylcarboxylate)s by catalyst-free click polymerization of butynoates and azides. *Chin. J. Polym. Sci.* **2020**, *38*, 1171–1177. [[CrossRef](#)]
65. Yang, J.-S.; Swager, T.M. Porous Shape Persistent Fluorescent Polymer Films: An Approach to TNT Sensory Materials. *J. Am. Chem. Soc.* **1998**, *120*, 5321–5322. [[CrossRef](#)]
66. Yang, J.-S.; Swager, T.M. Fluorescent Porous Polymer Films as TNT Chemosensors: Electronic and Structural Effects. *J. Am. Chem. Soc.* **1998**, *120*, 11864–11873. [[CrossRef](#)]
67. Zhao, D.; Swager, T.M. Sensory Responses in Solution vs. Solid State: A Fluorescence Quenching Study of Poly(Iptycenebutadiynylene)s. *Macromolecules* **2005**, *38*, 9377–9384. [[CrossRef](#)]
68. McQuade, D.T.; Pullen, A.E.; Swager, T.M. Conjugated Polymer-Based Chemical Sensors. *Chem. Rev.* **2000**, *100*, 2537–2574. [[CrossRef](#)]
69. Xu, B.; Wu, X.; Li, H.; Tong, H.; Wang, L. Selective detection of TNT and picric acid by conjugated polymer film sensors with donor–acceptor architecture. *Macromolecules* **2011**, *44*, 5089–5092. [[CrossRef](#)]
70. Lin, Y.; El-Khouly, M.E.; Chen, Y.; Supur, M.; Gu, L.; Li, Y.; Fukuzumi, S. A New Cyanofluorene-Triphenylamine Copolymer: Synthesis and Photoinduced Intramolecular Electron Transfer Processes. *Chem. Eur. J.* **2009**, *15*, 10818–10824. [[CrossRef](#)]
71. Lu, Q.; Cai, W.; Zhang, X.; Yang, C.; Ge, H.; Chen, Y.; Niu, H.; Wang, W. Multifunctional polymers for electrochromic, memory device, explosive detection and photodetector: Donor-acceptor conjugated isoindigo derivatives with strong fluorescence. *Eur. Polym. J.* **2018**, *108*, 124–137. [[CrossRef](#)]
72. Lin, X.; Lu, Q.; Yang, C.; Wang, Y.; Zhang, W.; Li, D.; Gao, Y.; Niu, H.; Wang, W. Multifunctional donor–acceptor conjugated polymers containing isoindigo and benzothiadiazole moieties for electrochromic, photoelectric sensor, 2,4,6-trinitrophenol detection and resistance memory device. *J. Mater. Sci.* **2021**, *56*, 12001–12017. [[CrossRef](#)]
73. Zhang, H.; Tang, B.Z. Through-Space Interactions in Clusteroluminescence. *JACS Au* **2021**, *1*, 1805–1814. [[CrossRef](#)] [[PubMed](#)]
74. Zhang, H.; Zhao, Z.; McGonigal, P.R.; Ye, R.; Liu, S.; Lam, J.W.; Kwok, R.T.; Yuan, W.Z.; Xie, J.; Rogach, A.L.; et al. Clusterization-triggered emission: Uncommon luminescence from common materials. *Mater. Today* **2020**, *32*, 275–292. [[CrossRef](#)]
75. Liu, J.; Wu, F.; Xie, A.; Liu, C.; Bao, H. Preparation of nonconjugated fluorescent polymer nanoparticles for use as a fluorescent probe for detection of 2,4,6-trinitrophenol. *Anal. Bioanal. Chem.* **2020**, *412*, 1235–1242. [[CrossRef](#)]
76. Liu, J.; Fu, T.; Liu, C.; Wu, F.; Wang, H. Sensitive detection of picric acid in an aqueous solution using fluorescent nonconjugated polymer dots as fluorescent probes. *Nanotechnology* **2021**, *32*, 355503. [[CrossRef](#)]
77. Swager, T.M. The Molecular Wire Approach to Sensory Signal Amplification. *Accounts Chem. Res.* **1998**, *31*, 201–207. [[CrossRef](#)]
78. Swager, T.M. Iptycenes in the Design of High Performance Polymers. *Accounts Chem. Res.* **2008**, *41*, 1181–1189. [[CrossRef](#)] [[PubMed](#)]
79. Correa, D.S.; Medeiros, E.S.; Oliveira, J.E.; Paterno, L.G.; Mattoso, L.H.C. Nanostructured Conjugated Polymers in Chemical Sensors: Synthesis, Properties and Applications. *J. Nanosci. Nanotechnol.* **2014**, *14*, 6509–6527. [[CrossRef](#)] [[PubMed](#)]
80. Thomas, S.W.I. *Molecules and Materials for the Optical Detection of Explosives and Toxic Chemicals*; Massachusetts Institute of Technology: Cambridge, MA, USA, 2006.
81. Zhou, Q.; Swager, T.M. Methodology for Enhancing the Sensitivity of Fluorescent Chemosensors: Energy Migration in Conjugated Polymers. *J. Am. Chem. Soc.* **1995**, *117*, 7017–7018. [[CrossRef](#)]
82. Zhou, Q.; Swager, T.M. Fluorescent Chemosensors Based on Energy Migration in Conjugated Polymers: The Molecular Wire Approach to Increased Sensitivity. *J. Am. Chem. Soc.* **1995**, *117*, 12593–12602. [[CrossRef](#)]
83. Levitsky, I.A.; Kim, J.; Swager, T.M. Energy Migration in a Poly(Phenylene Ethynylene): Determination of Interpolymer Transport in Anisotropic Langmuir–Blodgett Films. *J. Am. Chem. Soc.* **1999**, *121*, 1466–1472. [[CrossRef](#)]

84. Mei, J.; Hong, Y.; Lam, J.W.Y.; Qin, A.; Tang, Y.; Tang, B.Z. Aggregation-Induced Emission: The Whole Is More Brilliant than the Parts. *Adv. Mater.* **2014**, *26*, 5429–5479. [[CrossRef](#)]
85. Klanderman, B.H.; Faber, J.W.H. Novel Bridged Anthracene Derivatives and Polyesters and Copolyesters Therefrom. *J. Polym. Sci. Part A-1 Polym. Chem.* **1968**, *6*, 2955–2965. [[CrossRef](#)]
86. Chong, J.H.; MacLachlan, M.J. Iptycenes in Supramolecular and Materials Chemistry. *Chem. Soc. Rev.* **2009**, *38*, 3301–3315. [[CrossRef](#)] [[PubMed](#)]
87. Yang, J.-S.; Lin, C.-S.; Hwang, C.-Y. Cu²⁺-Induced Blue Shift of the Pyrene Excimer Emission: A New Signal Transduction Mode of Pyrene Probes. *Org. Lett.* **2001**, *3*, 889–892. [[CrossRef](#)]
88. Ali, M.A.; Shoaee, S.; Fan, S.; Burn, P.L.; Gentle, I.R.; Meredith, P.; Shaw, P.E. Detection of Explosive Vapors: The Roles of Exciton and Molecular Diffusion in Real-Time Sensing. *ChemPhysChem* **2016**, *17*, 3350–3353. [[CrossRef](#)]
89. Jimenez, E.R.; Rodríguez, H. Aggregation-Induced Emission: A Review of Promising Cyano-Functionalized AIEgens. *J. Mater. Sci.* **2020**, *55*, 1366–1387. [[CrossRef](#)]
90. Yamaguchi, S.; Swager, T.M. Oxidative Cyclization of Bis(Biaryl)Acetylenes: Synthesis and Photophysics of Dibenzo[g,p]Chrysene-Based Fluorescent Polymers [2]. *J. Am. Chem. Soc.* **2001**, *123*, 12087–12088. [[CrossRef](#)]
91. Zahn, S.; Swager, T.M. Three-Dimensional Electronic Delocalization in Chiral Conjugated Polymers. *Angew. Chem. Int. Ed.* **2002**, *41*, 4225–4230. [[CrossRef](#)]
92. Amara, J.P.; Swager, T.M. Synthesis and Properties of Poly(Phenylene Ethynylene)s with Pendant Hexafluoro-2-Propanol Groups. *Macromolecules* **2005**, *38*, 9091–9094. [[CrossRef](#)]
93. Thomas, W.S., III; Amara, J.P.; Bjork, R.E.; Swager, T.M. Amplifying Fluorescent Polymer Sensors for the Explosives Taggant 2,3-Dimethyl-2,3-dinitrobutane (DMNB). *Chem. Commun.* **2005**, *36*, 4572–4574. [[CrossRef](#)]
94. VanVeller, B.; Robinson, D.; Swager, T.M. Triptycene Diols: A Strategy for Synthesizing Planar π Systems through Catalytic Conversion of a Poly(p-Phenylene Ethynylene) into a Poly(p-phenylene vinylene). *Angew. Chem. Int. Ed.* **2012**, *51*, 1182–1186. [[CrossRef](#)]
95. Narayanan, A.; Varnavski, O.P.; Swager, T.M.; Goodson, T. Multiphoton Fluorescence Quenching of Conjugated Polymers for TNT Detection. *J. Phys. Chem. C* **2008**, *112*, 881–884. [[CrossRef](#)]
96. Malval, J.; Leray, I. Photophysical Properties of Poly(Triptycene Vinylene) Derivatives and Effect of Nitrotoluene Exposure. *Chem. Phys. Lett.* **2010**, *501*, 54–58. [[CrossRef](#)]
97. Ansari, M.; Bera, R.; Mondal, S.; Das, N. Triptycene-Derived Photoresponsive Fluorescent Azo-Polymer as Chemosensor for Picric Acid Detection. *ACS Omega* **2019**, *4*, 9383–9392. [[CrossRef](#)]
98. Swager, T.M. *Polymer Electronics for Explosives Detection*; Gardner, W.J., Jehuda, Y., Eds.; Springer: Dordrecht, The Netherlands, 2004; pp. 29–37.
99. Wang, Z. *Design, Synthesis and Characterization of Conjugated Polymers for the Detection of Nitroaromatic Explosives and Isocyanates*; Carleton University: Ottawa, ON, Canada, 2009.
100. Ayyavoo, K.; Velusamy, P. Pyrene Based Materials as Fluorescent Probes in Chemical and Biological Fields. *New J. Chem.* **2021**, *45*, 10997–11017. [[CrossRef](#)]
101. Ghorpade, T.K.; Palai, A.K.; Rath, S.K.; Sharma, S.K.; Sudarshan, K.; Pujari, P.K.; Patri, M.; Mishra, S.P. Pentriptycene-tbutylpyrene Based Poly(arylene-ethynylene)s: Highly Sensitive and Selective TNT Sensor in Aqueous as Well as Vapor Phase. *Sensors Actuators B Chem.* **2017**, *252*, 901–911. [[CrossRef](#)]
102. Sinha, J.; Kumar, A. Syntheses and Characterization of Amplified Fluorescence Poly(Aryleneethynylene)s Based on 3,4-Propylenedioxythiophenes and Their Application in TNT Sensing. *Synth. Met.* **2010**, *160*, 2265–2272. [[CrossRef](#)]
103. Dudhe, R.S.; Sinha, J.; Kumar, A.; Rao, V.R. Polymer Composite-Based OFET Sensor with Improved Sensitivity towards Nitro Based Explosive Vapors. *Sensors Actuators B Chem.* **2010**, *148*, 158–165. [[CrossRef](#)]
104. Ghosh, K.R.; Saha, S.K.; Wang, Z.Y. Ultra-Sensitive Detection of Explosives in Solution and Film as Well as the Development of Thicker Film Effectiveness by Tetraphenylethene Moiety in AIE Active Fluorescent Conjugated Polymer. *Polym. Chem.* **2014**, *5*, 5638–5643. [[CrossRef](#)]
105. Zyryanov, G.V.; Kopchuk, D.S.; Kovalev, I.S.; Nosova, E.V.; Rusinov, V.L.; Chupakhin, O.N. Chemosensors for Detection of Nitroaromatic Compounds (Explosives). *Russ. Chem. Rev.* **2014**, *83*, 783–819. [[CrossRef](#)]
106. Manandhar, E.; Wallace, K.J. Host–Guest Chemistry of Pyrene-Based Molecular Receptors. *Inorganica Chim. Acta* **2012**, *381*, 15–43. [[CrossRef](#)]
107. Demirel, G.B.; Daglar, B.; Bayindir, M. Extremely Fast and Highly Selective Detection of Nitroaromatic Explosive Vapours Using Fluorescent Polymer Thin Films. *Chem. Commun.* **2013**, *49*, 6140–6142. [[CrossRef](#)]
108. Jang, H.-S.; Cho, H.-S.; Uhrig, D.; Nieh, M.-P. Insight into the Interactions between Pyrene and Polystyrene for Efficient Quenching Nitroaromatic Explosives. *J. Mater. Chem. C* **2017**, *5*, 12466–12473. [[CrossRef](#)]
109. Beyazkılıç, P.; Yildirim, A.; Bayindir, M. Formation of Pyrene Excimers in Mesoporous Ormosil Thin Films for Visual Detection of Nitro-Explosives. *ACS Appl. Mater. Interfaces* **2014**, *6*, 4997–5004. [[CrossRef](#)]
110. Ilharco, L.M.; Santos, A.M.; Silva, M.J.; Martinho, J.M.G. Intramolecular Pyrene Excimer Probing the Sol-Gel Process. *Langmuir* **1995**, *11*, 2419–2422. [[CrossRef](#)]

111. Sun, X.; Brückner, C.; Nieh, M.-P.; Lei, Y. A Fluorescent Polymer Film with Self-Assembled Three-Dimensionally Ordered Nanopores: Preparation, Characterization and Its Application for Explosives Detection. *J. Mater. Chem. A* **2014**, *2*, 14613–14621. [[CrossRef](#)]
112. Sun, X.; Liu, Y.; Shaw, G.; Carrier, A.; Dey, S.; Zhao, J.; Lei, Y. Fundamental Study of Electrospun Pyrene–Polyethersulfone Nanofibers Using Mixed Solvents for Sensitive and Selective Explosives Detection in Aqueous Solution. *ACS Appl. Mater. Interfaces* **2015**, *7*, 13189–13197. [[CrossRef](#)]
113. Guo, L.; Zu, B.; Yang, Z.; Cao, H.; Zheng, X.; Dou, X. APTS and rGO co-Functionalized Pyrenated Fluorescent Nanonets for Representative Vapor Phase Nitroaromatic Explosive Detection. *Nanoscale* **2014**, *6*, 1467–1473. [[CrossRef](#)]
114. Shaligram, S.; Wadgaonkar, P.P.; Kharul, U.K. Fluorescent Polymeric Ionic Liquids for the Detection of Nitroaromatic Explosives. *J. Mater. Chem. A* **2014**, *2*, 13983–13989. [[CrossRef](#)]
115. Karadurmus, L.; Bilge, S.; Sinağ, A.; Ozkan, S.A. Molecularly imprinted polymer (MIP)-Based sensing for detection of explosives: Current perspectives and future applications. *TrAC Trends Anal. Chem.* **2022**, *155*, 116694. [[CrossRef](#)]
116. Zarejousheghani, M.; Lorenz, W.; Vanninen, P.; Alizadeh, T.; Cämmerer, M.; Borsdorf, H. Molecularly imprinted polymer materials as selective recognition sorbents for explosives: A review. *Polymers* **2019**, *11*, 888. [[CrossRef](#)] [[PubMed](#)]
117. Lv, P.; Xie, D.; Zhang, Z. Magnetic Carbon Dots Based Molecularly Imprinted Polymers for Fluorescent Detection of Bovine Hemoglobin. *Talanta* **2018**, *188*, 145–151. [[CrossRef](#)] [[PubMed](#)]
118. Xu, S.; Lu, H. Mesoporous structured MIPs@CDs fluorescence sensor for highly sensitive detection of TNT. *Biosens. Bioelectron.* **2016**, *85*, 950–956. [[CrossRef](#)]
119. Murugan, K.; Jothi, V.K.; Rajaram, A.; Natarajan, A. Novel Metal-Free Fluorescent Sensor Based on Molecularly Imprinted Polymer N-CDs@MIP for Highly Selective Detection of TNP. *ACS Omega* **2022**, *7*, 1368–1379. [[CrossRef](#)]
120. Apodaca, D.C.; Turner, N.; Bowyer, M.; Holdsworth, C.Z.; McCluskey, A. Tailoring the Preparation of Fluorescent Molecularly Imprinted Polymers (MIPs) toward the Detection of Chemical Warfare Agents. *Sens. Transducers* **2018**, *28*, 43–53.
121. Gorai, P.; Kumar, S.; Marques, C.; Singh, P.K.; Jha, R. Imprinted Polymer Functionalized Concatenated Optical Microfiber: Hypersensitive and Selective. *IEEE Sensors J.* **2023**, *23*, 329–336. [[CrossRef](#)]
122. Li, Z.; Yang, Y.-W. Conjugated macrocycle polymers. *Polym. Chem.* **2021**, *12*, 4613–4620. [[CrossRef](#)]
123. Chong, H.; Xu, Y.; Han, Y.; Yan, C.; Su, D.; Wang, C. Pillar [5] arene-based “Three-components” Supramolecular Assembly and the Performance of Nitrobenzene-based Explosive Fluorescence Sensing. *ChemistrySelect* **2021**, *6*, 9363–9367. [[CrossRef](#)]
124. Qin, P.; Yang, H.-H.; Zhao, X.-X.; Qu, W.-J.; Yao, H.; Wei, T.-B.; Lin, Q.; Shi, B.; Zhang, Y.-M. A supramolecular polymer network constructed by pillar[5]arene-based host–guest interactions and its application in nitro explosive detection. *J. Incl. Phenom. Macrocycl. Chem.* **2022**, *102*, 295–302. [[CrossRef](#)]
125. Barata, P.D.; Costa, A.I.; Prata, J.V. Calix[4]arene–carbazole-containing polymers: Synthesis and properties. *React. Funct. Polym.* **2012**, *72*, 627–634. [[CrossRef](#)]
126. Costa, A.I.; Ferreira, L.F.; Prata, J.V. Novel fluorescent (p-phenylene ethynylene)-calix[4]arene-based polymer: Design, synthesis, and properties. *J. Polym. Sci. Part A* **2008**, *46*, 6477–6488. [[CrossRef](#)]
127. Barata, P.D.; Prata, J.V. Cooperative Effects in the Detection of a Nitroaliphatic Liquid Explosive and an Explosive Taggant in the Vapor Phase by Calix[4]arene-Based Carbazole-Containing Conjugated Polymers. *ChemPlusChem* **2014**, *79*, 83–89. [[CrossRef](#)]
128. Barata, P.D.; Prata, J.V. Fluorescent calix[4]arene-carbazole-containing polymers as sensors for nitroaromatic explosives. *Chemosensors* **2020**, *8*, 128. [[CrossRef](#)]
129. Lin, H.; Cheng, X.; Yin, M.-J.; Bao, Z.; Wei, X.; Gu, B. Flexible porphyrin doped polymer optical fibers for rapid and remote detection of trace DNT vapor. *Anal.* **2020**, *145*, 5307–5313. [[CrossRef](#)]
130. Lei, T.; Guan, M.; Liu, J.; Lin, H.-C.; Pfattner, R.; Shaw, L.; McGuire, A.F.; Huang, T.-C.; Shao, L.; Cheng, K.-T.; et al. Biocompatible and totally disintegrable semiconducting polymer for ultrathin and ultralightweight transient electronics. *Proc. Natl. Acad. Sci. USA* **2017**, *114*, 5107–5112. [[CrossRef](#)]
131. Feng, H.T.; Wang, J.H.; Zheng, Y.S. CH₃– π Interaction of Explosives with Cavity of a TPE Macrocycle: The Key Cause for Highly Selective Detection of TNT. *ACS Appl. Mater. Interfaces* **2014**, *6*, 20067–20074. [[CrossRef](#)]
132. Zhou, H.; Wang, X.; Lin, T.T.; Song, J.; Tang, B.Z.; Xu, J. Poly(triphenyl ethene) and poly(tetraphenyl ethene): Synthesis, aggregation-induced emission property and application as paper sensors for effective nitro-compounds detection. *Polym. Chem.* **2016**, *7*, 6309–6317. [[CrossRef](#)]
133. Sun, R.; Huo, X.; Lu, H.; Feng, S.; Wang, D.; Liu, H. Recyclable fluorescent paper sensor for visual detection of nitroaromatic explosives. *Sensors Actuators B Chem.* **2018**, *265*, 476–487. [[CrossRef](#)]
134. Yan, C.; Qin, W.; Li, Z.; Zhou, Y.; Cui, Y.; Liang, G. Quantitative and rapid detection of explosives using an efficient luminogen with aggregation-induced emission characteristics. *Sens. Actuators B Chem.* **2020**, *302*, 127201. [[CrossRef](#)]
135. Lu, W.; Zhang, J.; Huang, Y.; Théato, P.; Huang, Q.; Chen, T. Self-Diffusion Driven Ultrafast Detection of ppm-Level Nitroaromatic Pollutants in Aqueous Media Using a Hydrophilic Fluorescent Paper Sensor. *ACS Appl. Mater. Interfaces* **2017**, *9*, 23884–23893. [[CrossRef](#)] [[PubMed](#)]
136. Cui, B.; Gao, C.; Fan, J.; Liu, J.; Feng, B.; Ruan, X.; Yang, Y.; Yuan, Y.; Chu, K.; Yan, Z.; et al. Integrating a Luminescent Porous Aromatic Framework into Indicator Papers for Facile, Rapid, and Selective Detection of Nitro Compounds. *Molecules* **2022**, *27*, 6252. [[CrossRef](#)] [[PubMed](#)]

137. Hussain, E.; Li, Y.; Cheng, C.; Zhuo, H.; Shahzad, S.A.; Ali, S.; Ismail, M.; Qi, H.; Yu, C. Benzo[ghi]perylene and coronene as ratiometric fluorescence probes for the selective sensing of nitroaromatic explosives. *Talanta* **2019**, *207*, 120316. [[CrossRef](#)]
138. Kovalev, I.S.; Taniya, O.S.; Slovesnova, N.V.; Kim, G.A.; Santra, S.; Zyryanov, G.V.; Kopchuk, D.S.; Majee, A.; Charushin, V.N.; Chupakhin, O.N. Fluorescent Detection of 2,4-DNT and 2,4,6-TNT in Aqueous Media by Using Simple Water-Soluble Pyrene Derivatives. *Chem. Asian J.* **2016**, *11*, 775–781. [[CrossRef](#)]
139. Guo, M.X.; Yang, L.; Jiang, Z.W.; Peng, Z.W.; Li, Y.F. Al-based metal-organic gels for selective fluorescence recognition of hydroxyl nitro aromatic compounds. *Spectrochim. Acta Part A Mol. Biomol. Spectrosc.* **2017**, *187*, 43–48. [[CrossRef](#)]
140. Guo, X.; Gao, B.; Cui, X.; Wang, J.; Dong, W.; Duan, Q.; Fei, T.; Su, Z. PL sensor for sensitive and selective detection of 2,4,6-trinitrophenol based on carbazole and tetraphenylsilane polymer. *Dye. Pigment.* **2021**, *191*, 109379. [[CrossRef](#)]
141. Lv, X.J.; Qi, L.; Gao, X.Y.; Wang, H.; Huo, Y.; Zhang, Z.Q. Selective detection of 2,4,6-trinitrophenol based on a fluorescent nanoscale bis (8-hydroxyquinoline) metal complex. *Talanta* **2016**, *150*, 319–323. [[CrossRef](#)] [[PubMed](#)]
142. Abuzalat, O.; Wong, D.; Park, S.S.; Kim, S. Highly selective and sensitive fluorescent zeolitic imidazole frameworks sensor for nitroaromatic explosive detection. *Nanoscale* **2020**, *12*, 13523–13530. [[CrossRef](#)] [[PubMed](#)]
143. Fan, Y.; Tao, T.; Wang, H.; Liu, Z.; Huang, W.; Cao, H. A Schiff base-functionalized graphene quantum dot nanocomposite for preferable picric acid sensing. *Dye. Pigment.* **2021**, *191*, 109355. [[CrossRef](#)]
144. Gonzalez, C.M.; Iqbal, M.; Dasog, M.; Piercey, D.G.; Lockwood, R.; Klapötke, T.M.; Veinot, J.G.C. Detection of high-energy compounds using photoluminescent silicon nanocrystal paper based sensors. *Nanoscale* **2014**, *6*, 2608–2612. [[CrossRef](#)]
145. Infantry: Electronic Nose for Explosives. *StrategyPage*, 28 June 2006.
146. Ma, J.; Bock, W. Fiber-Optic Sensors for Explosives Detection. *Open Opt. J.* **2013**, *7*, 141–158. [[CrossRef](#)]
147. Gardner, J.; Yinon, J. *Electronic Noses & Sensors for the Detection of Explosives*; Springer: Amsterdam, The Netherlands, 2004; ISBN 9781402023170.
148. Verma, P.; Goudar, R.H. Mobile phone based explosive vapor detection system (MEDS): A methodology to save humankind. *Int. J. Syst. Assur. Eng. Manag.* **2017**, *8*, 151–158. [[CrossRef](#)]
149. Kovalev, I.S.; Sadieva, L.K.; Taniya, O.S.; Yurk, V.M.; Minin, A.S.; Santra, S.; Zyryanov, G.V.; Charushin, V.N.; Chupakhin, O.N.; Tsurkan, M.V. Computer vision vs. spectrofluorometer-assisted detection of common nitro-explosive components with bola-type PAH-based chemosensors. *RSC Adv.* **2021**, *11*, 25850–25857. [[CrossRef](#)]
150. Wu, Z.; Duan, H.; Li, Z.; Guo, J.; Zhong, F.; Cao, Y.; Jia, D. Multichannel Discriminative Detection of Explosive Vapors with an Array of Nanofibrous Membranes Loaded with Quantum Dots. *Sensors* **2017**, *17*, 2676. [[CrossRef](#)]
151. Wu, W.; Shi, N.; Zhang, J.; Wu, X.; Wang, T.; Yang, L.; Yang, R.; Ou, C.; Xue, W.; Feng, X.; et al. Electrospun fluorescent sensors for the selective detection of nitro explosive vapors and trace water. *J. Mater. Chem. A* **2018**, *6*, 18543–18550. [[CrossRef](#)]
152. Zyryanov, G.V.; Palacios, M.A.; Anzenbacher, P., Jr. Simple molecule-based fluorescent sensors for vapor detection of TNT. *Org. Lett.* **2008**, *10*, 3681–3684. [[CrossRef](#)]
153. Khasanov, A.F.; Kopchuk, D.S.; Kovalev, I.S.; Taniya, O.S.; Giri, K.; Slepukhin, P.A.; Santra, S.; Rahman, M.; Majee, A.; Charushin, V.N.; et al. Extended cavity pyrene-based iptycenes for the turn-off fluorescence detection of RDX and common nitroaromatic explosives. *New J. Chem.* **2017**, *41*, 2309–2320. [[CrossRef](#)]
154. Liu, X.; Hu, Y.; Zhou, Y.; Zhang, P.; Gao, L.; Liu, B.; Wu, Z.; Zhang, L. PPV Nanotube Sensor Arrays for Explosives Identification by Excitation Wavelength Regulation. *Macromol. Mater. Eng.* **2021**, *306*, 2100276. [[CrossRef](#)]
155. Liu, R.; Li, Z.; Huang, Z.; Li, K.; Lv, Y. Biosensors for explosives: State of art and future trends. *TrAC Trends Anal. Chem.* **2019**, *118*, 123–137. [[CrossRef](#)]
156. Balan, B.; Vijayakumar, C.; Tsuji, M.; Saeki, A.; Seki, S. Detection and Distinction of DNT and TNT with a Fluorescent Conjugated Polymer Using the Microwave Conductivity Technique. *J. Phys. Chem. B* **2012**, *116*, 10371–10378. [[CrossRef](#)] [[PubMed](#)]
157. Shaw, P.E.; Chen, S.S.Y.; Wang, X.; Burn, P.L.; Meredith, P. High-Generation Dendrimers with Excimer-like Photoluminescence for the Detection of Explosives. *J. Phys. Chem. C* **2013**, *117*, 5328–5337. [[CrossRef](#)]
158. Abd-El-Aziz, A.S.; Abdelghani, A.A.; Wagner, B.D.; Abdelrehim, E.M. Aggregation enhanced excimer emission (AEEE) with efficient blue emission based on pyrene dendrimers. *Polym. Chem.* **2016**, *7*, 3277–3299. [[CrossRef](#)]
159. Santos, A.P.L.; Deokaran, G.O.; Costa, C.V.; Gama, L.I.; Júnior, E.G.M.; de Assis, A.M.; de Freitas, J.D.; de Araujo, W.R.; Dias, R.P.; da Silva, J.C.; et al. A “turn-off” fluorescent sensor based on electrospun polycaprolactone nanofibers and fluorene(bisthiophene) derivative for nitroaromatic explosive detection. *Forensic Sci. Int.* **2021**, *329*, 111056. [[CrossRef](#)]

Disclaimer/Publisher’s Note: The statements, opinions and data contained in all publications are solely those of the individual author(s) and contributor(s) and not of MDPI and/or the editor(s). MDPI and/or the editor(s) disclaim responsibility for any injury to people or property resulting from any ideas, methods, instructions or products referred to in the content.